

# Onset of Order in Lattice Systems: Kitaev Model and Hard Squares

A thesis submitted to  
Tata Institute of Fundamental Research, Mumbai, India  
for the degree of  
Doctor of Philosophy  
in  
Physics

By

Kabir Ramola

*Department of Theoretical Physics  
Tata Institute of Fundamental Research  
Mumbai - 400 005, India*

**July 2012**



## Declaration

This thesis is a presentation of my original research work. Wherever contributions of others are involved, every effort is made to indicate this clearly, with due reference to the literature, and acknowledgement of collaborative research and discussions.

The work was done under the guidance of Professor Deepak Dhar, at the Tata Institute of Fundamental Research, Mumbai.

(Kabir Ramola)

In my capacity as the supervisor of the candidate's thesis, I certify that the above statements are true to the best of my knowledge.

(Deepak Dhar)



## Acknowledgements

I am deeply grateful to Prof. Deepak Dhar for guiding me over the last five years. It has been a pleasure learning and working with him. I thank Kedar Damle for the many enthusiastic and informative discussions I have had with him. I would like to thank Vikram Tripathi and R. Palit for their advice and insight over the years. In addition, I would like to thank all the members of the Department of Theoretical Physics for the stimulating and helpful milieu they provided during my stay.

I would like to thank the DTP office staff Raju, Pawar, Girish and Mohan for all their efficient help over the years. A big thanks to Ajay and Kapil for their patience and help with the computer clusters.

I thank my friends Arnab, Loganayagam, Debasish, Jyotirmoy, Chirag, Kusum, Prithvi, Shamashis, Sayan, Rahul, Nikhil and Sambuddha for all the physics and the fun times we've shared. A special thanks to my friends Sayo, Dore, Kedar, Iyer and Aby, for all the good times.

Lastly, I would like to thank my sister and my parents for their constant support over the years.



## Collaborators

This thesis is based on work done in collaboration with several people.

The work presented in Chapter 2 is based on work done with Deepak Dhar and Samarth Chandra, and parts of it have appeared in print in *Phys. Rev. E* **82**, 031113. The work presented in Chapter 3 is based on work done with Deepak Dhar, Diptiman Sen, and R. Shankar, and parts of it have appeared in print in *Phys. Rev. B* **82**, 19543. The work presented in Chapter 4 is based on work done with Deepak Dhar and Kedar Damle, and parts of it have appeared in print in *Phys. Rev. E* **86**, 031135.

# Contents

<b>Synopsis</b>	<b>v</b>
<b>Publications</b>	<b>xix</b>
<b>1 Introduction</b>	<b>1</b>
1.1 Spin Models . . . . .	2
1.1.1 The XY and Heisenberg Models . . . . .	3
1.1.2 The Ashkin-Teller Model . . . . .	3
1.1.3 The Kitaev Model . . . . .	4
1.1.4 Order-by-Disorder . . . . .	6
1.2 Lattice Gas Models . . . . .	6
1.2.1 Hard-Core Lattice Gases . . . . .	6
1.2.2 The Hard Square Lattice Gas . . . . .	7
1.2.3 Columnar Order . . . . .	8
1.2.4 Solid-on-Solid Model and Surface Roughening . . . . .	9
1.3 Outline . . . . .	9
<b>References</b>	<b>14</b>
<b>2 The Kitaev Model with Classical Spins</b>	<b>15</b>
2.1 Introduction . . . . .	15
2.2 The Model . . . . .	16
2.3 The Ground States . . . . .	17
2.4 Effective Hamiltonian . . . . .	18
2.5 Two Dimensional Electrostatics . . . . .	19
2.6 Characterising the Ground State Manifold . . . . .	22
2.7 Finite Temperature Partition Function . . . . .	23
2.8 The Temperature Tending to Zero Limit . . . . .	23
2.9 Mapping to a Solid-on-Solid Model . . . . .	24
2.10 Correlations . . . . .	25
2.11 Monte Carlo Simulations . . . . .	26
2.12 The Spin- $S$ Quantum Kitaev Model . . . . .	30

2.13 Summary and Discussion . . . . .	32
<b>References</b>	<b>34</b>
<b>3 Spin-1 Kitaev Chain</b>	<b>35</b>
3.1 Introduction . . . . .	35
3.2 One-dimensional Kitaev Model . . . . .	36
3.3 The Invariants . . . . .	37
3.4 Dimension of the Subspaces . . . . .	38
3.5 Expectation Values of Operators . . . . .	41
3.6 The $S = 1$ Model . . . . .	43
3.7 Mapping to a Spin-1/2 Chain . . . . .	45
3.8 Variational Study of the Ground State . . . . .	46
3.9 Estimating the Energy Gap . . . . .	49
3.10 Study of Ground States in Other Sectors . . . . .	52
3.11 Summary . . . . .	55
<b>References</b>	<b>57</b>
<b>4 The Hard Square Lattice Gas</b>	<b>59</b>
4.1 Introduction . . . . .	59
4.2 The Model . . . . .	59
4.3 Expansion about the Crystalline Ordered State . . . . .	60
4.4 Expansion about the Columnar Ordered State . . . . .	62
4.4.1 Single Defect . . . . .	65
4.4.2 Two Defects . . . . .	66
4.4.3 Higher Orders . . . . .	67
4.5 High-Activity Expansion in terms of Rods . . . . .	68
4.5.1 High-Activity Expansion for the Free Energy . . . . .	73
4.5.2 Order Parameter Expansion . . . . .	74
4.6 Variational Study of the Free Energy . . . . .	74
4.7 Fluid to Columnar Order Transition . . . . .	77
4.8 Mapping to the Ashkin-Teller Model . . . . .	78
4.8.1 Ising Energy Densities . . . . .	79
4.9 Monte Carlo Simulations . . . . .	81
4.10 Hard-Cubes on the Cubic lattice . . . . .	88
4.11 Summary and Discussion . . . . .	89
<b>References</b>	<b>91</b>
<b>5 Conclusions</b>	<b>93</b>

---

<b>A</b>	<b>Height Correlations at Infinite Temperature</b>	<b>95</b>
<b>B</b>	<b>Additional Details for the High-Activity Expansion</b>	<b>99</b>
B.1	Three B-defects on the lattice: Exact Expression . . . . .	99
B.2	Regrouping the Terms . . . . .	100
B.2.1	Expansion for the Free Energy . . . . .	100
B.2.2	Expansion for the Order Parameter . . . . .	105
B.2.3	Summing the Binomial Series . . . . .	107

# Synopsis

## Introduction

Systems that are at the threshold of instability between order and disorder have been of continued interest in the field of Statistical Physics. In this thesis we discuss two models: the spin- $S$  Kitaev model in the limit of large  $S$  where the spins become classical 3-vector (Heisenberg) spins and the hard square lattice gas model. We investigate whether in this classical limit the Kitaev model displays order-by-disorder, a phenomenon whereby a system that is disordered at strictly zero temperature acquires a fluctuation induced order at temperatures just above zero. In addition, we analyse properties of a quantum spin- $S$  chain related to the Kitaev model. We then study the lattice gas of  $2 \times 2$  hard squares on the square lattice, where there is a vacancy-induced sliding instability that makes the crystalline order unstable, but a partial order survives in the form of columnar order where only two of the four possible ordered states mix with each other. We also analyse the nature of the transition from fluid to columnar order as a function of density in this system.

In the order-by-disorder mechanism, the relative weights of different ground states in the zero temperature limit of the partition function from finite temperatures differs from the actual sum over ground states that contribute at zero temperature. In this context we study the Kitaev model, an exactly soluble two dimensional quantum model in the classical limit. We find that this model has a manifold of ground states whose dimension is proportional to the size of the system and all ground states have an equal weight in the zero temperature limit. In the spin- $S$  quantum Kitaev model Baskaran *et. al.* [1] argued that the quantum fluctuations about the ground states induce an ordering in the system for large  $S$ . We investigate whether the thermal fluctuations in the  $S \rightarrow \infty$  limit of this model behave in the same way. We find that although the existence of order-by-disorder in the finite- $S$  quantum model seems plausible, the classical limit case does not behave in the same fashion. For the classical model, we develop an exact mapping to a height model and using this we are able to analyse the zero temperature limit without invoking a quadratic or quartic approximation to include the effects of fluctuations. We study this system at all temperatures and show that there is no incipient long range order in this system at temperatures tending to zero. At zero temperature the model is equivalent to a height

model which remains in the rough phase, this leads to a power law decay of the spin-spin correlation function with distance, with an exponent  $-2$ . We also develop exact bounds on the ground state energy of the quantum model in the large- $S$  spin limit.

In addition, we investigate properties of the spin-1 analogue of the Kitaev model on a 1D chain. We use a mapping to a classical lattice gas model to estimate the ground state energies and the energy gap of this 1D quantum spin chain.

In the second half of this thesis we study a classical lattice gas model of particles with nearest and next nearest neighbour exclusion (hard squares) on the square lattice. This problem has been the subject of several studies in the past [2] [3], however many aspects of it are still not well understood. The high density phase of this model displays columnar order, where the sublattice ordered state is unstable at large densities and particles preferentially align themselves along columns but do not have sublattice order. The columnar ordered state is difficult to treat theoretically in detail, and there have been few studies so far. For example, it has not been possible to develop a Peierls-type argument to show the stability of this phase. In this context we developed an exact series expansion about a state with perfect columnar order but no sublattice order. This expansion is a singular perturbation expansion, and contains fractional powers of fugacity. To understand the nature of the ordering in this system, we develop a novel Monte Carlo algorithm that avoids jamming problems effectively and can efficiently simulate the system near close-packed densities. We argue that the critical properties of this model corresponds to one point on the parameter space of a more general Ashkin-Teller model which possesses a line of critical points with continuously variable critical exponents. We locate the position of the hard squares critical point on this line by determining the sign of the coupling between the coarse grained Ising energy densities in the Ashkin-Teller description by simulations on lattices of sizes upto  $1600 \times 1600$ . We also obtain estimates for the critical exponents and other relevant quantities of this system.

## The Kitaev Model with Classical Spins

There has been a lot of interest in the Kitaev model in recent years as it is the first genuinely interacting two dimensional quantum spin model which is equivalent to a 3D classical statistical mechanical model. The quantum mechanical spin-1/2 Kitaev model can be exactly solved in 2D. The Hamiltonian can be diagonalized exactly in terms of Majorana fermions [4]. The model exhibits a phase transition from a phase with finite correlation length to one with long-range correlations as the ratios of coupling constants in different directions are varied [5, 6]. It has topological excitations, and their robustness with respect to noise makes it an interesting candidate for quantum computing [7]. Kitaev's pioneering work has led to a large amount of further research. The spectrum of the different phases of this model have been extensively studied [8]. Proposals for experimentally realising this

model using polar molecules and ultracold atoms trapped in optical lattices have recently been made [9, 10].

In a recent paper, Baskaran *et al.* studied a generalization of this model with spin- $S$  at each site and identified mutually commuting plaquette variables taking values  $\pm 1$  that are constants of motion for arbitrary  $S$  [1]. For large  $S$ , the spins can be approximated as classical  $O(3)$  vector spins. Baskaran *et al.* showed that the classical ground state of the model has a large degeneracy. They argued that for large  $S$ , the quantum fluctuations of spins have lower energy for a subset of the classical ground states. These states get more weight in the quantum mechanical ground state, and the quantum model shows long-range order in the ground state, an example of quantum order-by-disorder. It seems interesting to investigate whether the classical limit also shows order-by-disorder.

There is a fair amount of earlier work on order-by-disorder in classical systems [11, 12]. It has been studied a lot in the context of magnetic systems with frustration, such as spin systems with nearest neighbour antiferromagnetic interactions on different lattices [13, 14]. The prototypical example is the system of Heisenberg spins on a kagome lattice, with nearest neighbour antiferromagnetic couplings. The expectation of order-by-disorder in this classical system comes from theoretical and Monte Carlo studies, that suggest that at low temperatures, the spins lie on a single plane as  $T \rightarrow 0$  [15],[16]. By mapping this system to a height model at its critical point it can be shown that a single long-range ordered state (the  $\sqrt{3} \times \sqrt{3}$  state) is selected even amongst the coplanar ordered states [17],[18].

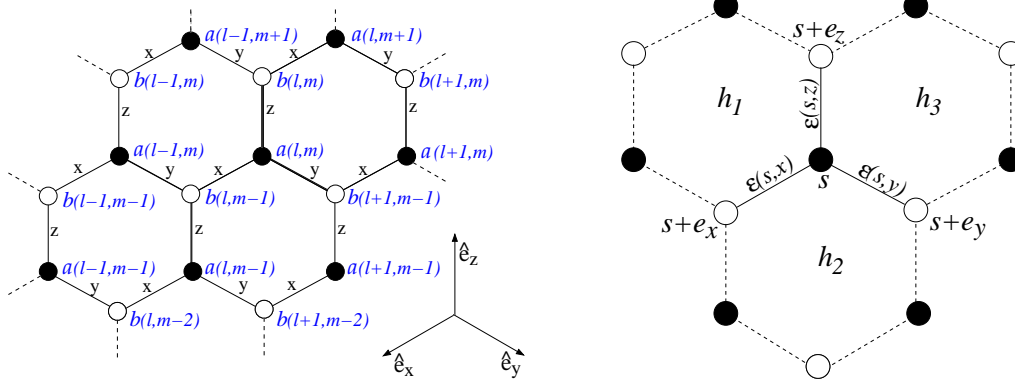


Figure 1: (Left) A hexagonal lattice depicting the labelling scheme for sites, and the  $x$ ,  $y$  and  $z$  bond classes. Sites in the A- and B- sublattices are denoted by filled and open circles respectively. (Right) Figure depicting the definition of the  $\epsilon$  and  $h$  variables on the bonds and plaquettes around an A-site  $s$ .

We consider classical Heisenberg spins on a hexagonal lattice with Kitaev couplings. The bonds of the lattice are divided into three classes,  $X$ ,  $Y$  and  $Z$ , according to their orientation (Fig. 2.1). At each lattice site  $i$  there is a three dimensional vector spin  $\vec{S}_i = (S_i^x, S_i^y, S_i^z)$  of unit magnitude. Thus  $S_i^x{}^2 + S_i^y{}^2 + S_i^z{}^2 = 1$  at every site. The Hamiltonian of the system is given by

$$H = -J \sum_{a \in A} [S_a^x S_{a+e_x}^x + S_a^y S_{a+e_y}^y + S_a^z S_{a+e_z}^z] \quad (1)$$

This Hamiltonian has spatially anisotropic interactions with spins interacting via their  $x, y$  and  $z$  components in the  $e_x, e_y$  and  $e_z$  directions respectively. We begin by characterising the ground state manifold of this model. We find that for a lattice of  $2N$  sites with periodic boundary conditions, the ground states form an  $(N + 1)$ -dimensional manifold.

Due to the bipartite nature of the lattice we can integrate out the spins on one of the sublattices in the partition function, yielding an effective Hamiltonian in terms of A-sublattice spins. For a given configuration of spins  $\{S^\alpha\}$ , to each bond  $(l, m; \alpha)$  of the lattice, we assign a bond-energy vector  $\epsilon(l, m; \alpha)\vec{e}_\alpha$ , with  $\epsilon(l, m; \alpha)$  given by

$$\epsilon(l, m; \alpha) = \left( S_{a(l,m)}^\alpha \right)^2 - \frac{1}{3}. \quad (2)$$

Clearly, the divergence of the field  $\epsilon$  at any site on the A-sublattice is 0. We find that the ground state ensemble is characterised by the constraint that the sum of bond energies at every B-site is also equal to 0. We thus have a divergence-free vector field on the bonds of the lattice at zero temperature. This allows us to map the zero temperature partition function of this model onto that of a height model with continuously variable heights. These height variables  $\{f(h_i)\}$  are associated with the hexagonal plaquettes of the lattice, where the  $h_i$  denotes a plaquette of the lattice. In the rough phase of this height model the correlations of the height field vary logarithmically. This leads to a power law decay of the spin-spin correlation function.

At finite temperatures, the ground state constraint is violated at every B-site. If we think of the  $\{\epsilon\}$  field as an electric field in two dimensions which at  $T = 0$  satisfies the divergence-free constraint  $\nabla \cdot \epsilon = 0$ , this is in effect equivalent to introducing finite charges at every B-site. We define a continuously variable charge at every B-site as follows

$$Q_{b(l,m)} = - \sum_{\alpha} \epsilon(b(l, m) - e_\alpha; \alpha). \quad (3)$$

We thus need additional variables to characterise the non-ground state configurations of the system. This can be achieved by introducing an electrostatic scalar potential  $\phi(s)$  at every site, where  $s$  denotes a site of the lattice. Given a configuration of spins on the A-sublattice, the  $f$  and  $\phi$  configurations can be generated using the corresponding lattice greens functions on the hexagonal lattice. We now take the zero temperature limit of this partition function using the height variables  $f$  and the charges  $Q$ . The partition function takes the form

$$Z[\beta] = (\text{Const.}) \left[ \prod_{l,m} \int df_{l,m} \int dQ_{b(l,m)} \right] \left[ \prod_{\text{bonds}} \left( \frac{1}{3} + \epsilon(\text{bond}) \right)^{-1/2} \right] \times \exp \left[ \sum_{l,m} F \left( \beta \sqrt{1 + Q_{b(l,m)}} \right) \right], \quad (4)$$

where,  $\Pi_{\text{bonds}}$  denotes the product over all bonds  $(l, m, \alpha)$  of the lattice and

$$F(x) = \log \left[ \frac{\sinh(x)}{x} \right]. \quad (5)$$

The linear term in  $Q$  in the above exponential vanishes due to the overall charge neutrality of the system. Hence the leading behaviour of the integral over the range of  $Q$  at large  $\beta$  can be determined exactly using a saddle point computation. While the range of the  $Q_s$  integrals depend on  $\{f_{l,m}\}$ , for large  $\beta$ , when the width of the peak is much smaller than the range of integration, and the peak is away from the end points of the range, each integration to leading order is independent of the configuration  $\{f_{l,m}\}$  and gives a factor  $C\beta^{-1/2}$  where  $C$  is a constant. Thus for all fixed  $\{f(l, m)\}$ , the integration over fluctuations in  $\{Q\}$  produces the same temperature-dependent weight factor, in the limit of large  $\beta$ . Thus we see that none of the ground states acquire a larger weight in the zero temperature limit of the partition function and this model does not exhibit thermal order-by-disorder.

The zero temperature height model has the symmetry that changing all heights by the same constant leaves the Hamiltonian unchanged. Though the interaction is a strongly non-linear function of difference of the heights, one expects that in the high-temperature phase of the height model, the long-wavelength hydrodynamical modes in the system will still be sound-like, with effective Hamiltonian  $|\nabla f|^2$ , which gives rise to the spectrum given by  $\omega^2 \propto k^2$ . Therefore for two sites  $s_1$  and  $s_2$  separated by a large distance  $R$  we have

$$\langle (f_{s_1} - f_{s_2})^2 \rangle \sim \log R \quad \text{which implies that} \quad \langle (S_{s_1}^\alpha)^2 (S_{s_2}^\beta)^2 \rangle_c \sim \frac{1}{R^2}. \quad (6)$$

As the temperature is increased, the height fluctuations are still logarithmic, but the spin correlators decay exponentially. At infinite temperature we are able to evaluate this quantity exactly, we have

$$\langle (f_R - f_0)^2 \rangle_{\beta=0} = \frac{2\sqrt{3}}{45\pi} \log[R] + \mathcal{O}(1) \quad \text{for large } R. \quad (7)$$

We perform Monte Carlo simulations on this model to verify our predictions. We simulate the effective Hamiltonian obtained by integrating out spins on the  $B$ -sublattice. For the finite temperature simulations, two kinds of moves were employed—single spin moves and 6-spin cluster moves (that efficiently thermalized the system at low temperatures). We looked for possible signatures of ordering in the system as the temperature was decreased by measuring various correlation functions and did not find any long range ordering in the system. The gauge symmetry of the model has a consequence that all correlation functions of the type  $\langle S_{s_1}^\alpha S_{s_2}^\beta \rangle$  with sites  $s_1$  and  $s_2$  not nearest neighbours are zero [19]. The simplest nontrivial correlation functions, for non-neighbour  $s_1$  and  $s_2$  are of the type  $\langle (S_{s_1}^\alpha)^2 (S_{s_2}^\beta)^2 \rangle$ . We computed correlations of the  $(S^\alpha)^2$ ,  $f$  and  $\phi$  fields at various temperatures. The  $\phi$  field was generated from the spin configuration by solving the discrete Poisson equation on the triangular lattice.

In addition, we also studied the quantum spin- $S$  version of this model with the Hamiltonian

$$H = -\frac{J}{S(S+1)} \sum_{a \in A} [S_a^x S_{a+e_x}^x + S_a^y S_{a+e_y}^y + S_a^z S_{a+e_z}^z] \quad (8)$$

We derived an exact lower bound for the ground state energy of this model. We have

$$\langle \psi | H | \psi \rangle \geq -JN \sqrt{\frac{S}{S+1}}. \quad (9)$$

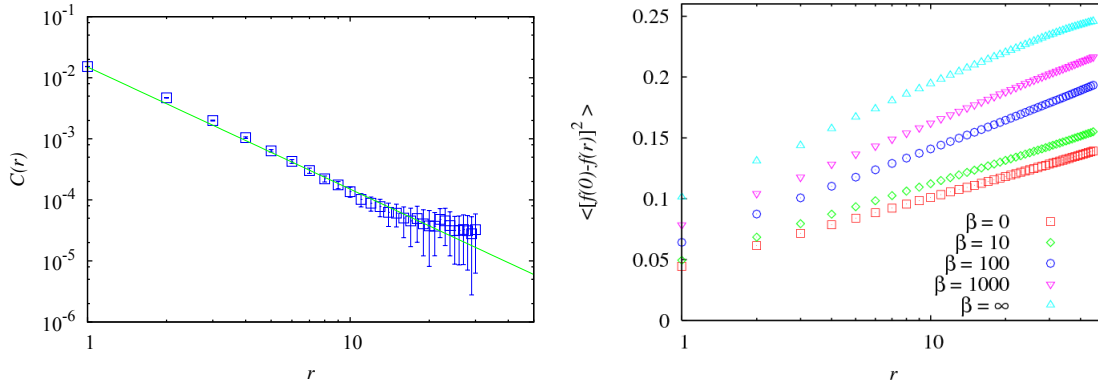


Figure 2: (Left): Plot of the zero temperature correlation function  $C(\vec{r}) = \langle S_A^{x2}(0) S_A^{x2}(\vec{r}) \rangle - \frac{1}{9}$  versus distance,  $r$  along the  $\hat{e}_x$  direction. These correlations follow a power law behaviour with exponent  $\simeq -2$ . The line has a slope of  $-2$ . (Right): Graph showing the finite temperature correlation function  $\langle (f(0) - f(r))^2 \rangle$  versus distance,  $r$  for various values of  $\beta = T^{-1}$ . The correlations are logarithmic at all temperatures, with the coefficient of  $\log(r)$  varying between  $(2.45 \pm 0.05) \times 10^{-2} \simeq \frac{2\sqrt{3}}{45\pi}$  at  $\beta = 0$  and  $(4.12 \pm 0.05) \times 10^{-2}$  at  $\beta = \infty$ .

## Spin-1 Kitaev Chain

Continuing with our study of the spin- $S$  Kitaev model, we analyse the 1D spin chain with the following Hamiltonian

$$H = \sum_n (J_{2n-1} S_{2n-1}^x S_{2n}^x + J_{2n} S_{2n}^y S_{2n+1}^y) \quad (10)$$

This is the Hamiltonian of the Kitaev model with the coupling in the  $e_z$  direction set to zero. The cases where  $S$  is integer and half-odd-integer are qualitatively different. We notice that there is a  $\mathbb{Z}_2$  valued conserved quantity  $W_n = \sum_n^y \sum_{n+1}^x$  for each bond  $(n, n+1)$  of the system, where  $\Sigma_n^a = e^{i\pi S_n^a}$ . The Hilbert space thus breaks up into sectors corresponding to different eigenvalues  $\{W_n\}$  with  $n = 1$  to  $N$ , where  $N$  is the number of sites on the chain. For integer  $S$ , the Hilbert space can be decomposed into  $2^N$  sectors, of unequal sizes.

We use the standard transfer matrix technique to count the number of states in each sector. In the limit when all the  $W_n$  are either  $+1$  or  $-1$ , the dimension of this subspace

can be computed explicitly. The number of states in the sector with all  $W_n = +1$  for the case  $S = 1$  grows as  $\gamma^N$ , where  $\gamma = (1 + \sqrt{5})/2$  is the golden ratio. For other sectors, given a  $\{W_i\}$ , the dimension can be expressed as a trace of explicit products of  $2 \times 2$  transfer matrices.

We next study the system with  $S = 1$ . We use exact diagonalizations of small systems and find that the ground state of this spin chain lies in the sector with all  $W_n = +1$  with an energy per site  $E_g = -0.60356058$ , and that the energy gap remains finite in the thermodynamic limit. In the ground state sector, the system can be mapped onto a spin-1/2 model and the excitations within the ground state sector about the fully polarised state in the  $z$  direction can be thought of as a dimer evaporation-deposition process. We develop variational wave functions to study the lowest energy states in the ground state and other sectors. We postulate a variational wavefunction of the type

$$|\psi\rangle = \sum_{\mathbf{C}} \sqrt{\text{Prob}(\mathbf{C})} |\mathbf{C}\rangle \quad (11)$$

where  $\text{Prob}(\mathbf{C})$  is chosen as the probability of the lattice gas configuration  $\mathbf{C}$  in some classical equilibrium ensemble corresponding to a suitably chosen lattice gas Hamiltonian. The simplest choice of the lattice-gas Hamiltonian is that of a classical lattice gas with nearest-neighbor exclusion, and a chemical potential  $\mu$ . Using this trial Hamiltonian state already gives a rather good estimate of the ground state energy of  $-0.60057$ . Extending the range of interaction to further neighbours and optimizing using the parameters yields better estimates of the ground state energy. An extension to the next nearest neighbour yields an estimate of  $-0.60333$  which agrees with the exact value obtained from exact diagonalization of finite size systems with an error  $< 0.1\%$ .

We then consider the sector with one  $W$  negative to obtain an estimate of the gap in the excitation spectrum. A single  $W = -1$  can be created on a bond by polarizing one of the bond spins in the  $x$  or  $y$  directions. We therefore use a trial wave function of the following type to study the ground state in the sector with one  $W$  negative and all others positive

$$|\psi\rangle = \frac{1}{\sqrt{2}} \left[ \sum_U \sqrt{\text{Prob}(U)} |xU\rangle - \sum_V \sqrt{\text{Prob}(V)} |Vy\rangle \right] \quad (12)$$

Here  $U$  and  $V$  are strings of length  $N - 1$ , consistent with  $W = +1$  at each bond, The  $x$  and  $y$  in the wavefunction above represent spins polarised in the  $x$  and  $y$  directions respectively. Using this trial state with position dependent weights for dimer evaporation/deposition and the probabilities derived from nearest neighbour lattice gas exclusion configurations, we are able to estimate the gap to the first excited state of this system. The energy gap converges quickly, and with a ten parameter wavefunction we obtain  $\Delta \simeq 0.15556$ .

## The Hard Square Lattice Gas

In the second half of the thesis, we study the system of particles with nearest and next-nearest-neighbour exclusion on the square lattice (hard squares). Equivalently, each particle is a  $2 \times 2$  square that occupies 4 elementary plaquettes of the square lattice (Fig. 4.1). Transfer matrix techniques indicate the existence of a phase transition in this model [2], [3], [20], [21]. Variational, density functional methods and virial expansions have also been used to study this problem [3], [22], [23]. These studies indicate that at high densities the sublattice ordered state is unstable but a “columnar ordered” state wherein one of the even or odd rows or columns is preferentially occupied over the others survives at high density (Fig. 4.1). Recent Monte Carlo evidence suggests that the transition from fluid to columnar order in this system is of second order, with exponents very close to the two dimensional Ising model [24], [25], [26].

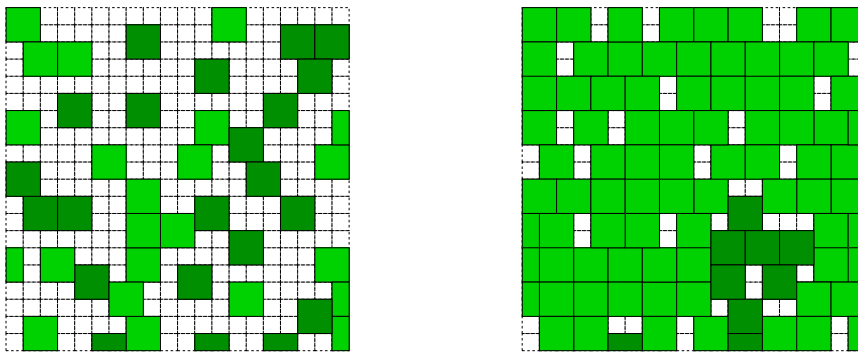


Figure 3: A typical configuration of hard squares on the lattice at (Left) low fugacity and (Right) high fugacity. The light green squares correspond to particles on row A, whereas the dark green squares correspond to particles on row B. At high densities, the system is in a columnar ordered phase.

The instability of the sublattice state at high densities is caused by the fact that a single square vacancy can break up into half-vacancies and be moved arbitrarily far apart in the horizontal or vertical direction. This is illustrated in Fig. 4 where, starting from a sublattice 1 ordered state we introduce a finite density of vacancies. The dark blue rectangles represent half-vacancies. The empty region is plaquettes covered by squares on sublattice 1, the horizontal rods are made of squares on sublattice 2 and the vertical rods are composed of squares on sublattice 3. The breaking of vacancies into half vacancies causes the standard high density expansion in powers of  $1/z$  to fail. It was realised quite early that the leading order correction to the high activity expansion is of order  $1/\sqrt{z}$  [27], where  $z$  is the fugacity associated with each particle, but a systematic expansion has not been developed so far. We note that there is as yet no rigorous proof of the existence of this type of order in this system. In this context it is worthwhile to develop exact series expansions in this phase and study their convergence.

We first develop a systematic expansion of the free energy in inverse powers of fugacity

in the columnar ordered state. This is a singular perturbation series in powers of  $1/\sqrt{z}$ . We introduce explicit symmetry breaking by ascribing different fugacities  $z_A$  and  $z_B$  to the particles on even and odd rows. The point  $z_B = 0$  corresponds to a fully columnar ordered configuration. The perturbation expansion about the ordered state in powers of  $z_B$  is a standard Mayer-like series [28].

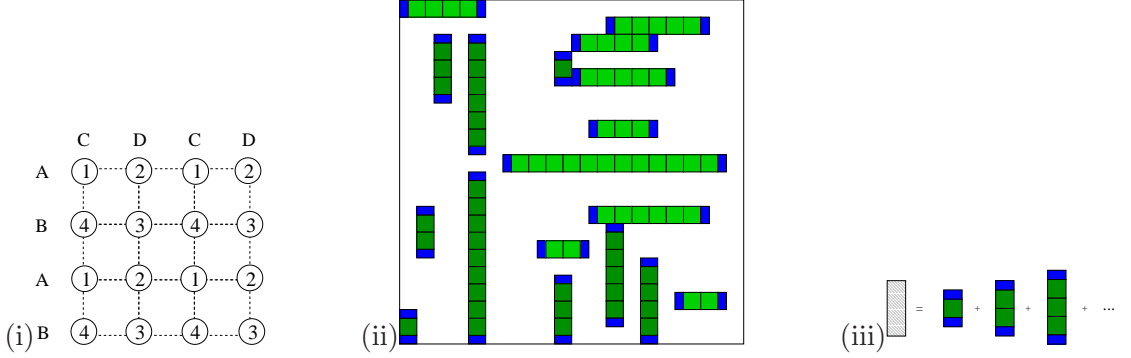


Figure 4: (i) We define four sublattices 1 through 4 on the square lattice. Rows containing the sites of sublattice 1 and 2 (3 and 4) will be called A (B) rows. Similarly, columns with sublattice sites 1 and 4 (2 and 3) will be called C (D) columns. (ii) A configuration near full packing consisting only of horizontal and vertical rod defects. (iii) Objects contributing to the expansion at order  $1/z$ . These are vertical rods with all the defects aligned along the Y direction.

We write the partition function of the system  $\Omega(z_A, z_B)$  as a formal expansion in terms of the fugacities of the particles on the B rows (defects) and the corresponding partition functions of the A rows. The partition function expansion about the columnar ordered state  $\Omega(z_A, 0)$  is

$$\frac{\Omega(z_A, z_B)}{\Omega(z_A, 0)} = 1 + z_B W_1(z_A) + \frac{z_B^2}{2!} W_2(z_A) + \dots \quad (13)$$

$W_n$  corresponds to the term arising from placing  $n$  B-particles on the lattice. Now, taking the logarithm of Eqn. 4.10 we arrive at the cumulant expansion

$$\frac{1}{N_B} \log \frac{\Omega(z_A, z_B)}{\Omega(z_A, 0)} = z_B \kappa_1(z_A) + \frac{z_B^2}{2!} \kappa_2(z_A) + \dots \quad (14)$$

where  $N_B = N/2 = L^2/2$  is the total number of B-sites in the system and  $\kappa_n$  denotes the connected part of the  $n$ 'th term in the expansion. When there are no B-particles in the lattice, the partition function of the system breaks up into a product of 1D partition functions of particles on the A-rows (particles on different A-rows do not interact). These A-particles thus behave as a 1D lattice gas with nearest neighbour exclusion. In general, any term involving an arbitrary number of B-particles can be decomposed into a product over 1D partition functions and hence can be evaluated using a product over two-particle correlators. We are thus able to exactly compute the first few terms in the cumulant expansion in defect fugacities. The contribution from a single B defect in the expansion

is given by the first term of the cumulant expansion  $\kappa_1(z_A)z_B$ , with  $\kappa_1(z_A) = \left(\frac{\rho_{1d}(z_A)}{z_A}\right)^2$ , where  $\rho_{1d}(z_A)$  is the density of particles in an infinite periodic chain of particles with nearest neighbour exclusion. When we set  $z_A = z_B = z$ , we obtain an expansion in inverse powers of  $z$  which contains fractional powers with the first term being of order  $1/z$  and the next being  $1/z^{3/2}$ . Similarly the two particle term also yields an expansion in terms of  $1/\sqrt{z}$  with the first correction of order  $1/z$  and so on. In general, terms at each order in inverse powers of  $z$  get contributions from an arbitrarily large number of defects.

For the case  $z_A = z_B = z$ , we find that the terms of the series can be regrouped and the resulting series can be thought of as a Mayer-like expansion of extended objects (vertical rods), but of arbitrary size. The order  $1/z$  term gets contributions only from defects aligned along the vertical direction (this excludes the least volume of A-particles). This is in effect the same object as a pair of half-vacancies separated by a vertical ‘‘rod’’ of B-sublattice particles. The term of order  $1/z^{\frac{n+1}{2}}$  involves at most  $n$  such objects and get contributions from all possible sizes of these objects.

We evaluate explicitly the contribution of terms corresponding to two rods which yields the exact high-activity expansion for the free energy per site  $f(z)$  and the density  $\rho(z)$  of the hard square lattice gas upto order  $1/z^{3/2}$ . We have

$$-f(z) = \frac{1}{4} \log z + \frac{1}{4z^{1/2}} + \frac{1}{4z} + \frac{(3 \log(\frac{9}{8}) + \frac{11}{96})}{z^{3/2}} + \mathcal{O}\left(\frac{1}{z^2}\right)$$

and

$$\rho(z) = \frac{1}{4} - \frac{1}{8z^{1/2}} - \frac{1}{4z} - \frac{(\frac{9}{2} \log(\frac{9}{8}) + \frac{11}{64})}{z^{3/2}} + \mathcal{O}\left(\frac{1}{z^2}\right) \quad (15)$$

We next investigate the nature of the phase transition from fluid to columnar order in this system. The correlations in the columnar ordered state are hard to describe theoretically using mean field like descriptions. All the well-known approximation schemes like the mean field theory and cluster variational approximations underestimate the value of the critical point  $z_c$  by an order of magnitude. Monte Carlo simulations are thus an important tool for analysing the nature of this transition.

At high densities the system can order in any one of four columnar ordered states. The four columnar ordered states are related to each other by a  $\frac{\pi}{2}$  rotational transformation about the centre of a plaquette. An anticlockwise rotation of an A-row ordered phase about a plaquette centre transforms the phase into a C-column ordered phase and so on. Hence these states belong to the symmetry group  $\mathbb{Z}_4$  and the transition is expected to lie in the universality class of a  $\mathbb{Z}_4$  transition. We define the following complex order parameter

$$O_{\mathbb{Z}_4} = 4\sqrt{2}[(\rho_1 - \rho_3) + i(\rho_2 - \rho_4)] \quad (16)$$

where  $\rho_i$  is the density of particles in the  $i$ th sublattice. The phase of the complex order

parameter  $O_{Z_4}$  takes the values  $\pi/4, -3\pi/4, -\pi/4$  and  $3\pi/4$  in the A, B, C, and D phases respectively.

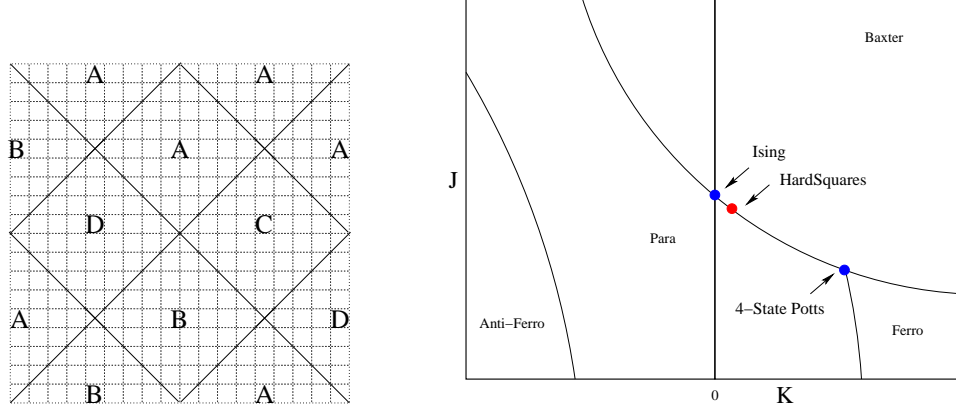


Figure 5: (Left) We coarse grain the system using a grid at an angle  $\frac{\pi}{4}$  with respect to the lattice. This ensures that the surface tensions between any two phases is symmetric. We assign a single phase label to each resulting diamond. (Right) The phase diagram of the Ashkin-Teller model depicting the critical lines and the position of the phase transition of the Hard Square lattice gas.

We now coarse grain the system using a grid at an angle  $\frac{\pi}{4}$  with respect to the lattice axes. We assign a single phase label to each resulting diamond corresponding to the majority rule (Fig. 4.8). In this coarse grained model, the phases have a finite surface tension with respect to each other. From symmetry we see that there are two types of surface tensions in this high density phase. These two surface tensions are  $\sigma_{AB} = \sigma_{CD}$ , where  $\sigma_{AB}$  denotes the surface tension between the A-phase and the B-phase, and  $\sigma_{AC} = \sigma_{CB} = \sigma_{BD} = \sigma_{DA}$ . We can relate this 4 state model to the Ashkin-Teller model with a Hamiltonian that has  $\mathbb{Z}_4$  symmetry. The Ashkin-Teller model is best described as a model of two coupled Ising models with a varying strength of interaction with the Hamiltonian

$$H = - \left[ \sum_{\langle i,j \rangle} J_2 \sigma_i \sigma_j + J_2 \tau_i \tau_j + J_4 \sigma_i \sigma_j \tau_i \tau_j \right] \quad (17)$$

This model has a line of critical points with continuously variable critical exponents, depending on the strength of the interactions. The surface tensions between the phases in the hard square gas correspond to the surface energies  $K$  and  $2J - K$  of the above Ashkin-Teller model, where  $J = \beta J_2$  and  $K = \beta J_4$ . Thus a likely universality class for the transition of this system is Ashkin-Teller criticality.

In the simulations of high density states of exclusion gases, one often encounters the problem of “jamming”, where the number of available local moves for a system become very small. Since the transition to the columnar ordered phase in this system occurs at densities very close to full packing, it becomes necessary to use efficient non-jamming algorithms. We devised the following novel Monte Carlo algorithm to simulate the hard square lattice gas.

We evaporate all particles that lie on an arbitrarily chosen 1D line (horizontal or vertical) of the system. The resulting empty line of particles breaks up into regions that are occupiable by particles and regions forbidden for occupation, depending on the configuration of particles on the lines immediately above and below. We then refill these smaller occupiable line segments using a configuration selected from the configuration space of a system of particles with nearest neighbour exclusion on a 1D chain of the corresponding length. Clearly, this update scheme obeys detailed balance. This algorithm thus updates an entire row or column at once, and is able to efficiently sample the phase space even at very high densities. Using this algorithm, we are able to obtain reliable estimates of thermodynamic quantities from lattices upto size  $1600 \times 1600$ .

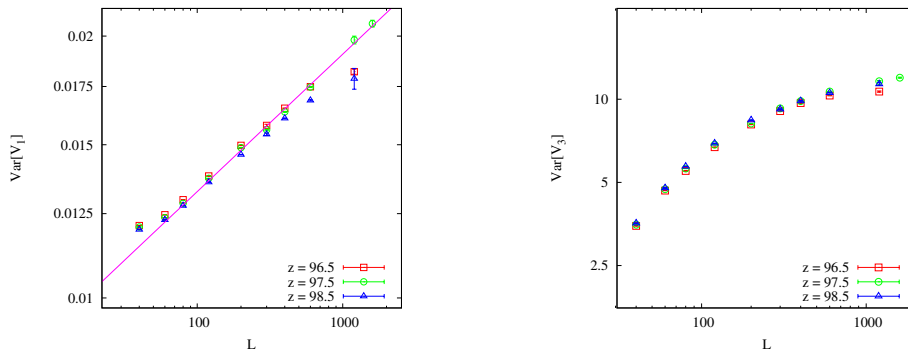


Figure 6: Variance of the observables  $V_1$  (Left) and  $V_3$  (Right). We see that the Variance of  $V_1$  rises with a detectable power with increasing system size whereas that of  $V_3$  saturates to a finite value.

Using finite size scaling, and Binder cumulant data, we obtain an estimate of the critical point as  $z_c = 97.5 \pm 0.5$ . The symmetry of the hard square lattice gas model suggests observables that are linear combinations of the sublattice densities  $\rho_i$  that have simple transformations under rotations by  $\frac{\pi}{2}$  as relevant quantities. These are  $V_i = \rho_1 + \omega_i \rho_2 + \omega_i^2 \rho_3 + \omega_i^3 \rho_4$ , where  $\omega_i$  with  $i = 1$  to 4 are the fourth roots of unity given by  $1, i, -1$  and  $-i$  respectively.

We measure the variance of these quantities in the system. At the critical point the variance of  $V_i$  varies as  $L^{a_i}$  where  $L$  is the size of the system, with  $a_1 \simeq 0.16$ ,  $a_2 = a_4 = \frac{7}{4}$  and  $a_3 = 0$ . We see that the variance of the observable  $V_1$  grows as a power law at large distances and the variance of  $V_3$  saturates to a finite value (Fig. 6). We are able to verify that the scaling exponent  $\gamma/\nu$  is equal to  $7/4$  to very high accuracy, consistent with the critical behaviour of the Ashkin-Teller model. Due to the large correlation lengths in the columnar ordered phase, the determination of the exponent  $\nu$  is slightly harder. At present our best estimates are  $\nu = 0.92 \pm 0.05$ . Using a mapping of the microscopic particle densities to a coarse grained Ising energy density, we are able to tentatively place the critical point of this model slightly to the ferromagnetic side of the Ising point on the critical line of the Ashkin-Teller model.

# Bibliography

- [1] G. Baskaran, D. Sen, and R. Shankar, Phys. Rev. B **78**, 115116 (2008)
- [2] A. Bellemans and R. Nigam, Phys. Rev. Lett. **16**, 23 (1966)
- [3] F. H. Ree and D. A. Chestnut, Phys. Rev. Lett. **18**, 5 (1967)
- [4] A. Kitaev, Ann. Phys. **321**, 2 (2006)
- [5] X. Y. Feng, G. M. Zhang, and T. Xiang, Phys. Rev. Lett. **98**, 087204 (2007)
- [6] V. Lahtinen and J. K. Pachos, Phys. Rev. B **81**, 245132 (2010)
- [7] C. Nayak, S. H. Simon, A. Stern, M. Freedman, and S. Das Sarma, Rev. Mod. Phys. **80**, 1083 (2008)
- [8] V. Lahtinen, G. Kells, A. Carollo, T. Stitt, J. Vala, and J. K. Pachos, Ann. Phys. **323**, 2286 (2008)
- [9] A. Micheli, G. K. Brennen, and P. Zoller, Nature Physics, **2**, 341 (2006)
- [10] L. M. Duan, E. Demler, and M. D. Lukin, Phys. Rev. Lett. **91**, 090402 (2003)
- [11] J. Villain, R. Bidaux, J. P. Carton, and R. Conteet, J. Phys. (Paris) **41**, 1263 (1980)
- [12] R. Moessner and J. T. Chalker, Phys. Rev. B **58**, 12049 (1998)
- [13] C. L. Henley, Phys. Rev. B **71**, 014424 (2005)
- [14] M. V. Gvozdkova and M. E. Zhitomirsky, JETP Lett. **81**, 236 (2005)
- [15] J. T. Chalker, P. C. W. Holdsworth, and E. F. Shender, Phys. Rev. Lett. **68**, 855 (1992)
- [16] M. E. Zhitomirsky, Phys. Rev. B **78**, 094423 (2008)
- [17] D. A. Huse and A. D. Rutenberg, Phys. Rev. B **45**, 7536 (1992)
- [18] C. L. Henley, Phys. Rev. B **80**, 180401 (2009)
- [19] G. Baskaran, S. Mandal, and R. Shankar, Phys. Rev. Lett. **98**, 247201 (2007)

- [20] R. M. Nisbet and I. E. Farquhar, *Physica* **76**, 2, 283-294 (1974)
- [21] W. Kinzel and M. Schick, *Phys. Rev. B* **24**, 324 (1981)
- [22] E. Aksenenko and Y. Shulepov, *J. Phys. A* **17**, 2109 (1984)
- [23] L. Lafuente and J. Cuesta, *J. Chem. Phys.* **119**, 10832 (2003)
- [24] H. C. M. Fernandes, J. J. Arenzon, and Y. Levin, *J. Chem. Phys.* **126**, 114508 (2007)
- [25] X. Feng, H. W. J. Blote, and B. Nienhuis, *Phys. Rev. E* **83**, 061153 (2011)
- [26] K. Ramola, K. Damle, and D. Dhar, in preparation
- [27] A. Bellemans and R. Nigam, *J. Chem. Phys.* **46**, 2922 (1967)
- [28] B. McCoy, *Advanced Statistical Mechanics* (International Series of Monographs on Physics) (Oxford University Press) (2010)

# Publications

## Papers relevant to the thesis work:

- Samarth Chandra, Kabir Ramola, Deepak Dhar, *Classical Heisenberg spins on a hexagonal lattice with Kitaev couplings*, Phys. Rev. E **82**, 031113 (2010)
- Diptiman Sen, R. Shankar, Deepak Dhar, Kabir Ramola, *Spin-1 Kitaev model in one dimension*, Phys. Rev. B **82**, 195435 (2010)
- Kabir Ramola, Deepak Dhar, *High-activity perturbation expansion for the hard square lattice gas*, Phys. Rev. E **86**, 031135 (2012)
- Kabir Ramola, Kedar Damle, Deepak Dhar, *Fluid to Columnar Order Transition in the Hard Square Lattice Gas* (in preparation)

## Other Papers:

- Kabir Ramola, *Fragment Formation in Biased Random Walks*, J. Stat. Mech., P10002 (2008)
- Kedar Damle, Deepak Dhar, Kabir Ramola, *Resonating Valence Bond Wave Functions and Classical Interacting Dimer Models*, Phys. Rev. Lett. **108**, 247216 (2012)



# Chapter 1

## Introduction

Systems that display phase transitions from disordered to long range ordered behaviour when thermodynamic parameters such as the temperature and density are varied are of fundamental importance in the field of Statistical Physics. Phase transitions represent an abrupt change in the macroscopic behaviour of a system. The phases are usually characterised by the existence of an order parameter that acquires a macroscopic value in an ordered phase, and is zero in the disordered phase. The best studied examples of phase transitions are the transitions from a ferromagnetic to a paramagnetic state in magnetic systems, and the melting of solids to a liquid state as the temperature is increased. Experimentally several novel phase transitions have been observed such as the transition of liquids to superfluid states and the insulator-superconductor transition. The onset of order in such systems is characterised by the existence of a critical point, that separates two phases. Systems approaching a critical point exhibit several characteristic features, which are manifest as diverging thermodynamic quantities such as the magnetic susceptibility or compressibility. Systems at criticality display the remarkable property of universality, in which several systems with different microscopic behaviour, display the same critical properties [1].

Simple theoretical models that capture the qualitative features of different phases across a transition are important tools to study critical behaviour. However, although such models are relatively easy to construct, theoretical results are harder to obtain. Simple theories such as the mean-field theory and cluster approximation techniques are usually insufficient to capture the complex nature of the scaling in these systems. In this context, two dimensional systems offer a fertile arena in which models that display non-trivial critical behaviour can be treated analytically. The best studied universality classes arise from the study of models of magnetism and lattice gases. Models that can be exactly solved are particularly interesting as they allow an accurate determination of the singular nature of the free energy of the system near the critical point [2], [3]. Although, very few models are integrable, there exist several models in two dimensions for which theoretical predictions can be made.

This thesis mainly deals with two models, The spin- $S$  Kitaev model, and the hard square lattice gas model. We analyse the spin- $S$  Kitaev model in the limit of large  $S$  where the

spins become classical 3-vector (Heisenberg) spins, and the hard square lattice gas model. We investigate whether in this classical limit the Kitaev model displays order-by-disorder, a phenomenon whereby a system that is disordered at strictly zero temperature acquires a fluctuation induced order at temperatures just above zero. We also analyse properties of a quantum spin-S chain related to the Kitaev model. We show that this model, with an added parameter, displays a quantum phase transition from a phase with a finite energy gap to a gapless phase. We then study the lattice gas of  $2 \times 2$  hard squares on the square lattice, where there is a vacancy-induced sliding instability that makes the crystalline order unstable, but a partial order survives in the form of columnar order where only two of the four possible ordered states mix with each other. We also analyse the nature of the transition from fluid to columnar order as a function of density in this system.

We now introduce a few well studied models that are relevant to the work presented in this thesis.

## 1.1 Spin Models

The magnetic properties of materials arise from the magnetic moments of individual spins in the system. To understand the cooperative nature of magnets at low temperatures, models that have interactions between the various spins at different sites of the system are needed. A simple interacting magnetic system can be modelled as spins at the vertices of a lattice interacting via the Hamiltonian

$$H = - \sum_{(i,j)} J_{ij} \mathbf{S}_i \mathbf{S}_j \quad (1.1)$$

where  $(i, j)$  represents a sum over any two sites on the lattice. The  $\mathbf{S}$  variables represent the spin degrees of freedom in the system, which could be classical vectors or quantum mechanical operators. Different types of interactions yield different magnetic behaviour in the system. There are several well known models that describe magnetic ordering in systems. We describe a few such models below.

The simplest model in this context is the Ising model where at each site, the spin is represented by a  $\mathbb{Z}_2$  variable that can take values  $+1$  or  $-1$ . When we limit ourselves to nearest neighbour interactions, this model can be exactly solved on a square lattice, i.e.- an analytic expression for the free energy of the system in the thermodynamic limit can be found [4], [5]. Exact solutions can also be obtained for all planar periodic two dimensional lattices [6],[7]. This model undergoes a transition from a long range magnetic ordered phase at low temperatures to a disordered phase above the critical temperature  $T_c$ . For the square lattice model the inverse critical temperature is  $\beta_c = \frac{1}{2J} \log(1 + \sqrt{2})$ . The critical exponents of this model define the Ising universality class. Several experimental systems have been observed to be Ising-like near their critical points [8].

### 1.1.1 The XY and Heisenberg Models

The spins in a magnetic system can also be represented as unit vectors that can have any orientation. Such a Hamiltonian is given by

$$H = - \sum_{\langle i,j \rangle} J \vec{S}_i \cdot \vec{S}_j \quad (1.2)$$

where  $\vec{S}_i$  represents a classical unit vector at each site  $i$ ,  $\langle i, j \rangle$  represents the sum over all nearest neighbour spins  $i$  and  $j$ , and the spins are coupled via a scalar product of the two vectors. For models with such continuous degrees of freedom and short range interactions, in two dimensions, the spontaneous magnetization remains zero at all finite temperature [10]. When the spins are classical three dimensional vectors, the model is referred to as the Heisenberg model. When the Hamiltonian involves only coupling in the x- and y- planes we arrive at the XY model [9].

The XY model does not display magnetic order at low temperatures, however the correlations between the spins decays algebraically at long distances, with a power that depends on the temperature of the system. This is sometimes referred to as ‘quasi long range order’ as the system does not possess true long range order, but the spin correlations are not short ranged. Above a critical temperature, the spins become uncorrelated, and the system is in a disordered phase. This is due to the creation of topological defects in the system, called vortices, that proliferate above the critical temperature. This is referred to as the Kosterlitz-Thouless transition, where vortices unbind and destroy the correlations between the spins [11], [12]. A very similar phase transition that is in the same universality class, arises in the problem of surface roughening which is described in Section 1.2.4.

The XY model is often used to model systems that have order parameters that possess symmetries of the same type, like superfluid helium and hexatic liquid crystals. These transitions are not accompanied by a symmetry breaking but by the proliferation of topological defects that leads to a vortex-unbinding transition from the low-temperature phase to the high-temperature disordered phase.

### 1.1.2 The Ashkin-Teller Model

Systems that have competing interactions between the various spins display a very rich phase structure, as, depending on the values of different parameters, the system can display several types of ordering. An interesting model of this type is the Ashkin-Teller-Potts model on the square lattice. This model describes a system with two Ising degrees of freedom at every site with a four spin coupling that has a varying strength of interaction. The Hamiltonian of the isotropic square lattice Ashkin-Teller model is given by

$$H = - \left[ \sum_{\langle i,j \rangle} J_2 \sigma_i \sigma_j + J_2 \tau_i \tau_j + J_4 \sigma_i \sigma_j \tau_i \tau_j \right] \quad (1.3)$$

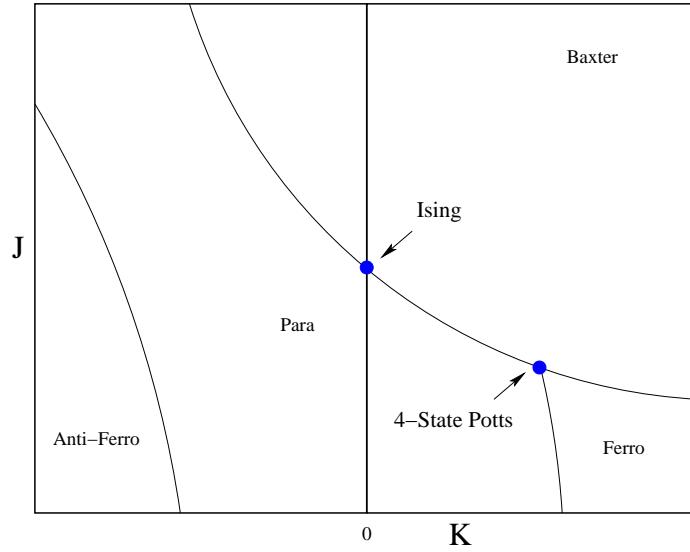


Figure 1.1: The phase diagram of the Ashkin-Teller model representing the different phases as the coupling parameters are varied.

where  $\sigma$  and  $\tau$  represent Ising spins at each site  $i$  of the square lattice. This model has several phases, separated by lines of critical points. The different phases of this model are characterised by the expectation values of the different Ising components [13]. Fig. 1.1 shows the phase diagram for this system for the different values of the coupling. In the case where  $K = \beta J_4$  is large and the individual Ising couplings  $J = \beta J_2$  are zero, the model can be thought of as a single Ising model with variables  $\sigma\tau$  at each site. In this case the expectation value  $\langle\sigma\tau\rangle$  is nonzero, showing ferromagnetic order for large  $K$  (above the Ising critical value  $K^* = \frac{1}{2} \log(1 + \sqrt{2})$ ), and antiferromagnetic order at large negative values of  $K$ . The individual fields remain disordered, i.e.-  $\langle\sigma\rangle = \langle\tau\rangle = 0$ . In the paramagnetic phase  $\langle\sigma\tau\rangle$ ,  $\langle\sigma\rangle$  and  $\langle\tau\rangle$  are all zero. These phases extend above the  $K = 0$  line for a finite value of the coupling  $J$ . The phase in which both  $J$  and  $K$  are large is sometimes referred to as the ‘Baxter Phase’, in this phase  $\langle\sigma\rangle$ ,  $\langle\tau\rangle$  and  $\langle\sigma\tau\rangle$  all acquire a nonzero expectation value. The line separating this phase from the paramagnetic phase is an exactly known critical curve with continuously varying critical exponents which terminates in the four-state Potts point ( $J = K$ ) where it bifurcates. The scaling exponent  $\gamma/\nu$  is equal to  $7/4$  along this entire line.

### 1.1.3 The Kitaev Model

An interesting model that has various competing interactions is the two-dimensional frustrated spin-1/2 model introduced by Kitaev [14]. The Hamiltonian of this system is given by

$$H = J_x \sum_{\langle ij \rangle_x} S_i^x S_j^x + J_y \sum_{\langle ij \rangle_y} S_i^y S_j^y + J_z \sum_{\langle ij \rangle_z} S_i^z S_j^z, \quad (1.4)$$

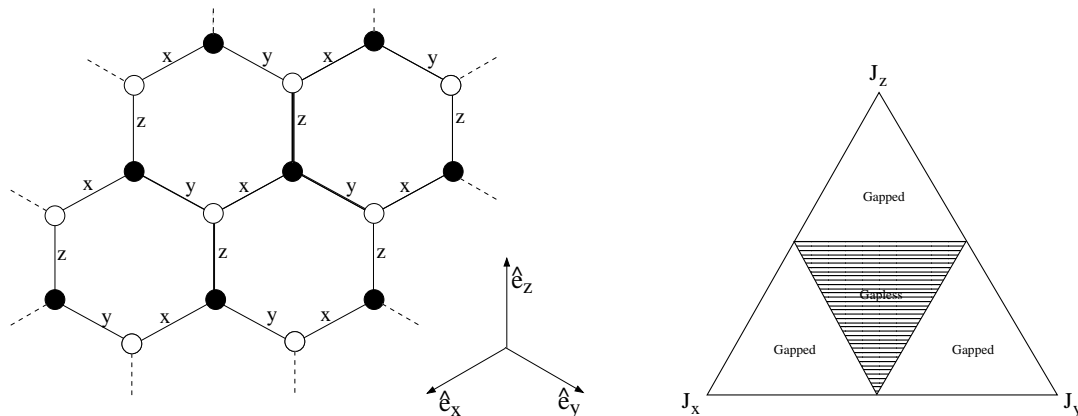


Figure 1.2: (Left) A hexagonal lattice depicting the coupling directions for the spins in the Kitaev model. (Right) The zero temperature phase diagram of the Kitaev model, showing the transition from a gapless to gapped phases as the coupling are varied.

where  $\langle ij \rangle_\alpha$  denote the nearest-neighbour bonds in the  $\alpha^{\text{th}}$  direction ( $\alpha \equiv x, y, z$ ) (Figure. 1.2). The couplings in this model are anisotropic and the Hamiltonian does not possess spin-rotation symmetry. A similar model, called the compass model, although not exactly solvable, was introduced by Kugel and Khomskii many years ago [15] to understand the magnetic properties of transition metal oxides which have orbital degeneracies.

In the spin-1/2 Kitaev model, a set of mutually commuting  $\mathbb{Z}_2$  valued constants of motion can be constructed on each hexagon of the lattice. This leads to a remarkable simplification in the structure of the model, and in fact this model can be exactly solved. This model has several fascinating properties which have been studied in great detail [16, 17, 18, 19, 20, 21, 22]. For instance, the model and its variants constitute the only known class of spin models in two dimensions or more dimensions that is fully integrable, being reducible to a system of non-interacting Majorana fermions. The Kitaev model has topological excitations, and their robustness with respect to noise makes it an interesting candidate for applications in quantum computation [14, 23, 24, 25]. Topological order implies the existence of invariants which, for topological reasons, are robust against a large class of perturbations. Such systems are often associated with a novel structure of the ground state and low-lying excitations.

The ground state of this model has recently been conjectured to be a spin liquid at the point  $J_x = J_y = J_z$  [26]. At zero temperature, the system can be in several possible phases, with finite correlation length and excitations with a finite energy gap, or one with long-range correlations, depending on the ratios of the coupling constants in different directions [16, 27]. As the couplings are varied, quantum phase transitions between the different phases are observed (Fig. 1.2). A quantum phase transition describes an abrupt change in the ground state of a many-body system due to its quantum fluctuations at strictly zero temperature [28].

Recently physical realizations of the spin-1/2 Kitaev model have been proposed in optical

lattice systems [29] and in quantum circuits [30].

#### 1.1.4 Order-by-Disorder

Systems that possess competing interactions do not have a unique ground state, because not all interactions can be satisfied at the same time. The word ‘frustration’ is sometimes used to refer to such systems with competing interactions that have a large number of states with energy near the minimum energy. Classical frustrated systems with a large degeneracy of ground states are interesting problems of study. In some cases, the system at  $T = 0$  is disordered (i.e.- a simple average over all the ground states has no order), whereas in the limit  $T \rightarrow 0$  some states acquire a higher weight over others because of a different density of nearby states and the system may exhibit signatures of order. This phenomenon is termed thermal “order-by-disorder” [31, 32]. In the  $T \rightarrow 0$  limit, ordered states have a larger entropy as compared to disordered states. Order-by-disorder in classical systems has been studied in the context of magnetic systems with frustration, such as spin systems with nearest neighbour antiferromagnetic interactions on different lattices. Entropy driven order in frustrated systems has been studied extensively for models on lattices such as the pyrochlore, diamond and face-centered cubic lattices [33],[34].

The extensive classical ground state degeneracy can also be lifted due to quantum fluctuations in the corresponding quantum spin model at  $T = 0$ , a phenomenon termed as quantum order-by-disorder. Quantum fluctuations typically remove this degeneracy with a linear superposition of ground states having a lower energy than the rest. In approximate calculations this is often done by looking at the density of low lying excited states (e.g. spin waves) about a classical ground state.

## 1.2 Lattice Gas Models

Real gases display a complex and rich phase diagram. To model even the behaviour of a large collection of simple molecules such as hydrogen represents a theoretical challenge. Although the ideal gas model, in which particles interact purely via elastic collisions yields qualitatively accurate results at low densities and high temperature, at high densities real gases display significant deviations from ideal behaviour. Lattice gas models, in which particles are constrained to be on the sites of a lattice, serve as the simplest models of complex physical systems such as simple fluids, structural glasses and granular materials. Lattice gas models provide an accurate description of physical systems such as gases adsorbed on substrates (e.g. adlayers of noble gases such as Xenon on graphite).

### 1.2.1 Hard-Core Lattice Gases

Real gases interact via complicated two body potentials that are repulsive at short distances and attractive at moderate distances. Since melting is dominated by strong short ranged

repulsive forces, a lattice gas in which particles interact exclusively through an extended hard core, where a particle on one site prevents the neighbouring sites from being occupied, is a good first approximation. In these systems temperature plays no role since the interaction energy is infinite inside the exclusion region and vanishes outside.

The Ising model can also be represented as a model of a lattice gas, where the excitations above the state with all spins  $+1$  can be thought of as particles on the lattice [35]. These particles have a finite energy of interaction between nearest neighbours, and two particles cannot sit directly on top of each other. This model represents a hard core lattice gas with nearest neighbour interaction.

When the interaction energy is set to infinity, the phase transitions in these systems as a function of density are the result of geometrical effects of excluded volume interactions. These have been called geometrical phase transitions, the best studied of which are the percolation transition [36] and phase transitions in assemblies of hard spheres [37]. Many systems with different shapes of particles have been studied in the literature, for example squares [38], rods [39], triangles [40] and L-shaped molecules [41]. The computation of the partition function of particles with finite exclusion volumes on a lattice remains an outstanding problem [42] [2]. The model of hard hexagons on the triangular lattice and related models are the only known exactly soluble systems of this kind [43], [44]. The difficulty and the scarcity of exact solutions have led to the development of various approximate theories to deal with more complex interaction potentials. Examples of these are the high and low activity expansions [45].

### 1.2.2 The Hard Square Lattice Gas

As the range of exclusion is varied, the universality class of the transition from the low density fluid state to a high density ordered state also changes. As we have seen, the nearest neighbour exclusion lattice gas belongs to the Ising universality class. The identification of the universality classes of gases with different exclusion radii is an interesting question.

In this thesis we study the lattice gas of particles with exclusion up to the next nearest neighbour on the square lattice. Equivalently, each particle is a  $2 \times 2$  square that occupies 4 elementary plaquettes of the lattice. This is known as the hard square lattice gas. This model has been the subject of many studies in the past. Unlike the nearest-neighbour exclusion lattice gas, this model does not have a sublattice ordered state at high densities [46, 47]. Transfer matrix techniques indicate the existence of a phase transition in this model [48, 49, 50, 51]. Variational, density functional methods and virial expansions have also been used to study this problem [49, 52, 53]. These studies indicate that at high densities the system is not sublattice ordered but exhibits “columnar order” wherein one of the even (odd) rows or columns is preferentially occupied over the other. However, there is as yet no rigorous proof of the existence of this type of order in this system. In this context it is worthwhile to develop exact series expansions and try to prove their convergence in this phase.

The nature of the transition from the low density disordered state to the columnar ordered state at high densities has been the subject of several studies. The hard square lattice gas also arises as a limiting case of spin models with interactions up to the second nearest neighbour on the square lattice [54, 55, 56]. In the Landau theory paradigm, the four columnar ordered states in this system give rise to an XY model with four fold anisotropy [57]. Such models are known to display non-universal behaviour with critical exponents that are governed by marginal operators, and naturally fall into the class of Ashkin-Teller-Potts models that exhibit such behaviour [58, 59, 60]. However, the critical exponents of this model have been hard to pin down from Monte Carlo simulations on small system sizes [51]. Recent Monte Carlo evidence suggests that the transition from fluid to columnar order in this system is of second order, with exponents very close to the two dimensional Ising model. In fact, the transition has been identified to be the Ising point in some studies [61], however, this does not seem to be the case [56, 62].

### 1.2.3 Columnar Order

There are several systems in which particles do not order into a periodic spatial pattern, but still display a long ranged ordered state. In some cases these particles are ordered in a particular orientation, such as nematic and smectic phases in liquid crystals [63]. A particularly interesting type of order in this category is columnar order, where the particles align along one dimensional lines that have weak correlations between them. There are several theoretical systems that display such ordered behaviour such as dimers with attractive interactions between them [64],[65] and the hard square lattice gas.

There have been only a few theoretical studies of the columnar ordered state in the hard square lattice gas so far, and the present understanding is not very satisfactory. Correlations in the columnar ordered state are hard to capture using mean-field like descriptions. For example, all the well-known approximation schemes like the mean-field theory and cluster variational approximations underestimate the value of the critical point  $z_c$  for the hard squares problem by an order of magnitude.

In many cases, the high density states exhibit crystalline order where one sublattice is preferentially occupied (for example hard hexagons on the triangular lattice and the nearest-neighbour-exclusion lattice gas on the square lattice). In such cases it is straightforward to develop high activity expansions for thermodynamic quantities [45]. In the case of the hard square lattice gas, the standard high density expansion in powers of  $1/z$  breaks down, and it was realised quite early that the leading order correction to the high activity expansion is of order  $1/\sqrt{z}$  [66], where  $z$  is the fugacity associated with each particle, but a systematic expansion has not been developed so far.

### 1.2.4 Solid-on-Solid Model and Surface Roughening

The condensation of fluids into crystalline structures is characterised by the coexistence of the two phases separated by an interface that grows as the system condenses. The properties of the interface between the two phases can be described well by a solid-on-solid model. The crystallization process occurs in steps in which layers are added to the growing surface. The heights  $\{h_i\}$  of the number of particles deposited at different lattice sites is represented by the height of the stack at each lattice site. The interaction between the different deposited items is of the type

$$H_{SOS} = \sum_{\langle i,j \rangle} V(h_i - h_j) \quad (1.5)$$

where  $V$  is a function of the difference in heights between the nearest neighbour columns. The energy of the surface is lowest when it is flat. The solid-on-solid model has a natural description in terms of the XY universality class, and can in fact be exactly mapped to the XY model via a duality transformation [67]. At low temperatures, the system is in a periodic state, where the surface is flat. At high temperatures, the variance in the difference of the height variables grows logarithmically with distance and the surface is said to be ‘rough’. This is sometimes referred to as the surface roughening transition.

## 1.3 Outline

This thesis is organised as follows. In Chapter 2 we analyse the low temperature properties of a system of classical Heisenberg  $O(3)$  spins on a hexagonal lattice interacting via the Kitaev Hamiltonian. We show that for a lattice of  $2N$  sites with periodic boundary conditions, the ground states form an  $(N + 1)$  dimensional manifold. We then map the ensemble of ground states onto a solid-on-solid model with continuously variable heights and nearest neighbour interactions. We see that the spin model at zero temperature maps onto the solid-on-solid model that is in its rough phase. We argue that the bond-energy bond-energy correlations at distance  $R$  decay as  $\frac{1}{R^2}$  at zero temperature. We find that as the temperature  $T$  tends to zero, all ground states have equal weight, and there is no order-by-disorder in this model. We perform Monte Carlo simulations to verify our predictions. We then discuss the quantum spin- $S$  Kitaev model for large  $S$ , and obtain a lower bound on the ground state energy of the quantum model.

In Chapter 3 we study a one-dimensional version of the Kitaev model on a ring of size  $N$ , in which there is a spin  $S > 1/2$  at each site. We find that cases where  $S$  is integer and half-odd-integer are qualitatively different. We show that there is a  $\mathbb{Z}_2$  valued conserved quantity for each bond of the system. For integer  $S$ , the Hilbert space can be decomposed into  $2^N$  sectors, of unequal sizes. The number of states in most of the sectors grows as  $d^N$ , where  $d$  depends on the sector. The largest sector contains the ground state, and for this sector, for  $S = 1$ , we show that  $d = (\sqrt{5} + 1)/2$ . In the ground state sector, the system

can be mapped to a spin-1/2 model. We develop variational wave functions to study the lowest energy states in the ground state and other sectors. The first excited state of the system is the lowest energy state of a different sector and we estimate its excitation energy. We consider a more general Hamiltonian, adding a term  $\lambda \sum_i W_i$ , and show that this has gapless excitations in the range  $\lambda_1^c \leq \lambda \leq \lambda_2^c$ . We use the variational wave functions to study how the ground state energy and the defect density vary near the two critical points  $\lambda_1^c$  and  $\lambda_2^c$ .

In Chapter 4 we study the lattice gas model of particles on a square lattice with nearest and next-nearest-neighbour exclusion (hard squares). In order to understand the nature of the columnar ordered phase in this model, we develop a high activity perturbation expansion for the free energy per site about a state with perfect columnar order. This is a singular perturbation series in powers of  $1/\sqrt{z}$ , where  $z$  is the fugacity associated with each particle. We show that the different terms of the series can be regrouped to get a Mayer-like series for a polydisperse system of interacting vertical rods in which the  $n$ -th term is of order  $z^{-(n+1)/2}$ . We sum this series to get the exact expansion to order  $1/z^{3/2}$ . We then analyse the nature of the transition from the columnar ordered phase at high density to the fluid phase at low density. Using a simple coarse grained picture, we argue that the critical properties of the model are that of a more general Ashkin-Teller model. We find a mapping of the local densities of the hard square lattice gas to the Ising energy densities in the corresponding Ashkin-Teller model. We then use Monte Carlo simulations to test our predictions. We locate the critical point of the system as  $z_c = 97.5 \pm 0.5$ . We also study the correlations between various quantities in the system in order to precisely locate the position of the transition on the Ashkin-Teller critical line.

# References

- [1] J. Cardy, *Scaling and Renormalization in Statistical Physics* (Cambridge University Press)(1996).
- [2] R. J. Baxter, *Exactly Solved Models in Statistical Mechanics* (Academic, London)(1982)
- [3] B. McCoy, *Advanced Statistical Mechanics* (International Series of Monographs on Physics) (Oxford University Press) (2010)
- [4] L. Onsager, Phys. Rev. **65** 117-149 (1944).
- [5] T. D. Schultz, D. C. Mattis, and E. H. Lieb, Rev. Mod. Phys. **36**, 856871 (1964).
- [6] G. H. Wannier, Phys. Rev. **79**, 357364 (1950).
- [7] P. W. Kasteleyn, J. Math. Phys., **4**, 287 (1963)
- [8] W. P. Wolf, Braz. J. Phys., **30**, 4 (2000).
- [9] There are two spin systems known by the name XY model in the literature. In both, the nearest-neighbour spin Hamiltonian involves only coupling in the x-y plane. In one, the spins are three-dimensional vectors (with no coupling of the z components) whereas in the other, spins are two-dimensional. We deal with the latter, also known as the “rigid rotor model”.
- [10] N. D. Mermin and H. Wagner, Phys. Rev. Lett. **17**, 11331136 (1966).
- [11] J. M. Kosterlitz and D. J. Thouless, J. Phys. C: Solid State Phys. **6** 1181 (1973).
- [12] V. Berezinskii Zh. Eksp. Teor. Fiz. **59**, 907 (1970); Sov. Phys., JETP **32**, 493 (1971).
- [13] R. V. Ditzian, J. R. Banavar, G. S. Grest, and L. P. Kadanoff, Phys. Rev. B **22**, 2542 (1980).
- [14] A. Kitaev, Ann. Phys. **321**, 2 (2006).
- [15] K. I. Kugel and D. I. Khomskii, Sov. Phys. Usp. **25**, 231 (1982).
- [16] X. Y. Feng, G. M. Zhang, and T. Xiang, Phys. Rev. Lett. **98**, 087204 (2007).

- 
- [17] G. Baskaran, S. Mandal, and R. Shankar, Phys. Rev. Lett. **98**, 247201 (2007).
- [18] D.-H. Lee, G.-M. Zhang, and T. Xiang, Phys. Rev. Lett. **99**, 196805 (2007).
- [19] H.-D. Chen and Z. Nussinov, J. Phys. A **41**, 075001 (2008).
- [20] Z. Nussinov and G. Ortiz, Phys. Rev. **B77**, 064302 (2008).
- [21] K. P. Schmidt, S. Dusuel, and J. Vidal, Phys. Rev. Lett. **100**, 057208 (2008).
- [22] K. Sengupta, D. Sen, and S. Mondal, Phys. Rev. Lett. **100**, 077204 (2008); S. Mondal, D. Sen, and K. Sengupta, Phys. Rev. **B78**, 045101 (2008).
- [23] M. A. Levin and X.-G. Wen, Phys. Rev. B **71**, 045110 (2005).
- [24] S. Das Sarma, M. Freedman, and C. Nayak, Physics Today **7**, 32 (2006).
- [25] C. Nayak, S. H. Simon, A. Stern, M. Freedman, and S. Das Sarma, Rev. Mod. Phys. **80**, 1083 (2008).
- [26] Hong Yao and Steven A. Kivelson, Phys. Rev. Lett. **99**, 247203 (2007).
- [27] V. Lahtinen, J. K. Pachos, Phys. Rev. B **81**, 245132 (2010).
- [28] S. Sachdev, *Quantum Phase Transitions* (Cambridge University Press) (1999).
- [29] L.-M. Duan, E. Demler, and M. D. Lukin, Phys. Rev. Lett. **91**, 090402 (2003).
- [30] J. Q. You, X.-F. Shi, X. Hu and F. Nori, Phys. Rev. B **81**, 014505 (2010).
- [31] J. Villain, R. Bidaux, J. P. Carton, and R. J. Conte, J. Phys. (Paris) **41**, 1263 (1980).
- [32] R. Moessner and J. T. Chalker, Phys. Rev. B **58**, 12049 (1998).
- [33] C. L. Henley, Phys. Rev. B **71**, 014424 (2005).
- [34] M. V. Gvozdkova and M. E. Zhitomirsky, JETP Lett. **81**, 236 (2005).
- [35] T. D. Lee and C. N. Yang, Phys. Rev. **87**, 410419 (1952).
- [36] A. Aharony and D. Stauffer, *Introduction to Percolation Theory* (Taylor and Francis, London, 1994). Percolation does not have any interactions except on-site repulsion, one studies the geometrical properties of connected clusters of particles.
- [37] B.J. Alder and T.E. Wainwright, Phys. Rev. **127**, 359 (1962).
- [38] P. A. Pearce and K. A. Seaton, J. Stat. Phys. **53**, 1061 (1988).
- [39] A. Ghosh and D. Dhar, Euro. Phys. Lett. **78**, 20003 (2007).
- [40] A. Verberkmoes and B. Nienhuis, Phys. Rev. Lett. **83**, 3986 (1999).

- 
- [41] B. C. Barnes, D. W. Siderius and L. D. Gelb, *Langmuir* **25**, 6702 (2009).
- [42] L. K. Runnels and L. L. Combs, *J. Chem. Phys.* **45**, 2482 (1966).
- [43] R. J. Baxter, *J. Phys. A*, **13**, L61 (1980).
- [44] J. Bouttier, P. Di Francesco and E. Guitter, *J. Phys. A: Math. Gen.* **35** 3821 (2002).
- [45] D. S. Gaunt and M. E. Fisher, *J. Chem. Phys.* **43**, 2840 (1965).
- [46] R. L. Dobrushin, *Theor. Prob. Appl.* **10** No 2 (1965).
- [47] O. J. Heilmann, *Commun. Math. Phys.* **36** 91 (1974).
- [48] A. Bellemans and R. Nigam, *Phys. Rev. Lett.* **16**, 23 (1966).
- [49] F. H. Ree and D. A. Chestnut, *Phys. Rev. Lett.* **18**, 5 (1967).
- [50] R. M. Nisbet and I. E. Farquhar, *Physica* **76**, 2, 283-294 (1974).
- [51] W. Kinzel and M. Schick, *Phys. Rev. B* **24**, 324 (1981).
- [52] E. Aksenenko and Y. Shulepov, *J. Phys. A* **17**, 2109 (1984).
- [53] L. Lafuente and J. Cuesta, *J. Chem. Phys.* **119**, 10832 (2003).
- [54] K. Binder and D. P. Landau, *Phys. Rev. B* **21**, 1941 (1980).
- [55] J. Amar, K. Kaski, and J. D. Gunton, *Phys. Rev. B* **29**, 1462 (1984).
- [56] M. Zhitomirsky and H. Tsunetsugu, *Phys. Rev. B* **75**, 224416 (2007).
- [57] E. Domany, M. Schick, J. S. Walker, and R. B. Griffiths, *Phys. Rev. B* **18**, 2209 (1978).
- [58] L. P. Kadanoff, *Phys. Rev. Lett.* **39**, 903 (1977).
- [59] J. V. José, L. P. Kadanoff, S. K. Kirkpatrick, and D. R. Nelson, *Phys. Rev. B* **16**, 1217 (1977).
- [60] L. P. Kadanoff, *Ann. Phys. (N.Y.)* **120**, 39 (1979).
- [61] H. C. M. Fernandes, J. J. Arenzon and Y. Levin, *J. Chem. Phys.* **126**, 114508 (2007).
- [62] X. Feng, H. W. J. Blote and B. Nienhuis, *Phys. Rev. E* **83**, 061153 (2011).
- [63] P. M. Chaikin, and T. C. Lubensky, *Principles of Condensed Matter Physics* (Cambridge University Press) (1995).
- [64] F. Alet, Y. Ikhlef, J. L. Jacobsen, G. Misguich, and V. Pasquier, *Phys. Rev. E* **74**, 041124 (2006).
- [65] S. Papanikolaou, E. Luijten, and E. Fradkin, *Phys. Rev. B* **76**, 134514 (2007).

[66] A. Bellemans and R. Nigam, *J. Chem. Phys.* **46**, 2922 (1967).

[67] H. J. F. Knops, *Phys. Rev. Lett.* **39**, 766769 (1977).

## Chapter 2

# The Kitaev Model with Classical Spins

### 2.1 Introduction

In this chapter, we analyse the low temperature properties of a system of classical Heisenberg spins on a hexagonal lattice with Kitaev couplings. The simple nature of the Hamiltonian allows us to perform many calculations that are not possible in other, more complex spin models.

We investigate whether this model displays order-by-disorder, wherein the thermal fluctuations at low temperatures induce a long range order in the system. We are able to parametrise the ground states and excitations of the system exactly and we show that the ground states for a lattice of  $2N$  sites with periodic boundary conditions form an  $(N + 1)$  dimensional manifold. Our parametrisation allows us to take the temperature  $T \rightarrow 0$  limit of the partition function exactly and prove that there is no incipient long range order as the temperature approaches zero. For  $T$  tending to zero we find that all ground states have equal weight, and there is no order-by-disorder in this model. We show that at zero temperature, the ensemble of ground states is equivalent to that of a solid-on-solid model with continuously variable heights and nearest neighbour interactions at a finite temperature. We argue that the bond-energy bond-energy correlations at distance  $R$  decay as  $\frac{1}{R^2}$  at zero temperature. This is verified by Monte Carlo simulations. We also discuss the relation to the quantum spin- $S$  Kitaev model and obtain a lower bound on the ground state energy of the quantum model.

In a recent interesting paper, Baskaran *et al.* studied a generalisation of this model with spin- $S$  at each site and identified mutually commuting  $\mathbb{Z}_2$  variables that are constants of motion for arbitrary  $S$  [1]. For large  $S$ , the spins can be approximated as classical  $O(3)$  vector spins. Baskaran *et al.* showed that the classical ground state of the model has a large degeneracy. They argued that though a naive averaging over these ground state configurations would suggest that the system is disordered at zero temperature, for large

$S$ , the quantum fluctuations of spins have lower energy for a subset of the classical ground states. These states acquire a larger weight in the quantum mechanical ground state, and the quantum model shows long-range order in the ground state, an example of quantum order-by-disorder.

The finite-temperature fluctuations in the classical model behave qualitatively like the zero-point fluctuations in the quantum model, and it is interesting to ask if temperature fluctuations can induce order-by-disorder in the model of classical Heisenberg spins with Kitaev couplings, just as the quantum fluctuations are expected to in the large- $S$  quantum model. We see that there is a qualitative difference between the classical and quantum mechanisms of order-by-disorder. For the classical Kitaev model, the contribution of nearby states to the restricted partition function in the limit of very small temperature, with states summed only over the neighbourhood of a given classical ground state, is exactly the same for almost all ground states.

## 2.2 The Model

We consider classical Heisenberg spins on a hexagonal lattice. We consider a finite lattice, with periodic boundary conditions. There are  $L$  hexagons in each row, and  $M$  rows of hexagons ( $L$  and  $M$  both assumed even). The total number of hexagons is  $N = LM$ , and the number of sites is  $2N$ . The bonds of the lattice are divided into three classes,  $X, Y$  and  $Z$ , according to their orientation (Fig. 2.1). The hexagonal lattice consists of two sublattices denoted by  $A$  and  $B$ . We label sites in the  $A$  sublattice by  $a(l, m)$  and the corresponding  $B$  sublattice site connected to it via a  $Z$  bond by  $b(l, m)$ . We define three bond vectors  $e_x, e_y, e_z$  as the vectors from any  $A$ -site to its three neighbours via the  $X, Y$  and  $Z$  bonds respectively (Fig. 2.1). Thus we have  $a(l, m) + e_x = b(l, m - 1)$ ,  $a(l, m) + e_y = b(l + 1, m - 1)$  and  $a(l, m) + e_z = b(l, m)$ . We define the hexagonal plaquette  $(l, m)$  to be the hexagon whose topmost point is  $a(l, m)$ . A bond will be specified by the  $(l, m)$  coordinate of its  $A$ -lattice end point and its class  $X, Y$  or  $Z$ . For instance,  $(a(l, m); x) \equiv (l, m; x)$  is an  $X$ -bond with  $a(l, m)$  at one of its ends. The periodic boundary conditions are implemented by making  $a(l, m) = a(l + L, m) = a(l - \frac{M}{2}, m + M)$ .

At each lattice site  $i$  there is a three dimensional vector spin  $\vec{S}_i = (S_i^x, S_i^y, S_i^z)$  of unit magnitude. Thus  $S_i^{x^2} + S_i^{y^2} + S_i^{z^2} = 1$  at every site. The Hamiltonian of the system is given by

$$H = -J \sum_{a \in A} [S_a^x S_{a+e_x}^x + S_a^y S_{a+e_y}^y + S_a^z S_{a+e_z}^z] \quad (2.1)$$

As the hexagonal lattice is bipartite, for classical spins, without loss of generality we assume  $J > 0$ . The Hamiltonian does not have rotational symmetry in the spin space, but it has a local symmetry : for any bond  $(l, m; \alpha)$ , the Hamiltonian is invariant under the transformation  $S_{a(l, m)}^\alpha \rightarrow -S_{a(l, m)}^\alpha, S_{a(l, m)+e_\alpha}^\alpha \rightarrow -S_{a(l, m)+e_\alpha}^\alpha$ .

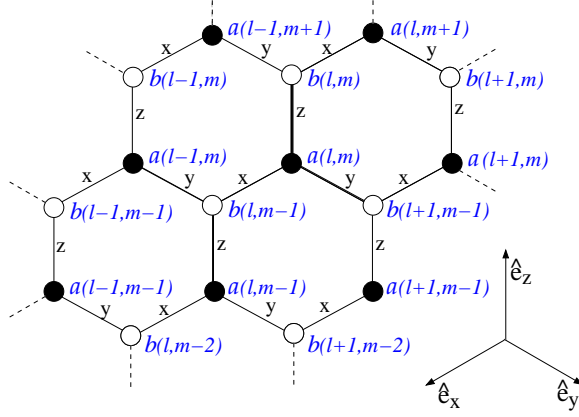


Figure 2.1: A hexagonal lattice depicting the labelling scheme for sites, and the x, y and z bond classes. Sites in the  $A$ - and  $B$ - sublattices are denoted by filled and open circles respectively.

## 2.3 The Ground States

We begin by obtaining the ground states of this system. We express the Hamiltonian  $H$  as a sum of individual Hamiltonians at every  $B$ -site

$$H = \sum_{(l,m)} H_{b(l,m)}, \quad (2.2)$$

where  $H_{b(l,m)}$  is a Hamiltonian containing only the couplings of the  $B$ -sublattice site  $b(l, m)$ . We have

$$H_{b(l,m)} = -J \left( S_{a(l,m+1)}^x S_{b(l,m)}^x + S_{a(l-1,m+1)}^y S_{b(l,m)}^y + S_{a(l,m)}^z S_{b(l,m)}^z \right).$$

Each  $B$ -sublattice spin  $\vec{S}_b$  experiences a field  $\vec{F} = \left( S_{a(l,m+1)}^x, S_{a(l-1,m+1)}^y, S_{a(l,m)}^z \right)$  due to the surrounding  $A$ -sites. The Hamiltonian for every  $B$ -site is thus  $H_b = -J \vec{S}_b \cdot \vec{F}$ . This energy is minimised when  $\vec{S}_b$  is parallel to the vector  $\vec{F}$ , with the minimum energy equal to  $-J \sqrt{S_{b-e_x}^x{}^2 + S_{b-e_y}^y{}^2 + S_{b-e_z}^z{}^2}$ .

Now, given a specified configuration of spins on the  $A$ -sublattice  $\{\vec{S}_a\}$  we can obtain  $E_{min}(\{\vec{S}_a\})$ , the minimum value of  $H$  for the configuration  $\{\vec{S}_a\}$ , by minimising over the  $B$ -spins as above (since the  $B$ -spins are uncoupled in the Hamiltonian, each minimisation can be performed independently). We thus obtain the minimum energy for a given configurations of  $A$ -spins. We have

$$E_{min}(\{\vec{S}_a\}) = -J \sum_{(l,m)} \sqrt{S_{a(l,m+1)}^x{}^2 + S_{a(l-1,m+1)}^y{}^2 + S_{a(l,m)}^z{}^2}.$$

Now,  $\sqrt{x}$  is a convex function of  $x$  for all real positive  $x$ . We use the convexity inequality

$$\sum_{i=1}^N \sqrt{x_i} \leq N \sqrt{\frac{\sum_{i=1}^N x_i}{N}}, \quad (2.3)$$

with equality holding when all the  $x_i$  are equal. Using this identity for the sum of the square roots above we immediately get

$$E_{min}(\{\vec{S}_a\}) \geq -JN. \quad (2.4)$$

Here we have used the fact that the sum of the spin squared components of all the  $A$ -spins is equal to  $N$ , the number of  $A$ -sites. It is easy to see that there exist spin states of the Hamiltonian for which the above energy is actually attained, for instance, when all spins are aligned along the  $z$  direction. Thus, the ground state energy is  $-JN$ . In fact Baskaran *et al.* studied such states terming them ‘‘Cartesian States’’, but no proof that these were the true ground states was given.

In the inequality (2.3), the equality sign holds when all the terms within the square root are equal. Thus the ground state condition is

$$S_{a(l,m+1)}^x{}^2 + S_{a(l-1,m+1)}^y{}^2 + S_{a(l,m)}^z{}^2 = 1, \text{ for each } b \in B. \quad (2.5)$$

The above conditions are necessary and sufficient to attain the ground state. For each given configuration of  $A$ -site spins  $\{\vec{S}_a\}$ , there is a unique configuration of  $B$ -spins  $\{\vec{S}_b\}$  that minimises the Hamiltonian. The components of each  $B$ -spin are  $S_b^\alpha = S_{b-e_\alpha}^\alpha$ .

## 2.4 Effective Hamiltonian

We next derive an effective Hamiltonian for the model by integrating out the contributions from the  $B$ -sublattice sites. The partition function of the system at finite temperature  $Z[\beta]$  is given by

$$Z[\beta] = \int \prod_s \left( \frac{d\vec{S}_s}{4\pi} \right) \exp[-\beta H] \quad (2.6)$$

where  $\beta^{-1} = T$ . The index  $s$  runs over all sites of the lattice. The integral over each  $B$ -site is of the form  $W_{l,m} = \int d\vec{S}_{b(l,m)} \exp[-\beta \vec{S}_{b(l,m)} \cdot \vec{F}]$  where  $\vec{F} = S_{a(l,m+1)} \hat{i} + S_{a(l-1,m+1)} \hat{j} + S_{a(l,m)} \hat{k}$ . This can in turn be evaluated as

$$W_{l,m} = \frac{1}{2} \int_{-1}^1 d(\cos \theta) \exp \left( -\beta \cos \theta \sqrt{S_{a(l,m+1)}^x{}^2 + S_{a(l-1,m+1)}^y{}^2 + S_{a(l,m)}^z{}^2} \right),$$

where  $\theta$  is the angle between the vector  $\vec{S}_{b(l,m)}$  and  $\vec{F}$ . This immediately yields

$$W_{l,m} = \frac{\sinh\left(\beta\sqrt{S_{a(l,m+1)}^x{}^2 + S_{a(l-1,m+1)}^y{}^2 + S_{a(l,m)}^z{}^2}\right)}{\beta\sqrt{S_{a(l,m+1)}^x{}^2 + S_{a(l-1,m+1)}^y{}^2 + S_{a(l,m)}^z{}^2}}. \quad (2.7)$$

Therefore

$$Z[\beta] = \int \prod_{(l,m)} \frac{d\vec{S}_{a(l,m)}}{4\pi} \prod_{(l,m)} W_{l,m}. \quad (2.8)$$

We thus obtain the effective Hamiltonian for the spins on the  $A$ -sublattice alone as

$$H_{eff}(\{\vec{S}_a\}, \beta) = -\frac{1}{\beta} \sum_{(l,m)} F\left(\beta\sqrt{S_{a(l,m+1)}^x{}^2 + S_{a(l-1,m+1)}^y{}^2 + S_{a(l,m)}^z{}^2}\right), \quad (2.9)$$

where

$$F(x) = \log\left(\frac{\sinh(x)}{x}\right). \quad (2.10)$$

We note that the temperature of the Kitaev Hamiltonian enters as a parameter in  $H_{eff}$  in a nontrivial manner.

## 2.5 Two Dimensional Electrostatics

In this section we map the model of  $A$ -spins interacting via an effective Hamiltonian onto that of a two dimensional electrostatics problem with continuously variable real valued charges at every  $B$ -site. For a given configuration of  $A$ -spins  $\{S_a^\alpha\}$ , to each bond  $(l, m; \alpha)$  of the lattice, we assign a vector  $\epsilon(l, m; \alpha)\vec{e}_\alpha$ , with  $\epsilon(l, m; \alpha)$  given by

$$\epsilon(l, m; \alpha) = S_{a(l,m)}^\alpha{}^2 - \frac{1}{3}. \quad (2.11)$$

We define the discrete divergence of the  $\epsilon$ -field on the sites of the lattice as the sum of the  $\epsilon$ 's on the bonds attached to the site, we have

$$\nabla \cdot \epsilon \equiv \sum_{\alpha} \epsilon(a(l, m); \alpha) \text{ at site } a(l, m), \quad (2.12)$$

$$\equiv \sum_{\alpha} \epsilon(b(l, m) - e_\alpha; \alpha) \text{ at site } b(l, m). \quad (2.13)$$

Clearly, the divergence of the field  $\epsilon$  at any site on the  $A$ -sublattice is 0. The flux of the  $\epsilon$  field out of any polygon on the dual lattice is therefore zero. In addition, from Eq. (2.5)

we see that *for ground state configurations* even for bonds meeting at any site,  $b \in B$ , we have

$$\sum_{\alpha} \epsilon(b(l, m) - e_{\alpha}; \alpha) = 0, \text{ for all sites } b \in B. \quad (2.14)$$

We thus have a divergence-free vector field living on the bonds of the lattice. This can be thought of as an electric field configuration with no net charges present on the lattice sites. For non-ground state configurations, the sum of  $\epsilon$  variables at each  $B$ -site is no longer zero, and possesses a finite divergence. We parametrise this deviation using a real valued charge variable  $Q$  placed on the  $B$ -sublattice sites, defined as

$$Q_{b(l, m)} = - \sum_{\alpha} \epsilon(b(l, m) - e_{\alpha}; \alpha). \quad (2.15)$$

There are no charges on the  $A$ -sites and we define  $Q_{a(l, m)} = 0$ , for all sites  $a(l, m)$ . Given the values of these charges, we can construct the corresponding electrostatic potential field  $\phi$  defined at all sites  $s$  of the lattice such that

$$\nabla^2 \phi(s) = -Q_s; \text{ for all sites } s. \quad (2.16)$$

Here  $\nabla^2$  is the discrete laplacian on the lattice, and the above equation is just the discrete Poisson equation on the lattice. These equations can be solved explicitly and the potential  $\phi(s)$  can be determined completely, up to an overall additive constant, so long as the total charge in the system is zero. Explicitly, we have

$$\phi(s) = \sum_{s'} G(s, s') Q_{s'}, \quad (2.17)$$

where  $G(s, s')$  is the lattice Green's function. Then, as  $\nabla^2 \phi(s) = -Q_s = -\nabla \cdot \epsilon(s)$ , we see that  $\epsilon + \nabla \phi$  has no divergence and can be expressed in terms of the curl of a new scalar field  $\{f\}$ . We define the height field  $f(l, m) \equiv f_{l, m}$  attached to the hexagonal plaquettes of the lattice (as shown in Fig. 2.2) such that the difference in the  $f$ -field between two neighbouring plaquettes is equal to the value of  $\epsilon + \nabla \phi$  along the shared bond. This satisfies the divergence-free condition for the field  $\epsilon + \nabla \phi$ . Let  $s$  be any site on the  $A$ -sublattice with its neighbours as sites  $s + e_x, s + e_y, s + e_z$ . We label the three hexagons to which  $s$  belongs as  $h_1, h_2$  and  $h_3$  (Fig. 2.2).

If the site  $s \equiv a(l, m)$ , then  $h_1$  will have coordinates  $(l - 1, m + 1)$ , and similarly for the other hexagons. Then, for all sites  $s$ , the  $f$ -field is defined by

$$\begin{aligned} \epsilon(s, x) &= \phi(s) - \phi(s + e_x) + f(h_1) - f(h_2) \\ \epsilon(s, y) &= \phi(s) - \phi(s + e_y) + f(h_2) - f(h_3) \\ \epsilon(s, z) &= \phi(s) - \phi(s + e_z) + f(h_3) - f(h_1) \end{aligned} \quad (2.18)$$

Given the fields  $\epsilon(s, \alpha)$  and  $\phi(s)$ , we assign any fixed value to  $f(l, m)$  at one particular hexagon, then the value of the  $f$ -field at neighbouring hexagons is completely determined. Thus for a given configuration  $\{S_a^\alpha\}$ , we can determine the  $f$ -fields at all hexagons up to an overall additive constant.

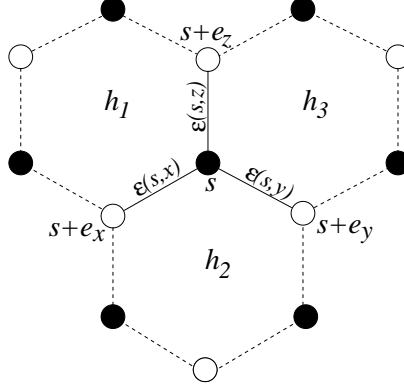


Figure 2.2: Figure depicting the definition of the  $\epsilon$  and  $h$  variables on the bonds and plaquettes around an  $A$ -site  $s$ .

We will now use the values of  $\{Q_s\}$  and  $\{f_{l,m}\}$ , instead of  $\{S_a^{\alpha 2}\}$  to specify the spin-configurations. The number of variables  $S_a^{\alpha 2}$  are  $3N$  in number, with  $N$  constraints between them, thus there are  $2N$  independent real variables. As the variables  $Q_s$  satisfy the constraint  $\sum_s Q_s = 0$ , there are  $N - 1$  independent parameters  $Q_s$ . Also, there are only  $(N - 1)$  independent parameters  $f(l, m)$ , as these are defined only up to an overall additive constant. We need two additional linearly independent variables to complete our new set of coordinates. We choose these to be  $R_1 = \sum_l \epsilon(l, m; z) + \phi(b(l, m)) - \phi(a(l, m))$  and  $R_2 = \sum_m \epsilon(l, m; y) + \phi(b(l + 1, m - 1)) - \phi(a(l, m))$ , which lead to

$$\begin{aligned} f(l + L, m) &= f(l, m) + R_1 \\ f(l - \frac{M}{2}, m + M) &= f(l, m) + R_2 \end{aligned} \quad (2.19)$$

Assuming that the  $\phi$ -field, obtained in Eq.(2.17) is periodic on the torus, with  $\phi(a(l, m)) = \phi(a(l + L, m)) = \phi(a(l - M/2, m + M))$ ,  $R_1$  is independent of  $m$  (and  $R_2$  of  $l$ ), and these correspond to fixing the boundary conditions for the  $f(l, m)$ .

The range of each  $S_a^{\alpha 2}$  is  $[0, 1]$ , which leads to the condition  $2/3 \geq \epsilon(s, \alpha) \geq -1/3$  at each bond. This implies constraints on the allowed range of  $f(l, m)$  and  $Q(l, m)$ . Now, given the values of the  $Q$ -,  $f$ - and  $\phi$ -fields, one can systematically reconstruct the  $\epsilon$ -field (and thus the spin configuration). The value of  $\epsilon$  at any bond in the bulk can be evaluated from the  $f$ 's at the neighbouring plaquettes and the  $\phi$  at the ends of the bond as shown in Eq. (2.18). The  $\epsilon$ 's at the edges of the lattice are determined by the values of  $f$  at the plaquettes next to the edge, which can be obtained from  $R_1$  (or  $R_2$ ) using Eq. (2.19). Thus, in the allowed range, the transformation from  $\{Q, f, R\}$  to  $\{S_a^{\alpha 2}\}$  is invertible.

## 2.6 Characterising the Ground State Manifold

In this section we use the new height variables  $\{f\}$  to completely characterise the ground state manifold of the system. Baskaran *et al.* defined Cartesian states as states where each spin is aligned in the direction along a Cartesian axis (x-, y- or z-) [1]. We can construct a Cartesian ground state of  $H$ , by constructing a dimer covering of the hexagonal lattice. Spins at the ends of a dimer lying on a bond of type  $\alpha$  ( $\alpha = X, Y$  or  $Z$ ) are aligned parallel to each other in the direction  $\alpha$  (either both having  $S^\alpha = +1$  or both having  $S^\alpha = -1$ ). This state has an energy  $-NJ$ . Then corresponding to a dimer covering, there are  $2^N$  Cartesian ground states. The number of dimer coverings of the hexagonal lattice increases as  $1.38^N$  [2], hence the number of Cartesian ground states increases as  $2.76^N$ . Baskaran *et al.* also showed that for any two Cartesian states, there is a one-parameter family of ground states that connects them, thus forming a network of ground states. In this section we characterise the entire set of ground states of this model, which is a larger manifold than the network described above. The derivation of the ground state energy and constraint was provided in section 2.3. We provide an alternative derivation below.

In the large  $\beta$  limit,  $F(x)$  in the effective Hamiltonian for the  $A$ -sites can be replaced by  $x$ . Therefore the ground state energy  $E_0$  of the system is given by

$$E_0 = -J \text{Max} \left[ \sum_{(l,m)} \sqrt{1 + Q_{(l,m)}} \right]. \quad (2.20)$$

Once again, as the energy is a sum of square roots, we can use the convexity inequality (Eq. (2.3)) and arrive at the ground state energy of the system (Eq. (2.4)). Alternatively, we can also obtain the ground state constraint by noting that  $F(\beta\sqrt{x})$  is itself a convex function for all  $\beta, x > 0$ . As the sum in Eq. (2.20) is maximised when all the terms are equal, the necessary and sufficient condition for the ground state configuration is

$$Q_b = 0, \text{ for all sites } b \in B. \quad (2.21)$$

Since the  $Q$ -field, and hence also the  $\phi$ -field are exactly zero everywhere in the ground states, the manifold is described only by the  $f$ -field. Correspondingly, the equations (2.18) simplify to

$$\begin{aligned} \epsilon(s, x) &= f(h_1) - f(h_2) \\ \epsilon(s, y) &= f(h_2) - f(h_3) \\ \epsilon(s, z) &= f(h_3) - f(h_1) \end{aligned} \quad (2.22)$$

The set of states forms an  $N + 1$  dimensional manifold, parametrised by the variables  $\{f\}$ , with the boundary conditions on these given by  $R_1$  and  $R_2$ . It is a convex set whose extremal points correspond to the Cartesian states studied by Baskaran *et al.*

## 2.7 Finite Temperature Partition Function

In this section we express the partition function of the model in terms of the new  $\{Q\}$ ,  $\{f\}$  and  $\{\phi\}$  variables. We begin by analysing the phase space factors in the partition function as we change variables from  $\{\vec{S}\}$  to  $\{f, Q\}$ . The phase space integral for each  $A$ -site spin is

$$\int d\vec{S} = \int dS_a^x dS_a^y dS_a^z \delta(S_a^{x^2} + S_a^{y^2} + S_a^{z^2} - 1). \quad (2.23)$$

We now change our integration variables from  $S_a^x$  to  $S_a^{x^2}$ . We have  $dS_a^x = dS_a^{x^2} / (2\sqrt{S_a^{x^2}})$  and similarly for the  $y$  and  $z$  components. The  $f$ 's and  $Q$ 's are linear functions of the  $S_a^{\alpha^2}$ 's (with  $\alpha = x, y, z$ ), hence the Jacobian matrix of transformation for this change of variables is a  $2N \times 2N$  constant matrix. Also, the determinant is non-zero as the transformation is invertible. The partition function at finite temperature, up to an unimportant constant, is thus given by

$$Z[\beta] = \text{Const.} \int dR_1 dR_2 \int \prod_{l,m} df_{l,m} \int dQ_{b(l,m)} \left( \prod_{\text{bonds}} \left( \frac{1}{3} + \epsilon(\text{bond}) \right)^{-1/2} \right) \times \exp \left( \sum_{l,m} F \left( \beta \sqrt{1 + Q_{b(l,m)}} \right) \right), \quad (2.24)$$

where  $\prod_{\text{bonds}}$  denotes the product over all bonds  $(l, m; \alpha)$  of the lattice, with the  $\epsilon$ ,  $Q$  and  $f$  variables defined in Section 2.5 and  $F(x)$  defined by Eq. (2.10).

## 2.8 The Temperature Tending to Zero Limit

In this section we take the limit of temperature tending to zero in the partition function by integrating over the variables that quantify the deviation about the ground state configurations, namely the charges  $\{Q\}$ . Our exact characterisation of the ground state manifold and excitations allow us to take this limit without any approximation. We define the restricted partition function for a fixed configuration of heights  $\{f_{l,m}\}$  by integrating over the charges  $\{Q\}$  as

$$Z[\{f_{l,m}\}, \beta] = \int \prod_{(l,m)} dQ_{b(l,m)} \exp(-\beta H_{eff}[\{f, Q\}]). \quad (2.25)$$

For large  $\beta$ , the integrand in Eq.(2.25) is sharply peaked at  $Q_s = 0$ . We can use the method of steepest descent to find the value of this integral (integrating over the  $N - 1$   $Q$  variables). We expand  $H_{eff}$  in a power series in  $Q$ 's

$$H_{eff} = E_0 + \sum_s Q_s^2 + \dots \quad (2.26)$$

The linear term in  $Q$  in the function  $H_{eff}$  vanishes since  $\sum_s Q_s = 0$ . While the range of the  $Q_s$  integrals depend on  $\{f_{l,m}\}$ , for large  $\beta$ , when the width of the peak is much smaller than the range of integration, and the peak is away from the end points of the range, each integration to leading order is independent of  $\{f_{l,m}\}$  and gives a factor  $C\beta^{-1/2}$  where  $C$  is a constant. The restricted partition function  $Z[\{f\}, \beta]$  in the limit of very small temperature to leading order in  $\beta$ , is  $\beta^{-(N-1)/2} Z_0[\{f\}]$ . Where  $Z_0[\{f\}]$  is given by

$$Z_0[\{f\}] = \lim_{\beta \rightarrow \infty} \beta^{(N-1)/2} Z[\{f\}, \beta] = \text{Const.} \left[ \prod_{\text{bonds}} \left( \frac{1}{3} + \epsilon(\text{bond}) \right)^{-1/2} \right]. \quad (2.27)$$

Thus for each configuration  $\{f_{l,m}\}$ , the integration over fluctuations in  $\{Q\}$  produces the same temperature dependent weight factor in the limit of large  $\beta$ . In order to evaluate averages in the limit of low temperatures we can thus ignore the  $Q$ -degrees of freedom, and set them equal to zero. Now, the zero-temperature partition function, i.e.- the partition function in the limit  $\beta \rightarrow \infty$  defined as

$$Z_0 = \lim_{\beta \rightarrow \infty} \beta^{(N-1)/2} Z[\beta] = \int dR_1 dR_2 \int \prod_{(l,m)} df_{l,m} Z_0[\{f\}] \quad (2.28)$$

can be expressed as

$$Z_0 = \int dR_1 dR_2 \int \prod_{(l,m)} df_{l,m} \exp \left( - \sum_{\langle i,j \rangle} V(f_i - f_j) \right), \quad (2.29)$$

where

$$\begin{aligned} V(x) &= \frac{1}{2} \log \left( \frac{1}{3} + x \right), \text{ for } -1/3 \leq x \leq +2/3; \\ &= +\infty, \text{ otherwise.} \end{aligned} \quad (2.30)$$

and the sum over  $\langle i, j \rangle$  denotes the summation over all nearest neighbour hexagons  $i$  and  $j$ .

## 2.9 Mapping to a Solid-on-Solid Model

We note that  $Z_0$  may be interpreted as the partition function of a solid-on-solid (SOS) model, with a real height variable  $f_{l,m}$  located at sites  $(l, m)$  of a triangular lattice and interacting via an effective Hamiltonian  $H_{SOS}$ . This Hamiltonian depends on the temperature  $T$  of the spin model. At a finite temperature  $H_{SOS}$  is determined by integrating over the  $Q$  variables in the restricted partition function in Eq. (2.25).  $H_{SOS}(T > 0)$  has some weak long range couplings. However at  $T = 0$  the  $Q$ -field is identically zero, which leads to a

purely nearest-neighbour, but non-quadratic coupling between the height variables given by

$$H_{SOS}(T=0) = - \sum_{(l,m)} [V(f_{l,m-1} - f_{l-1,m}) + V(f_{l,m} - f_{l,m-1}) + V(f_{l-1,m} - f_{l,m})].$$

We note that the Hamiltonian has a term  $\log(\frac{1}{3} + \epsilon(\text{bond}))$ , which diverges when  $\epsilon(\text{bond})$  tends to  $-1/3$ . Thus the Cartesian states of Baskaran *et al.* have a large relative weight, which has a divergent density. However, this divergence is an integrable divergence, and the actual measure of the Cartesian states in the ensemble of states at zero temperature is zero.

## 2.10 Correlations

The model has the following local symmetry: the Hamiltonian is invariant under the transformation  $S_{a(l,m)}^\alpha \rightarrow -S_{a(l,m)}^\alpha, S_{a(l,m)+e_\alpha}^\alpha \rightarrow -S_{a(l,m)+e_\alpha}^\alpha$  on each bond  $(l, m; \alpha)$  of the lattice. This implies that all correlation functions of the type  $\langle S_{s_1}^\alpha S_{s_2}^\beta \rangle$  with sites  $s_1$  and  $s_2$  not nearest neighbours are zero [3]. The simplest non-trivial correlation functions, for non-neighbour  $s_1$  and  $s_2$  are of the type  $\langle S_{s_1}^{\alpha 2} S_{s_2}^{\beta 2} \rangle$ . The convergence of the high temperature expansion of the partition function implies that these correlations fall exponentially with distance, at small  $\beta$ . As there is no phase transition as  $\beta \rightarrow \infty$ , we expect this behaviour for all  $0 \leq \beta < \infty$  as well, with the correlation length increasing as a function of  $\beta$ .

We now discuss the asymptotic behaviour of the height and spin-squared correlations at zero temperature. The SOS model has the symmetry that changing all heights by the same constant leaves the Hamiltonian unchanged. Though the interaction is a strongly non-linear function of  $f_{b(l,m)+e_\alpha} - f_{b(l,m)+e_{\alpha'}}$ , we expect that in the high-temperature phase of the SOS model, the long-wavelength hydrodynamical modes in the system will still be sound-like, with effective Hamiltonian  $|\nabla f|^2$ , which gives rise to the spectrum given by  $\omega^2 \propto k^2$ . This implies that, for two sites  $s_1$  and  $s_2$  separated by a large distance  $R$

$$\langle (f_{s_1} - f_{s_2})^2 \rangle \sim \log R, \quad (2.31)$$

which leads to

$$\langle \nabla f_{s_1} \cdot \nabla f_{s_2} \rangle \sim \frac{1}{R^2}. \quad (2.32)$$

Since the energy density variables  $S_s^{\alpha 2}$  are proportional to  $\nabla f$  (at zero temperature), we conclude that the connected part of the bond-energy bond-energy correlation function

$$\langle S_{s_1}^{\alpha 2} S_{s_2}^{\beta 2} \rangle_c \sim \frac{1}{R^2}. \quad (2.33)$$

At infinite temperature, the spins at different sites are completely uncorrelated. This

is not true for the  $f$  variables, which have non-trivial correlations even for  $\beta = 0$ . In the Appendix A we calculate the leading behaviour of  $\langle (f_R - f_0)^2 \rangle$  at large  $R$  for  $\beta = 0$ . We have, at infinite temperature

$$\langle (f_R - f_0)^2 \rangle_{\beta=0} = \frac{2\sqrt{3}}{45\pi} \log[R] + \mathcal{O}(1) \quad \text{for large } R. \quad (2.34)$$

## 2.11 Monte Carlo Simulations

In this section we present results from Monte Carlo studies of this model for zero temperature as well as for non-zero temperatures. We simulated the effective Hamiltonian  $H_{eff}$  (Eq. 2.9), obtained by integrating out spins on the  $B$ -sublattice. For the finite temperature simulations, two kinds of moves were employed—single spin moves and cluster moves.

### Single Spin Moves

We discuss single spin moves first. In any given state, we choose a site,  $a(l, m)$ . We generate a gaussian random vector  $\vec{r} = (r_x, r_y, r_z)$ , whose variance is proportional to the temperature  $T$ . The proposed single spin move is then to change the spin at site  $a(l, m)$  from  $\vec{S}_{a(l,m)}$  to  $\vec{S}'_{a(l,m)}$ , given by

$$\vec{S}'_{a(l,m)} = \frac{\vec{S}_{a(l,m)} + \vec{r}_s}{|\vec{S}_{a(l,m)} + \vec{r}_s|}. \quad (2.35)$$

If the change in the effective Hamiltonian by the move is  $\Delta H$ , the move is accepted according to the Metropolis rule, i.e.- with probability  $\text{Min}[1, e^{-\beta\Delta H}]$ . Clearly, this satisfies the detailed balance condition.

### Plaquette Moves

While the single spin moves, in principle, are sufficient for correctly sampling the entire phase space, we also employed hexagon update moves to speed up the simulations at low temperatures. Given any configuration, we randomly choose a hexagon on the honeycomb lattice. To obtain the new configuration of spins we move along this hexagon, alternately adding and subtracting a quantity,  $\Delta$ , to the bond-energies, and then computing the spin components which give rise to these bond-energies. In Fig. 2.3, suppose the topmost  $A$ -site is  $s_1$ , then  $\epsilon_1 = S_{s_1}^x{}^2 - \frac{1}{3}$  and  $\epsilon_2 = S_{s_1}^y{}^2 - \frac{1}{3}$ . Now  $\epsilon_1$  is changed to  $\epsilon_1 + \Delta$  and  $\epsilon_2$  to  $\epsilon_2 - \Delta$ . This then fixes the new  $S_{s_1}^x$  and  $S_{s_1}^y$  (up to a randomly chosen sign), leaving  $S_{s_1}^z$  unchanged. Clearly, this leaves the sum of squares of the spin components unchanged. This change is also made to the four other bonds on the hexagon [Fig. 2.3]. The value of  $\Delta$  is chosen uniformly in the interval  $[-a, a]$ , where  $a$  is a parameter. The proposed move is rejected if any of the bond-energies fall outside the interval  $[-\frac{1}{3}, \frac{2}{3}]$ . Since the sum of bond-energies at each site (A and B) remains constant, these hexagon update moves leave the value of the effective

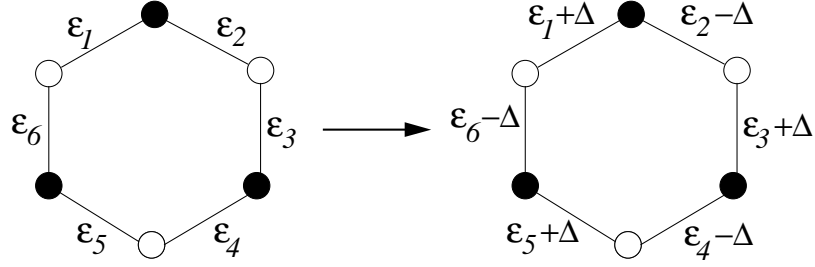


Figure 2.3: The hexagon update move in the Monte Carlo simulations. The  $\epsilon$ 's depict the bond-energy variables associated with each  $A$ -site (depicted by filled circles). A random number uniformly distributed between  $-a$  and  $+a$  is alternately added to and subtracted from the bond energies on the hexagon. The move is rejected if any of the bond energies fall outside the interval  $[-\frac{1}{3}, \frac{2}{3}]$ .

Hamiltonian unchanged. These moves therefore play a crucial role in efficiently sampling the configurations close to the ground states at very low temperatures. We take the ratio of the phase space factors of the two states and accept or reject the proposed configuration according to the Metropolis rule. Clearly, this also satisfies the detailed balance condition. For the zero temperature simulations only the hexagonal updates were used.

## Results

Monte Carlo simulation data presented in this section has been computed for  $L \times L$  triangular lattices of  $A$ -sublattice spins of various sizes, with  $L$  ranging from 30 to 256.  $6 \times 10^6$  Monte Carlo updates were made per site of which the first  $6 \times 10^5$  were not used in computing the correlation functions. Correlation functions were calculated after every 6 updates per site.

We calculated the correlation function  $C(\vec{r}) = \langle S_{a(l,m)}^z S_{a(l',m')}^z \rangle - \frac{1}{9}$  for various lattice sizes and temperatures. Here  $\vec{r}$  is the vector from site  $a(l, m)$  to  $a(l', m')$ . We find that this correlation decays quite fast, and at finite temperatures, is very small except for a few points around the origin. At zero temperature,  $C(\vec{r})$  is oscillatory along the  $(1, 0)$  direction (and is periodically negative). We observe a clear  $\frac{1}{R^2}$  behaviour along the  $\hat{e}_z$  direction, as plotted in Fig. 2.4.

We looked for a signal of possible order in the ground state ensemble of the type proposed by Baskaran *et al.* but did not detect any signal of long range order. One way of determining if there is any periodic order in the system is to study the structure factor which we define as the Fourier transform of  $C(\vec{r})$

$$S(\vec{k}) = \frac{1}{\sqrt{LM}} \sum_{(l',m')} \left( \langle S_{a(l,m)}^z S_{a(l',m')}^z \rangle - \frac{1}{9} \right) \exp(i\vec{k} \cdot \vec{r}), \quad (2.36)$$

where the summation is over all sites  $a(l', m')$  for a fixed  $a(l, m)$  with  $\vec{r}$  as defined earlier. If there was an ordering of the type suggested in [1], the structure factor  $S(\vec{k})$  would have a peak at  $\vec{k} = (\frac{2\pi}{3}, -\frac{2\pi}{3})$  and  $\vec{k} = (-\frac{2\pi}{3}, \frac{2\pi}{3})$ , with the heights scaling as a power of the system

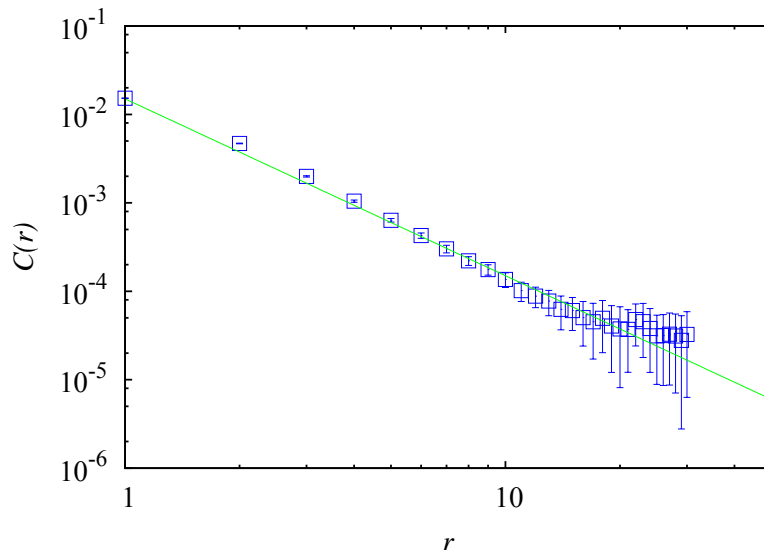


Figure 2.4: Plot of the zero temperature correlation function  $C(\vec{r}) = \langle S_A^{x^2}(0)S_A^{x^2}(\vec{r}) \rangle - \frac{1}{9}$  versus distance,  $r$  along the  $\hat{e}_x$  direction. These correlations follow a power law behaviour with exponent  $\simeq -2$ . The line has a slope of  $-2$ . The data plotted is for a lattice of size  $L = 120$ .

size. On calculating the structure factor for various  $(k_1, k_2)$  at zero temperature, we find that  $S(\vec{k})$ , apart from some fluctuation all through, has two clearly visible peaks at wave vectors  $(\frac{2\pi}{3}, -\frac{2\pi}{3})$  and  $(-\frac{2\pi}{3}, \frac{2\pi}{3})$ , see Fig. 2.5. However, the height of these peaks are only about three times the average value, and they do not become sharper with system size. Thus, we find no evidence of even incipient long-range order (hexatic-like, with power-law decay of the two-point correlation function) in the system at  $T = 0$ .

We also computed correlations of the  $f$ - and  $\phi$ -fields at various temperatures. At the end of each Monte Carlo step the  $\phi$ -field was generated from the spin configuration by solving the discrete Poisson equation on the triangular lattice (Eq. (A.4)). This was done by inverting the Poisson equation in Fourier space as shown in Eq.(A.5). The Fourier transforms were calculated using the fast Fourier transform code provided in [4]. The spin configuration and the  $\phi$ -field was then used to generate the  $f$ -field using Eq.(2.18). In Fig. 2.6, we have plotted the zero temperature correlation function  $\langle (f_{l,m} - f_{l',m'})^2 \rangle \equiv \langle (f(0) - f(r))^2 \rangle$  versus  $\log r$  where  $r$  is the distance between the two sites. We see that this correlation function increases logarithmically with distance. Note that a logarithmic dependence of this function implies a  $1/r^2$  dependence of the bond-energy bond-energy correlation function (Eq. (2.33)). Fig. 2.7 shows the correlation function  $\langle (f(0) - f(r))^2 \rangle$  at various values of  $\beta$ . These correlations vary as  $\log(r)$  at all temperatures with the coefficient varying between  $(2.45 \pm 0.05) \times 10^{-2} \simeq \frac{2\sqrt{3}}{45\pi}$  at  $\beta = 0$  and  $(4.12 \pm 0.05) \times 10^{-2}$  at  $\beta = \infty$ .

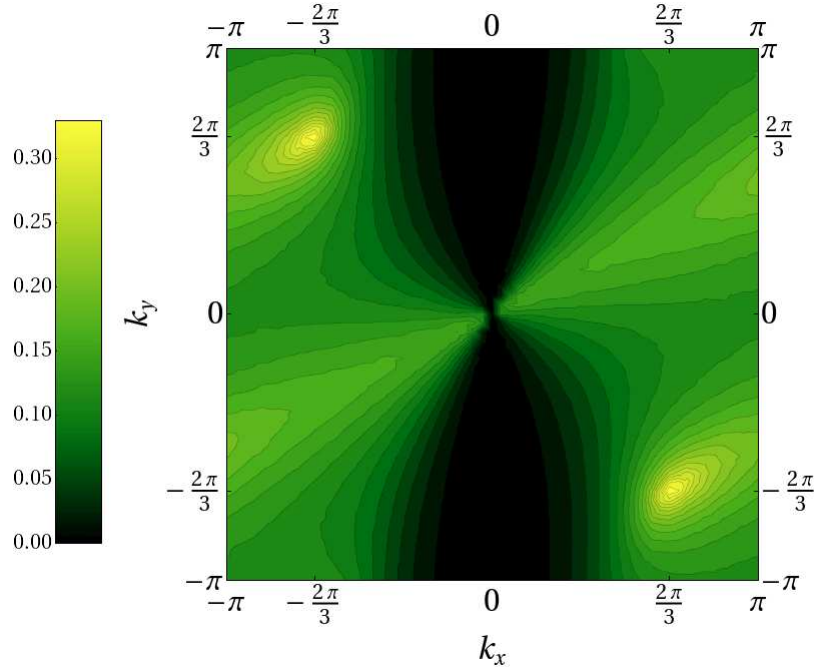


Figure 2.5: Plot of  $|S(\vec{k})|$ , the  $s_A^{z^2}$  structure factor, defined as  $S(\vec{k}) = \frac{1}{\sqrt{LM}} \sum_{\vec{r}} (\langle s_A^{z^2}(0) s_A^{z^2}(\vec{r}) \rangle - \frac{1}{9}) \exp(i\vec{k} \cdot \vec{r})$ , where the  $\vec{r}$  summation extends over all lattice sites. Two prominent peaks are visible at  $(-\frac{2\pi}{3}, \frac{2\pi}{3})$  and  $(\frac{2\pi}{3}, -\frac{2\pi}{3})$ . However, these peaks do not diverge with system size in our simulations.

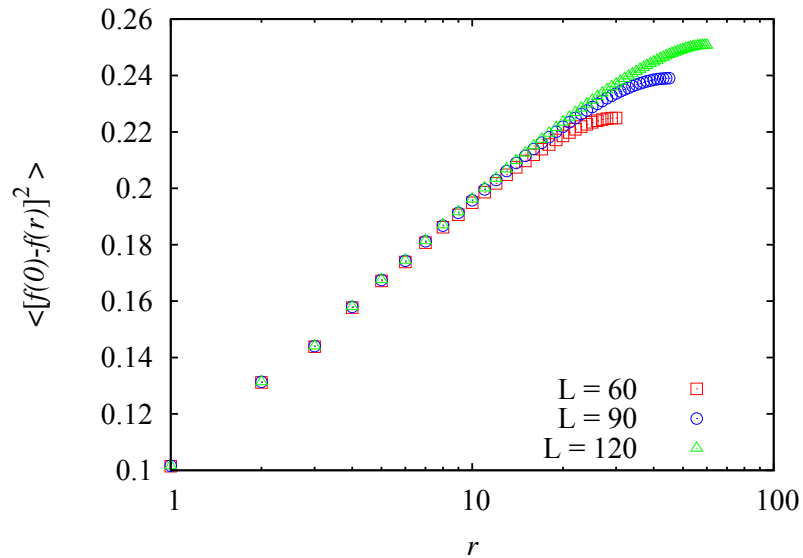


Figure 2.6: Graph of the zero temperature correlation function  $\langle (f(0) - f(r))^2 \rangle$  versus distance,  $r$ , for different lattice sizes  $L$ , showing a  $\log r$  dependence in accordance with the mapping to a height model at a finite temperature.

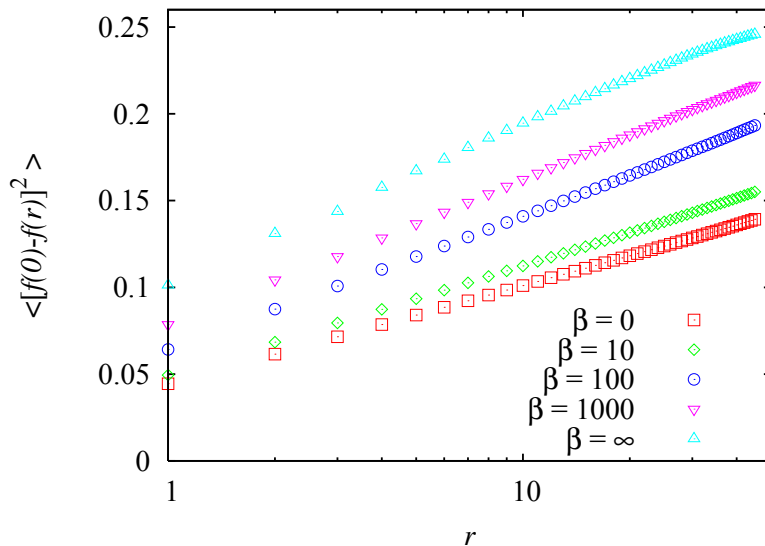


Figure 2.7: Graph showing the finite temperature correlation function  $\langle (f(0) - f(r))^2 \rangle$  versus distance,  $r$  for various values of  $\beta = T^{-1}$ . The correlations are logarithmic at all temperatures, with the coefficient of  $\log(r)$  varying between  $(2.45 \pm 0.05) \times 10^{-2} \simeq \frac{2\sqrt{3}}{45\pi}$  at  $\beta = 0$  and  $(4.12 \pm 0.05) \times 10^{-2}$  at  $\beta = \infty$ . The data plotted is for a lattice of size  $L = 120$

## 2.12 The Spin- $S$ Quantum Kitaev Model

In this section we discuss the ground state energy of the quantum spin- $S$  Kitaev model, where there is a spin- $S$  at each site interacting via the Kitaev Hamiltonian. This model has been studied by Baskaran *et al.* [1] where they identified mutually commuting  $\mathbb{Z}_2$  plaquette variables that are the invariants of this system. However, this model is not exactly soluble as in the spin-1/2 case and thus needs to be treated using different techniques. We derive an exact lower bound for the ground state energy of this system below. Our quantum mechanical Hamiltonian is normalised by the size of the spins. We have

$$\mathbf{H} = -\frac{J}{S(S+1)} \sum_{a \in A} \left( \mathbf{S}_a^x \mathbf{S}_{a+e_x}^x + \mathbf{S}_a^y \mathbf{S}_{a+e_y}^y + \mathbf{S}_a^z \mathbf{S}_{a+e_z}^z \right).$$

Here  $\mathbf{S}_s^\alpha$  ( $\alpha = x, y, z$ ) are quantum mechanical spin- $S$  operators at each site  $s$ . Using the operator inequality  $\mathbf{A}\mathbf{B} \geq -(\mathbf{A}^2 + \mathbf{B}^2)/2$ , where  $\mathbf{A}$  and  $\mathbf{B}$  are any commuting Hermitian operators, it is easily seen that  $\mathbf{H}$  satisfies the lower bound

$$E_G \geq -JN, \quad (2.37)$$

where  $E_G$  denotes the ground state energy of the Hamiltonian. This is essentially the classical ground state energy. A better bound may be proved by using a technique similar to the one used in Section 2.3 which involves the minimisation of the Hamiltonian at every  $B$ -site. We write the Hamiltonian  $\mathbf{H}$  as a sum of individual Hamiltonians at every  $B$ -site

$$\mathbf{H} = \frac{1}{S(S+1)} \sum_{(l,m)} \mathbf{H}_{b(l,m)}, \quad (2.38)$$

where  $\mathbf{H}_{b(l,m)}$  is a 4-site spin Hamiltonian containing only the couplings of the site  $b(l,m)$  on the  $B$ -sublattice and its neighbours

$$\mathbf{H}_{b(l,m)} = -J \left( \mathbf{S}_{a(l,m+1)}^x \mathbf{S}_{b(l,m)}^x + \mathbf{S}_{a(l-1,m+1)}^y \mathbf{S}_{b(l,m)}^y + \mathbf{S}_{a(l,m)}^z \mathbf{S}_{b(l,m)}^z \right).$$

The operators  $\mathbf{H}_{b(l,m)}$  can be diagonalised in a Hilbert space of 4-spins, i.e. a  $(2S+1)^4$  dimensional Hilbert space. We note that  $\mathbf{S}_{a(l,m+1)}^x$ ,  $\mathbf{S}_{a(l-1,m+1)}^y$  and  $\mathbf{S}_{a(l,m)}^z$  are operators that belong to different sites, therefore they commute amongst each other and with  $\mathbf{H}_{b(l,m)}$ . Hence we can move to a basis in which these are diagonal. We now work in the subspace in which the basis vectors are eigenvectors of  $\mathbf{S}_{a(l,m+1)}^x$ ,  $\mathbf{S}_{a(l-1,m+1)}^y$  and  $\mathbf{S}_{a(l,m)}^z$  with eigenvalues  $s_{a(l,m+1)}^x$ ,  $s_{a(l-1,m+1)}^y$ ,  $s_{a(l,m)}^z$  respectively. Thus the eigenvalues  $\lambda$  of  $H_{b(l,m)}$  satisfy the relation

$$\lambda^2 \leq (JS)^2 \left( s_{a(l,m+1)}^x{}^2 + s_{a(l-1,m+1)}^y{}^2 + s_{a(l,m)}^z{}^2 \right). \quad (2.39)$$

This is true for all eigenvalues  $s_{a(l,m+1)}^x$ ,  $s_{a(l-1,m+1)}^y$ ,  $s_{a(l,m)}^z$  and hence is valid as an operator inequality

$$\mathbf{H}_{b(l,m)}^2 \leq (JS)^2 \left( \mathbf{S}_{a(l,m+1)}^x{}^2 + \mathbf{S}_{a(l-1,m+1)}^y{}^2 + \mathbf{S}_{a(l,m)}^z{}^2 \right). \quad (2.40)$$

Therefore, for any wave function  $|\psi\rangle$  of all the  $2N$  spins on the lattice we have

$$\langle \psi | \mathbf{H}_{b(l,m)}^2 | \psi \rangle \leq (JS)^2 \left( \langle \mathbf{S}_{a(l,m+1)}^x{}^2 \rangle + \langle \mathbf{S}_{a(l-1,m+1)}^y{}^2 \rangle + \langle \mathbf{S}_{a(l,m)}^z{}^2 \rangle \right), \quad (2.41)$$

where  $\langle \mathbf{S}_{a(l,m+1)}^x{}^2 \rangle = \langle \psi | \mathbf{S}_{a(l,m+1)}^x{}^2 | \psi \rangle$  and so on. Using the fact that  $\langle \psi | \mathbf{H}_{b(l,m)} | \psi \rangle^2 \leq \langle \psi | \mathbf{H}_{b(l,m)}^2 | \psi \rangle$  and taking the square root we get

$$\langle \psi | \mathbf{H}_{b(l,m)} | \psi \rangle \geq -JS \sqrt{\langle \mathbf{S}_{a(l,m+1)}^x{}^2 \rangle + \langle \mathbf{S}_{a(l-1,m+1)}^y{}^2 \rangle + \langle \mathbf{S}_{a(l,m)}^z{}^2 \rangle}.$$

This immediately gives

$$\langle \psi | \mathbf{H} | \psi \rangle \geq \sum_{(l,m)} -JS \sqrt{\langle \mathbf{S}_{a(l,m+1)}^x{}^2 \rangle + \langle \mathbf{S}_{a(l-1,m+1)}^y{}^2 \rangle + \langle \mathbf{S}_{a(l,m)}^z{}^2 \rangle}, \quad (2.42)$$

where the sum is over all the sites of the  $B$ -sublattice. Note that the terms in each of the square roots are all real numbers. Using Eq. (2.3) in Eq. (2.42) and observing that for any site on the  $A$ -sublattice  $\mathbf{S}_{a(l,m)}^x{}^2 + \mathbf{S}_{a(l,m)}^y{}^2 + \mathbf{S}_{a(l,m)}^z{}^2 = S(S+1)$  we arrive at

$$\langle \psi | \mathbf{H} | \psi \rangle \geq -JN \sqrt{\frac{S}{S+1}}. \quad (2.43)$$

For large  $S$ ,

$$\frac{E_G}{JN} \geq -1 + \frac{1}{2S} + O\left(\frac{1}{S^2}\right) \quad (2.44)$$

is a lower bound, which shows an increase in the ground state energy due to quantum fluctuations. We note that the bound (2.43) is valid for all spins  $S$  and not just for large  $S$ .

### 2.13 Summary and Discussion

We have shown that the Kitaev model with classical spins shows no order-by-disorder, while there are plausible arguments that the quantum model does. We have mapped the finite and zero temperature problem of classical spins onto a height-model interacting via an effective Hamiltonian  $H_{SOS}$ . This effective Hamiltonian depends on the temperature of the spin model. We have shown that the correlations of the height variables vary as  $\log(r)$ , where  $r$  is the distance between the sites, for all temperatures of the spin model. The discrete height model with a pinning potential in two dimensions undergoes a roughening transition from a phase in which it is ordered to one with logarithmic correlations between the height variables [5]. In the rough phase ( $T > T_R$ ) of the height model, the coefficient of  $\log(r)$  gives us a measure of the temperature [6],[7]. So we see that the range of temperature  $[0, \infty]$  of the spin model maps onto a range of temperature of the height model which is in the rough phase. Note that as the temperature of the Kitaev Hamiltonian is decreased,  $\langle (f(0) - f(r))^2 \rangle$  in the SOS model increases. The increased fluctuations in  $\{f\}$  are accompanied by a decrease in fluctuations of the  $\phi$ -field, and the fluctuations of the spins  $\{\vec{S}\}$  decrease with temperature, as expected.

The difference in the nature of the low temperature ordering in the classical and quantum case is because the mechanism of order-by-disorder in classical and quantum models is somewhat different. Consider a classical model, whose ground states form an  $M$ -dimensional manifold. Let  $G$  be one of the ground states. We expand the energy in the coordinates orthogonal to the manifold, and look for small perturbations about the ground state. Keeping terms in the deviations from the ground state to quadratic order, and going into the normal mode coordinates, we get a quadratic approximation to the Hamiltonian in the transverse coordinates as

$$\delta H = \sum_j \left[ \frac{1}{2m_j(G)} p_j^2 + m_j(G) \omega_j(G)^2 q_j^2 \right], \quad (2.45)$$

where the sum over  $j$  extends over the  $n$  transverse degrees of freedom. Then, the corresponding quantum mechanical partition function in the quadratic approximation is

$$Z_{quad} \approx \prod_j \frac{e^{-\beta \hbar \omega_j / 2}}{1 - e^{-\beta \hbar \omega_j}}. \quad (2.46)$$

For low temperatures, the  $G$  having the minimum value of the effective quantum me-

chanical free energy is obtained by minimising the “zero-point energy”  $f_q(G) = \sum_j \frac{1}{2} \hbar \omega_j$ . However, the classical partition function corresponds to the case  $\beta \omega_j \ll 1$ , and at low temperature  $T$  is easily seen to be proportional to  $T^n / \prod \omega_j(G)$ . Thus the relative weights of different points  $G$  on the manifold are determined by an effective free energy  $f_{cl}(G)$  proportional to  $\sum_j \log \omega_j$ . Clearly  $f_q$  and  $f_{cl}$  are quite different, and states which are favoured by one need not be favoured by the second. In particular,  $f_{cl}$  depends more sensitively on the low frequency modes.

If some of the  $\omega_j$ 's are zero, in this approximation, the classical partition function diverges, but the quantum weight has no singularity. This problem of zero modes also occurs in the calculation of [1]. In fact the zero frequency eigenvalue has a large degeneracy.

More generally, finite  $\hbar$  corrections in a quantum mechanical system correspond to a finite temperature classical model but in one higher dimension, and can be qualitatively different. A simple example of this is a system of masses coupled by nearest neighbour springs in one dimension. In the classical case, the variance of displacements of masses at distance  $R$  varies as  $TR$  for large  $R$ , and small  $T$ , but this quantity grows only as  $\log R$ , both in the quantum case at zero temperature, and the classical case in *two* dimensions.

In the path-integral formulation, the large- $S$  quantum Kitaev model becomes a set of classical spins on a  $2+1$  dimensional lattice, with Kitaev couplings in two spatial directions, and ferromagnetic couplings in the time/inverse-temperature direction. It is quite plausible that in this 3-dimensional model, there is long-range order for low “effective temperature”, but in the 2-dimensional classical Kitaev model, the destabilising effect of fluctuations is too strong.

There are several interesting classical two dimensional systems, where thermal order-by-disorder is expected. The best studied example for a continuous spin model in two dimensions is the system of Heisenberg spins on a kagome lattice, with nearest neighbour antiferromagnetic couplings. The expectation of order-by-disorder in this classical system comes from theoretical and Monte Carlo studies, that suggest that at low temperatures, the spins lie on a single plane as  $T \rightarrow 0$  [8],[9]. This model can also be related to the height model at its critical point, within the quadratic approximation, suggesting that a single long-range ordered state (the  $\sqrt{3} \times \sqrt{3}$  state) is selected over the coplanar ones [10],[11]. It would be interesting to identify the main reason for the difference in the behaviours in these models and the case studied here.

# References

- [1] G. Baskaran, D. Sen and R. Shankar, Phys. Rev. B **78**, 115116 (2008).
- [2] P. W. Kasteleyn, J. Math. Phys., **4**, 287 (1963)
- [3] G. Baskaran, S. Mandal, and R. Shankar, Phys. Rev. Lett. **98**, 247201 (2007).
- [4] William H. Press, Brian P. Flannery, Saul A. Teukolsky, William T. Vetterling, Numerical Recipes in Fortran 77 and 90 (1992).
- [5] J. V. José, L. P. Kadanoff, S. K. Kirkpatrick, and D. R. Nelson, Phys. Rev. B **16**, 1217 (1977).
- [6] S. T. Chui, J. D. Weeks, Phys. Rev. B **14**, 4978 (1976).
- [7] T. Ohta and K. Kawasaki, Prog. Theor. Phys. Vol. 60 No. 2 pp. 365-378 (1978).
- [8] J. T. Chalker, P. C. W. Holdsworth, and E. F. Shender, Phys. Rev. Lett. **68**, 855 (1992).
- [9] M. E. Zhitomirsky, Phys. Rev. B **78**, 094423 (2008).
- [10] D. A. Huse and A. D. Rutenberg, Phys. Rev. B **45**, 7536 (1992).
- [11] C. L. Henley, Phys. Rev. B **80**, 180401 (2009).

## Chapter 3

# Spin-1 Kitaev Chain

### 3.1 Introduction

The integrable nature of the spin-1/2 Kitaev model makes it a very useful testing ground for analysing properties of one and two dimensional quantum spin systems. Variants of the model have been the subject of a large amount of research in recent years. Several related models have been studied in two dimensions [1, 2, 3, 4, 5, 6, 7, 8, 9], three dimensions [10, 11] and also on quasi-one-dimensional lattices [12, 13, 14].

In this chapter, we study the Kitaev model with spin- $S$  at every site. The two-dimensional model appears difficult to analyse, but even the one-dimensional version of it has a lot of interesting structure. For the Kitaev model with spin  $S > 1/2$ , there is a  $\mathbb{Z}_2$  invariant associated with each plaquette for arbitrary spin- $S$ , which reduces to the conserved  $\mathbb{Z}_2$  gauge flux for the spin-1/2 case [15]. However, the model does not seem to be fully integrable. The spin- $S$  Kitaev model has been studied in the large  $S$  limit using spin wave theory [15], and the classical version of the Kitaev model has been studied at finite temperatures using analytical and Monte Carlo techniques [16]. We have seen in the previous chapter that while the phenomenon of order-by-disorder [17, 18, 19, 20] may occur in the quantum mechanical Kitaev model, it does not in the corresponding classical model [16].

We begin by considering the spin- $S$  Kitaev chain, obtained by setting the coupling along one of the directions in the two dimensional model to zero. We show that this model has local, mutually commuting conserved quantities  $W_n$ , for integer  $S$ . The eigenvalues of  $W_n$  are  $\pm 1$ . For open boundary conditions, there are some additional conserved quantities at the ends of the system. The existence of these conserved quantities implies that the Hilbert space of a  $N$ -site system can be decomposed into a sum of  $2^N$  disjoint subspaces. The dimensions of these subspaces are not equal. We describe a procedure to compute the dimension of these sectors. For large  $N$ , the dimension varies as  $d^N$  in most sectors, with the constant  $d$  depending on the sector. The sectors show complicated spatial structures, arising from the spatial structure of  $\{W_n\}$ .

We then consider the spin-1 chain. The ground state lies in the sector in which  $W_n = +1$  for all  $n$ , as verified by numerical studies [21]. In this sector, there is a gap between the ground state and the first excited state. The lowest excited state of the system is the ground state of a different sector; and the energy-gap seems to approach a non-zero value in the limit of the system size going to infinity. We consider the sector containing the ground state, and show that the Hamiltonian is equivalent to the Hamiltonian of a deposition-evaporation process of a nearest-neighbour-exclusion lattice gas model, which can be written as a spin-1/2 system with local interactions with a range extending to at most next-nearest neighbours. The Hamiltonian seems to be difficult to diagonalize exactly, we present a variational study of the ground state. The variational estimate of the ground state energy is found to agree well with the results obtained numerically for small systems. We also analyse the first excited state of the Hamiltonian. We then consider a more general Hamiltonian, obtained by adding a term  $\lambda \sum_n W_n$ , and discuss its ground states as a function of  $\lambda$ . We show that the ground state of this new Hamiltonian is gapless for a range of couplings  $\lambda_1^c \leq \lambda \leq \lambda_2^c$ , and gapped otherwise. We argue that for  $\lambda$  just above  $\lambda_1^c$ , in the sector containing the ground state, the density of negative  $W$ 's is of order  $|\frac{1}{\log(\lambda - \lambda_1^c)}|$ . For  $\lambda$  just below  $\lambda_2^c$ , the density of positive  $W$ 's goes to zero as  $(\lambda_2^c - \lambda)^{1/2}$ .

## 3.2 One-dimensional Kitaev Model

In this section, we discuss a one-dimensional spin- $S$  model which is obtained by considering a single row of the Kitaev model in two dimensions. The Kitaev model on the honeycomb lattice is governed by the Hamiltonian

$$H = J_x \sum_{\langle ij \rangle_x} S_i^x S_j^x + J_y \sum_{\langle ij \rangle_y} S_i^y S_j^y + J_z \sum_{\langle ij \rangle_z} S_i^z S_j^z, \quad (3.1)$$

where  $\langle ij \rangle_\alpha$  denote the nearest-neighbour bonds in the  $\alpha^{\text{th}}$  direction ( $\alpha \equiv x, y, z$ ). If we set  $J_z = 0$ , we get a set of decoupled chains, which we refer to as Kitaev chains. The Hamiltonian is given by

$$H = \sum_n (J_{2n-1} S_{2n-1}^x S_{2n}^x + J_{2n} S_{2n}^y S_{2n+1}^y). \quad (3.2)$$

In general, the couplings  $J_m$  could be all different from each other. If some of the couplings are negative, we can change the signs of those couplings by performing the unitary transformation

$$S_m^x \rightarrow -S_m^x, \quad S_m^y \rightarrow -S_m^y, \quad \text{and} \quad S_m^z \rightarrow S_m^z \quad (3.3)$$

on appropriate sites. We consider only the simple case, where all couplings have the same value,  $J_m = J$ . Without any loss of generality, we set  $J = 1$ . Finally, the Hamiltonian can be unitarily transformed to a more convenient form by the following transformation on the

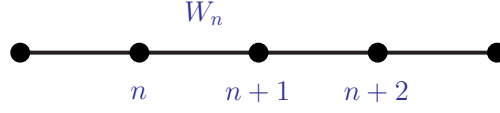


Figure 3.1: Picture of the Kitaev chain showing one of the conserved quantities  $W_n$ .

even sites,

$$S_{2n}^x \rightarrow S_{2n}^y, \quad S_{2n}^y \rightarrow S_{2n}^x, \quad \text{and} \quad S_{2n}^z \rightarrow -S_{2n}^z. \quad (3.4)$$

The Hamiltonian in Eq. (3.2) then takes the translationally invariant form

$$H_K = \sum_n S_n^x S_{n+1}^y. \quad (3.5)$$

### 3.3 The Invariants

The Hamiltonian in Eq. (3.5) has the following local symmetries for all  $S$ . We introduce the operators on sites

$$\Sigma_n^\alpha = e^{i\pi S_n^\alpha}, \quad (3.6)$$

and operators on bonds

$$W_n = \Sigma_n^y \Sigma_{n+1}^x. \quad (3.7)$$

We then find that

$$[W_n, H] = 0. \quad (3.8)$$

The eigenvalues of  $\Sigma_n^\alpha$  are  $\pm 1$  for integer  $S$  and  $\pm i$  for half-odd-integer  $S$ . Thus for any value of the spin  $S$ , the eigenvalues of  $W_n$  are  $\pm 1$ .

However, there is a qualitative difference between integer and half-odd-integer values of  $S$ . For integer values of  $S$ , all the matrices  $\Sigma_n^\alpha$  commute with each other, whereas for half-odd-integer values,  $\Sigma_n^\alpha$  commutes with  $\Sigma_m^\beta$  for  $n \neq m$  but anticommutes with  $\Sigma_n^\beta$  for  $\alpha \neq \beta$ . Consequently, for integer  $S$ , all the invariants  $W_n$  commute, but for half-odd-integer  $S$ ,  $W_n$  anti-commutes with its neighbouring invariants,  $W_{n\pm 1}$ , and commutes with  $W_m$ ,  $m \neq n, n \pm 1$ . We will now show that this implies that all the eigenstates of the chain with half-odd-integer  $S$  are  $2^{N/2}$  fold degenerate.

The invariants for half-odd-integer  $S$  can be combined in the following way to form a set of mutually commuting angular momentum operators, one per every two bonds,

$$\mu_n^z = W_{2n}, \quad \mu_n^x = W_{2n-1} \prod_{m < n} W_{2m-1}, \quad \mu_n^y = i\mu_n^x \mu_n^z. \quad (3.9)$$

It can be verified that

$$\left[ \mu_n^\alpha, \mu_m^\beta \right] = 2i\delta_{nm}\epsilon^{\alpha\beta\gamma}\mu^\gamma, \quad (3.10)$$

$$\left\{ \mu_n^\alpha, \mu_n^\beta \right\} = 2\delta^{\alpha\beta}. \quad (3.11)$$

The  $\mu_n^\alpha$  commute with the Hamiltonian as they are made by multiplying conserved operators. Hence Eq. (3.10) shows that the Hamiltonian has a  $(SU(2))^{N/2}$  symmetry, where  $N$  is the number of sites. Thus each eigenstate is  $2^{N/2}$ -fold degenerate. There is no reason for such a degeneracy for integer  $S$  and the ground state for  $S = 1$  is non-degenerate.

We note that the spin- $S$  Kitaev model in two dimensions also has a  $\mathbb{Z}_2$  valued invariant associated with every hexagon of the honeycomb lattice [15]. When they are restricted to a single chain, the invariants take the form

$$V_n = \Sigma_n^y \Sigma_{n+1}^z \Sigma_{n+2}^x, \quad (3.12)$$

which involves three neighbouring sites. The invariants given in Eq. (3.7) are simpler because they only involve two sites. For any spin  $S$ , we find that  $\Sigma_n^x \Sigma_n^y \Sigma_n^z = I$  and  $(\Sigma_n^\alpha)^2 = (-1)^{2S}$ ; hence the invariants in Eqs. (3.7) and (3.12) are related to each other as

$$V_n = (-1)^{2S} W_n W_{n+1}. \quad (3.13)$$

Open chains have extra symmetries at the edges. If the site labels of the open chain are  $1, \dots, N$ , then  $S_1^x$  and  $S_N^y$  also commute with the Hamiltonian. Thus at the first and last sites, we have a  $U(1)$  symmetry group generated by these operators. Note that a  $\mathbb{Z}_2$  subgroup of this group, consisting of the operators  $\Sigma_1^x$  and  $\Sigma_N^y$ , also commutes with all the invariants. If we combine the operators  $S_1^x$  and  $S_N^y$  with the  $W_n$  invariants on the first and last bonds, we have a larger symmetry group made of  $W_1$ ,  $S_1^x$  and their products at the first bond, and the group made of  $W_N$ ,  $S_N^y$  at the last bond. As we will show in section 3.6, for the  $S = 1$  case the group formed is  $SU(2) \times U(1)$  at each end.

### 3.4 Dimension of the Subspaces

In this section we develop a procedure to count the number of states in a given sector for integer  $S$ . First, we look at the dimension of sectors with  $\{W\}$  configurations given by  $\mathcal{W} \equiv \{W_N, \dots, W_2, W_1\}$  for a closed chain of  $N$  sites and  $\mathcal{W} \equiv \{W_{N-1}, \dots, W_2, W_1\}$  for an open chain. The states of a chain can be classified by the eigenvalues of  $\Sigma_i^x$  and  $\Sigma_i^y$  as

$$(y_N x_N) \cdots (y_2 x_2)(y_1 x_1), \quad (3.14)$$

where  $x_i, y_i = \pm 1$  are the eigenvalues of  $\Sigma_i^x$  and  $\Sigma_i^y$  respectively. The invariants are then  $W_i = x_{i+1} y_i$ .

We now calculate the number of states in a given sector  $\mathcal{W}$  using a standard transfer matrix technique. Consider the allowed states of  $r$  sites, when the values of  $(r-1)$  constants  $W_j$ , with  $j = 1$  to  $(r-1)$  have been specified. We denote this set of values by  $\mathcal{W}$ . Let  $Z_r(y|\mathcal{W})$  denote the number of allowed states of this set of sites with  $\Sigma_r^y = y$  where  $y$  takes values  $\pm 1$ . We now add a site  $(r+1)$  to the chain, and also specify  $W_r$ . Let the new set of  $\{W\}$  be denoted by  $\mathcal{W}'$ .

Consider first the case  $W_r = +1$ . Clearly, we can have two possibilities:  $\Sigma_{r+1}^x = \Sigma_r^y = +1$ , or  $\Sigma_{r+1}^x = \Sigma_r^y = -1$ . Let  $\nu(p, p')$  denote the number of states of a single site with  $\Sigma^y = p$ , and  $\Sigma^x = p'$ . Then, we clearly have the recursion equation

$$Z_{r+1}(y|\mathcal{W}') = \nu(y, +1)Z_r(+1, \mathcal{W}) + \nu(y, -1)Z_r(-1, \mathcal{W}). \quad (3.15)$$

This equation can be written as a matrix equation

$$\begin{bmatrix} Z_{r+1}(+1|\mathcal{W}') \\ Z_{r+1}(-1|\mathcal{W}') \end{bmatrix} = \mathbb{T}_+ \begin{bmatrix} Z_r(+1|\mathcal{W}) \\ Z_r(-1|\mathcal{W}) \end{bmatrix}, \quad (3.16)$$

where  $\mathbb{T}_+$  is a  $2 \times 2$  matrix given by

$$\mathbb{T}_+ = \begin{bmatrix} \nu(+1, +1) & \nu(+1, -1) \\ \nu(-1, +1) & \nu(-1, -1) \end{bmatrix}, \quad (3.17)$$

thus

$$\mathbb{T}_+ = \frac{1}{2} \begin{bmatrix} S-1 & S+1 \\ S+1 & S+1 \end{bmatrix} \quad \text{for } S \text{ odd}, \quad (3.18)$$

$$= \frac{1}{2} \begin{bmatrix} S+2 & S \\ S & S \end{bmatrix} \quad \text{for } S \text{ even}. \quad (3.19)$$

Similarly, when  $W_n = -1$ , the corresponding recursion equation is

$$\begin{bmatrix} Z_{r+1}(+1|\mathcal{W}') \\ Z_{r+1}(-1|\mathcal{W}') \end{bmatrix} = \mathbb{T}_- \begin{bmatrix} Z_r(+1|\mathcal{W}) \\ Z_r(-1|\mathcal{W}) \end{bmatrix}, \quad (3.20)$$

where the matrix  $\mathbb{T}_-$  is given by

$$\mathbb{T}_- = \begin{bmatrix} \nu(+1, -1) & \nu(+1, +1) \\ \nu(-1, -1) & \nu(-1, +1) \end{bmatrix}. \quad (3.21)$$

Thus

$$\begin{aligned} \mathbb{T}_- &= \mathbb{T}_+ \tau^x \\ \text{where } \tau^x &= \begin{pmatrix} 0 & 1 \\ 1 & 0 \end{pmatrix}. \end{aligned} \quad (3.22)$$

It is then clear that for a given set of invariants  $\mathcal{W}$ , the number of states can be written in terms of a product of the matrices  $\mathbb{T}_+$  and  $\mathbb{T}_-$ . For example, for an open chain of  $N$  sites, and  $\mathcal{W} = \{W_{N-1}, \dots, W_3, W_2, W_1\} = \{+1, \dots, +1, -1, -1\}$ , we have

$$\begin{bmatrix} Z_N(+1|+--) \\ Z_N(-1|+--) \end{bmatrix} = \mathbb{T}_+ \dots \mathbb{T}_+ \mathbb{T}_- \mathbb{T}_- \begin{bmatrix} Z_1(+1|\phi) \\ Z_1(-1|\phi) \end{bmatrix}, \quad (3.23)$$

where  $\phi$  denotes the null string, and  $Z_1(y|\phi)$  denotes the number of states of the spin at site 1 with  $\Sigma_1^y = y$ . Thus  $Z_1(+1|\phi) = S + 1$ ,  $Z_1(-1|\phi) = S$ , when  $S$  is an even integer, and  $Z_1(+1|\phi) = S$ ,  $Z_1(-1|\phi) = S + 1$  when  $S$  is an odd integer. The total number of states in this sector is then given by

$$\Gamma(\mathcal{W}) = Z_N(+1|\mathcal{W}) + Z_N(-1|\mathcal{W}). \quad (3.24)$$

For a closed chain, there is an additional invariant  $W_N = y_N x_1$  and the number of states in the sector becomes

$$\Gamma(\mathcal{W}) = \text{Tr} \left( \prod_{n=1}^N \mathbb{T}_{W_n} \right), \quad (3.25)$$

where  $\mathbb{T}_{W_n} \equiv \mathbb{T}_\pm$  for  $W_n = \pm 1$  and  $\prod_{n=1}^N$  is an ordered product of  $\mathbb{T}_\pm$  matrices, from site 1 to  $N$ . We now calculate the dimensions of some sectors for a closed chain of length  $N$ . It is easy to get an explicit answer for the two extreme limits when  $W_n = \pm 1$  for all  $n$ . In these cases, the number of states,  $\Gamma^\pm$ , is

$$\Gamma^\pm = (d_1^\pm)^N + (d_2^\pm)^N, \quad (3.26)$$

where  $d_1^\pm(S)$  and  $d_2^\pm(S)$  are the larger and smaller eigenvalues of  $\mathbb{T}_\pm$  respectively. The eigenvalues can be computed to give

$$d_{1(2)}^+ = \frac{1}{2} \left( S \pm \sqrt{S^2 + 2S + 2} \right) \quad \text{for } S \text{ odd,} \quad (3.27)$$

$$= \frac{1}{2} \left( S + 1 \pm \sqrt{S^2 + 1} \right) \quad \text{for } S \text{ even,} \quad (3.28)$$

$$d_{1(2)}^- = \frac{1}{2} \left( S + 1 \pm \sqrt{S^2 - 1} \right) \quad \text{for } S \text{ odd,} \quad (3.29)$$

$$= \frac{1}{2} \left( S \pm \sqrt{S^2 + 2S} \right) \quad \text{for } S \text{ even.} \quad (3.30)$$

For  $S = 1$ ,  $d_1^+$  is equal to the golden ratio,  $\gamma = (1 + \sqrt{5})/2$ , and  $d_2^+ = -1/\gamma$ . As  $N \rightarrow \infty$ , the dimension of the Hilbert space in the sector with all  $W_n = 1$  grows as  $\gamma^N$ . On the other hand,  $d_1^- = d_2^- = 1$ . The dimension of the sector with all  $W_n = -1$  is therefore equal to 2. With the exception of  $S = 1$ , the larger of the two eigenvalues  $d_1^\pm$  is always greater than 1, and in the  $N \rightarrow \infty$  limit, we have

$$\Gamma^\pm(S) = (d_1^\pm(S))^N. \quad (3.31)$$

$d_1^\pm(S)$  is sometimes referred to as the quantum dimension of the sector. As can be seen it is, in general, fractional for any  $S$ . In the limit  $S \rightarrow \infty$ , the quantum dimension tends to  $S + 1/2$  for both the sectors. It is interesting to note that it is a half-odd-integer in this limit.

### 3.5 Expectation Values of Operators

In this section we derive expressions for the expectation values of the  $\Sigma_n^\alpha$  operators ( $\alpha \equiv x, y, z$ ) in various sectors. We will assume periodic boundary conditions. Our calculation will average over all the states of a given sector considered with equal weight; this can be considered as a calculation in the limit that the temperature  $T \rightarrow \infty$ , so that it does not depend on the Hamiltonian. We evaluate the expectation values of  $\Sigma_r^\alpha$  by inserting projection operators at site  $r$  in the product of transfer matrices in Eq.(3.25).

The expectation value of a  $\Sigma_r^\alpha$  operator (at infinite temperature) located at a position  $r$  in an arbitrary sector with  $W$ -configuration  $\mathcal{W}$  can be calculated by summing all the states with  $\Sigma_r^\alpha = +1$  with a coefficient  $+1$  and all the states with  $\Sigma_r^\alpha = -1$  with a coefficient  $-1$ . The elements of the transfer matrices  $\mathbb{T}_\pm$  from site  $r - 1$  to  $r$  are given by the values of  $\nu(y_r, x_r)$ . In the calculation of the expectation value of  $\Sigma_r^\alpha$  placed at site  $r$ , we define a modified transfer matrix  $\mathbb{T}_+^x$  at site  $r$  that sums over the states at  $r$ , with the appropriate sign of the state  $x_r$ . The rest of the transfer matrices remain the same and contribute to the sum over all possible states. We have

$$\begin{aligned}
\mathbb{T}_+^x &= \begin{bmatrix} \nu(+1, +1) & -\nu(+1, -1) \\ \nu(-1, +1) & -\nu(-1, -1) \end{bmatrix}, \\
&= \mathbb{T}_+ \tau^z \\
\text{where } \tau^z &= \begin{pmatrix} 1 & 0 \\ 0 & -1 \end{pmatrix},
\end{aligned} \tag{3.32}$$

and

$$\begin{aligned}
\mathbb{T}_-^x &= \begin{bmatrix} -\nu(+1, -1) & \nu(+1, +1) \\ -\nu(-1, -1) & \nu(-1, +1) \end{bmatrix}, \\
&= -\mathbb{T}_- \tau^z.
\end{aligned} \tag{3.33}$$

Similarly for  $\Sigma_r^y$

$$\begin{aligned}
\mathbb{T}_+^y &= \begin{bmatrix} \nu(+1, +1) & \nu(+1, -1) \\ -\nu(-1, +1) & -\nu(-1, -1) \end{bmatrix}, \\
&= \tau^z \mathbb{T}_+,
\end{aligned} \tag{3.34}$$

and

$$\begin{aligned}
\mathbb{T}_-^y &= \begin{bmatrix} \nu(+1, -1) & \nu(+1, +1) \\ -\nu(-1, -1) & -\nu(-1, +1) \end{bmatrix}, \\
&= \tau^z \mathbb{T}_-.
\end{aligned} \tag{3.35}$$

Using the fact that the action of  $\Sigma_r^z$  on the states is  $\Sigma_r^x \Sigma_r^y$  we can write the modified transfer matrix for  $\Sigma_r^z$

$$\begin{aligned}
\mathbb{T}_+^z &= \begin{bmatrix} \nu(+1, +1) & -\nu(+1, -1) \\ -\nu(-1, +1) & \nu(-1, -1) \end{bmatrix}, \\
&= \tau^z \mathbb{T}_+ \tau^z,
\end{aligned} \tag{3.36}$$

and

$$\begin{aligned}
\mathbb{T}_-^z &= \begin{bmatrix} -\nu(+1, -1) & \nu(+1, +1) \\ \nu(-1, -1) & -\nu(-1, +1) \end{bmatrix}, \\
&= -\tau^z \mathbb{T}_- \tau^z.
\end{aligned} \tag{3.37}$$

Thus we can write the following formula for the expectation value of the  $\Sigma_r^\alpha$  operator in a general sector with a  $W$ -configuration  $\mathcal{W}$

$$\langle \Sigma_{r+1}^\alpha \rangle_{\mathcal{W}} = \text{Tr} \left[ \left( \prod_{j=r+1}^N \mathbb{T}_{W_j} \right) \mathbb{T}_{W_r}^\alpha \left( \prod_{i=1}^{r-1} \mathbb{T}_{W_i} \right) \right] / \Gamma(\{\mathcal{W}\}),$$

where

$$\begin{aligned} \mathbb{T}_{W_r}^x &= W_r \mathbb{T}_{W_r} \tau^z, \\ \mathbb{T}_{W_r}^y &= \tau^z \mathbb{T}_{W_r}, \\ \mathbb{T}_{W_r}^z &= W_r \tau^z \mathbb{T}_{W_r} \tau^z. \end{aligned} \quad (3.38)$$

We now compute the expectation values of  $\Sigma_r^\alpha$  in two sectors: the sector  $\mathcal{W}_0$  with all  $W_n = +1$ , and the sector  $\mathcal{W}_1$  in which one of the  $W_n = -1$  and all the other  $W_n = +1$  (without loss of generality we pick  $W_N = -1$ ). The expressions for  $\langle \Sigma_r^\alpha \rangle_{\mathcal{W}_{0,1}} \equiv \langle \Sigma_r^\alpha \rangle_{0,1}$  can be evaluated to be

$$\begin{aligned} \langle \Sigma_r^x \rangle_0 &= \langle \Sigma_r^y \rangle_0 = \text{Tr} [\tau^z \mathbb{T}_+^N] / \Gamma(\{\mathcal{W}_0\}), \\ \langle \Sigma_r^z \rangle_0 &= \text{Tr} [\tau^z \mathbb{T}_+ \tau^z \mathbb{T}_+^{N-1}] / \Gamma(\{\mathcal{W}_0\}), \end{aligned} \quad (3.39)$$

and

$$\begin{aligned} \langle \Sigma_r^x \rangle_1 &= \text{Tr} [\mathbb{T}_+^{N-r+1} \tau^z \mathbb{T}_+^{r-1} \tau^x] / \Gamma(\{\mathcal{W}_1\}), \\ \langle \Sigma_r^y \rangle_1 &= \text{Tr} [\mathbb{T}_+^{N-r} \tau^z \mathbb{T}_+^r \tau^x] / \Gamma(\{\mathcal{W}_1\}), \\ \langle \Sigma_r^z \rangle_1 &= \text{Tr} [\mathbb{T}_+^{N-r} \tau^z \mathbb{T}_+ \tau^z \mathbb{T}_+^{r-1} \tau^x] / \Gamma(\{\mathcal{W}_1\}). \end{aligned} \quad (3.40)$$

A similar procedure can be used to evaluate the spin-textures of various operators in the different  $\{\mathcal{W}\}$  sectors of this model.

### 3.6 The $S = 1$ Model

We now focus on the Kitaev chain with spin-1's at each site. We work with the natural spin-1 representation in which

$$(S^\alpha)_{\beta\gamma} = i\epsilon_{\alpha\beta\gamma}. \quad (3.41)$$

In this representation, the matrices  $\Sigma^\alpha$  are diagonal and are given by

$$\begin{aligned}
\Sigma^x &= \begin{pmatrix} 1 & 0 & 0 \\ 0 & -1 & 0 \\ 0 & 0 & -1 \end{pmatrix}, \\
\Sigma^y &= \begin{pmatrix} -1 & 0 & 0 \\ 0 & 1 & 0 \\ 0 & 0 & -1 \end{pmatrix}, \\
\Sigma^z &= \begin{pmatrix} -1 & 0 & 0 \\ 0 & -1 & 0 \\ 0 & 0 & 1 \end{pmatrix}.
\end{aligned} \tag{3.42}$$

We note that these matrices satisfy  $\Sigma^x \Sigma^y \Sigma^z = I$ . We denote the basis vectors by  $|x\rangle$ ,  $|y\rangle$  and  $|z\rangle$  defined as

$$|x\rangle = \begin{pmatrix} 1 \\ 0 \\ 0 \end{pmatrix}, \quad |y\rangle = \begin{pmatrix} 0 \\ 1 \\ 0 \end{pmatrix}, \quad |z\rangle = \begin{pmatrix} 0 \\ 0 \\ 1 \end{pmatrix}. \tag{3.43}$$

We then see that the 9 possible states at sites  $(n, n+1)$  are given by

$$|xy\rangle, |xz\rangle, |yx\rangle, |zy\rangle \text{ and } |zz\rangle \text{ with } W_n = 1, \tag{3.44}$$

and

$$|xx\rangle, |yy\rangle, |yz\rangle \text{ and } |zx\rangle \text{ with } W_n = -1. \tag{3.45}$$

From Eq. (3.41) we have,

$$\begin{aligned}
S^x|x\rangle &= 0, & S^y|x\rangle &= i|z\rangle, & S^z|x\rangle &= -i|y\rangle, \\
S^x|y\rangle &= -i|z\rangle, & S^y|y\rangle &= 0, & S^z|y\rangle &= i|x\rangle, \\
S^x|z\rangle &= i|y\rangle, & S^y|z\rangle &= -i|x\rangle, & S^z|z\rangle &= 0.
\end{aligned} \tag{3.46}$$

Eqs. (3.42) and (3.46) imply that  $(S^\alpha)^2 = (1 - \Sigma^\alpha)/2$ . For the 5 states in Eq. (3.44) satisfying  $W_n = 1$ , we have the following actions of the relevant term in the Hamiltonian,

$$\begin{aligned}
S_1^x S_2^y |xy\rangle &= 0, \\
S_1^x S_2^y |xz\rangle &= 0, \\
S_1^x S_2^y |zy\rangle &= 0, \\
S_1^x S_2^y |zz\rangle &= |yx\rangle, \\
S_1^x S_2^y |yx\rangle &= |zz\rangle.
\end{aligned} \tag{3.47}$$

For the 4 states in Eq. (3.45) satisfying  $W_n = -1$ , the actions of the relevant term in the Hamiltonian are given by

$$\begin{aligned}
S_1^x S_2^y |xx\rangle &= 0, \\
S_1^x S_2^y |yy\rangle &= 0, \\
S_1^x S_2^y |yz\rangle &= -|zx\rangle, \\
S_1^x S_2^y |zx\rangle &= -|yz\rangle.
\end{aligned} \tag{3.48}$$

As mentioned earlier, for an open chain with sites numbered from 1 to  $N$ , we find that  $S_1^x$  and  $S_N^y$  commute with  $H$ . We define the operators,

$$\tau^1 \equiv iW_1 S_1^x, \quad \tau^2 \equiv S_1^x, \tag{3.49}$$

$$\tau^3 \equiv -S_1^x W_1 S_1^x, \quad \tau^0 \equiv \frac{1}{2} (1 - (S_1^x)^2). \tag{3.50}$$

It can be verified that these operators obey a  $SU(2) \times U(1)$  algebra. Exactly the same construction on the last bond, with  $S_1^x \rightarrow S_N^y$  and  $W_1 \rightarrow W_N$ , yields the same algebra on that bond.

### 3.7 Mapping to a Spin-1/2 Chain

For a given value of the state of the spin at site  $n$ , and a given value of  $W_n$ , there are at most two choices for the spin state at site  $n+1$ . Hence it is clear that the Hilbert space of a given sector can be mapped into the Hilbert space of a spin-1/2 chain, with some states excluded which correspond to infinite energy. However, in general, the corresponding Hamiltonian would have a rather complicated form, with long-ranged interactions. The mapping is easy to construct explicitly in the sector with all  $W_n = +1$ , and the corresponding Hamiltonian has only local interactions. This is what we now proceed to show.

Consider the state  $zzzz \dots$  that belongs to the sector with all  $W_n = +1$ . The only allowed process in this sector is  $zz \rightleftharpoons yx$  [Eqs. (3.47)]. We may think of this process as a quantum dimer deposition-evaporation model. The  $z$ -spins are treated as empty sites; two empty sites can be changed to being occupied by a dimer  $yx$  by a ‘deposition’ process, and conversely,  $yx$  can ‘evaporate’ and become  $zz$  again. The dimers have a hard-core constraint, and a site cannot be shared by two dimers. The dimers are oriented: the ‘head’  $x$  being to the right of the ‘tail’  $y$ .

This dimer deposition-evaporation model can also be described as a deposition-evaporation of a nearest-neighbour exclusion lattice gas. We just think of the heads as particles, and do not distinguish between the tails and empty sites, except for ensuring that we deposit a particle at a site only if it is empty and both its nearest neighbours are also empty. Then

this model is described by the Hamiltonian

$$H_d = -\frac{1}{4} \sum_n (1 - \sigma_{n-1}^z) \sigma_n^x (1 - \sigma_{n+1}^z). \quad (3.51)$$

We note that this model is different from the dimer deposition-evaporation models studied earlier [22], in that the two ends of the dimer are distinct, and there is no reconstitution. Also, this Hamiltonian does not have an interpretation as the evolution operator of a classical Markov process, as there are no diagonal terms corresponding to probability conservation. We have introduced a minus sign in the Hamiltonian for later convenience. This does not change the eigenvalue spectrum as the eigenvalues of  $H_d$  occur in pairs  $\pm e_i$ .

### 3.8 Variational Study of the Ground State

We will now use a variational approach to study the ground state of the Hamiltonian  $H_d$  with periodic boundary conditions. We use the  $z$ -basis, and denote the  $\uparrow$  state at the site  $i$  by an occupied site ( $n_i = 1$ ), and the  $\downarrow$  state by an empty state ( $n_i = 0$ ). Since two adjacent sites cannot be simultaneously occupied, the state space is that of hard-core particles with nearest-neighbour exclusion on a line. A configuration  $\mathbf{C}$  is specified by an  $N$ -bit binary string  $0010010101\dots$ , which gives the values of all the  $N$  occupation numbers  $n_i$ . We note that in the basis where all the  $n_i$  are diagonal, the Hamiltonian  $H_d$  has all matrix elements non-positive. This implies that the (real) eigenvector corresponding to the lowest energy will have all components of the same sign in this basis.

For the ground state of  $H_d$ , we consider a variational wave function of the form

$$|\psi\rangle = \sum_{\mathbf{C}} \sqrt{\text{Prob}(\mathbf{C})} |\mathbf{C}\rangle, \quad (3.52)$$

where  $\text{Prob}(\mathbf{C})$  is chosen as the probability of the lattice gas configuration  $\mathbf{C}$  in some classical equilibrium ensemble corresponding to a suitably chosen lattice gas Hamiltonian. Clearly, this trial vector is normalized, with

$$\langle\psi|\psi\rangle = 1. \quad (3.53)$$

With this choice,  $\text{Prob}(\mathbf{C})$  is also the probability of the configuration  $\mathbf{C}$  in the quantum mechanical variational state  $|\psi\rangle$ .

The simplest choice of the lattice-gas Hamiltonian is that of a classical lattice gas with nearest-neighbour exclusion, and a chemical potential  $\mu$ , with a Hamiltonian given by

$$H_{cl} = +\infty \sum_i n_i n_{i+1} - \mu \sum_i n_i, \quad (3.54)$$

where we use the convention that  $0 \cdot \infty = 0$ ; hence the first term in (3.54) allows states with  $n_i n_{i+1} = 0$  but disallows states with  $n_i n_{i+1} = 1$ . Let us denote  $z = \exp(\beta\mu)$ . It is

straightforward to determine various correlation functions in the thermal equilibrium state corresponding to  $H_{cl}$ . The probability of a configuration  $\mathbf{C}$  is given by

$$\text{Prob}(\mathbf{C}) = \exp[-\beta H_{cl}(\mathbf{C})]/\Omega_N(z), \quad (3.55)$$

where  $\Omega_N(z)$  is the grand partition function for a ring of  $N$  sites. The grand partition function  $\Omega_N(z)$  can be determined using the standard transfer matrix technique. For the nearest neighbour exclusion gas we use the basis states given by the occupation numbers at each site  $\{(0), (1)\}$ . We thus have the  $2 \times 2$  matrix  $\mathbf{T}_2$  given by

$$\mathbf{T}_2 = \begin{bmatrix} 1 & 1 \\ z & 0 \end{bmatrix}, \quad (3.56)$$

with eigenvalues

$$\lambda_{\pm} = (1 \pm \sqrt{1 + 4z})/2, \quad (3.57)$$

We now calculate the expectation value of the Hamiltonian  $\langle \Psi | H_d | \Psi \rangle$ . The matrix element of the  $i$ -th term is clearly zero, unless  $n_{i-1} = n_{i+1} = 0$ . Now, in the calculation of the expectation value of  $\langle \Psi | H_d | \Psi \rangle$  the only configurations that have a nonzero contribution are the those with the configuration  $n_{i-1}n_i n_{i+1} = 010$  in  $|\Psi\rangle$  along with  $n_{i-1}n_i n_{i+1} = 000$  in  $\langle \Psi |$  and vice versa, since the action of the Hamiltonian deposits or evaporates particles at a given position. The corresponding coefficients of the terms in the wave function are  $\sqrt{z \text{Prob}(000)}$  and  $\sqrt{\text{Prob}(000)}$  respectively. Thus we have

$$\langle H_d \rangle / N = -2\sqrt{z} \text{Prob}(000) = \frac{-2}{\sqrt{z}} \text{Prob}(010). \quad (3.58)$$

Here  $\text{Prob}(000)$  denotes the probability that three randomly selected consecutive sites in the ring will be empty in the classical ensemble, and a similar definition for  $\text{Prob}(010)$ . This is easily calculated for the Hamiltonian  $H_{cl}$  in the limit of large  $N$ . We have

$$\text{Prob}(010) = \text{Prob}(1) = \rho, \quad (3.59)$$

where  $\rho$  is the density per site given by

$$\rho = z \frac{d}{dz} \log(\lambda_+) = \frac{1}{2} - \frac{1}{2\sqrt{1+4z}}. \quad (3.60)$$

This yields the following expression for the expectation value of the Hamiltonian

$$\langle H_d \rangle = -\frac{2}{\sqrt{z}} \left( \frac{1}{2} - \frac{1}{2\sqrt{1+4z}} \right). \quad (3.61)$$

Extremizing  $\langle H_d \rangle$  with respect to  $z$ , we find that the minimizing value occurs for  $z = 0.405$ , yielding  $\langle H_d \rangle = -0.60057$ . This gives us the variational bound on the ground state energy per site  $E_0$

$$E_0 \leq -0.60057. \quad (3.62)$$

This energy is somewhat higher than the energy obtained by exact diagonalisation [21] indicating that the correlations in the classical Hamiltonian  $H_{cl}$  do not exactly reproduce the correlations in the quantum ground state of  $H_d$ .

We can attempt a better variational calculation by considering a classical lattice gas with an additional next-nearest-neighbour interaction. The Hamiltonian of this lattice gas is

$$H'_{cl} = +\infty \sum_i n_i n_{i+1} - K \sum_i n_i n_{i+2} - \mu \sum_i n_i. \quad (3.63)$$

Let us denote  $z = \exp(\beta\mu)$ , and  $u = \exp(\beta K)$ . In this case, since the interactions extend to the next-nearest-neighbour, the basis states need to contain the occupation numbers of two consecutive sites. We thus have a  $3 \times 3$  transfer matrix in the two-site occupation number basis  $\{(00), (10), (01)\}$  given by

$$\mathbf{T}_3 = \begin{bmatrix} 1 & 0 & 1 \\ z & 0 & zu \\ 0 & 1 & 0 \end{bmatrix}. \quad (3.64)$$

The probability of the configuration  $\mathbf{C}$  in the equilibrium ensemble is given by

$$\text{Prob}(\mathbf{C}) = \exp[-\beta H'_{cl}(\mathbf{C})] / \Omega_N(z, u), \quad (3.65)$$

where  $\Omega_N(z, u)$  is the grand partition function for a ring of  $N$  sites. We then get

$$\begin{aligned} -\langle H_d \rangle / N &= 2\text{Prob}(00000)\sqrt{z} + 4\text{Prob}(10000)\sqrt{zu} \\ &\quad + 2\text{Prob}(10001)\sqrt{zu^2}, \end{aligned} \quad (3.66)$$

Here  $\text{Prob}(00000)$  is the probability of finding a randomly selected set of five consecutive sites all unoccupied in the equilibrium ensemble corresponding to the Hamiltonian  $H'_{cl}$ . These probabilities are also easily calculated. Treating  $z$  and  $u$  as variational parameters, we find that  $\langle H_d \rangle$  is minimized for  $z = 0.35198$  and  $u = 1.3752$ . For these values one finds that the density is  $\rho = 0.1952$ ,  $\text{Prob}(00000) = 0.28066$ ,  $\text{Prob}(10000) = 0.082804$ , and  $\text{Prob}(10001) = 0.02443$ .

These give

$$E_0 \leq -0.60333, \quad (3.67)$$

which is an improvement over Eq. (3.62), and quite close to the extrapolated value of  $-0.60356$  obtained from exact diagonalisation. This estimate may be further improved by taking third-neighbour interactions in the classical Hamiltonian.

### 3.9 Estimating the Energy Gap

Exact diagonalisation studies suggest that the first excited state of the 1-dimensional spin-1 Kitaev model lies in the sector with one  $W_n = -1$  and the rest  $+1$  [21]. We thus study this sector using the variational techniques of Section 3.8 and try to estimate the gap of the first excited state (the lowest energy state in this sector) from the ground state energy of the system. We set  $W_N = -1$  and the rest of the  $W_n$ 's equal to  $+1$ . Two states with this configuration of  $W_n$ 's are  $|xzz\dots zzz\rangle$ , where the state at site 1 is  $|x\rangle$  and the rest of the sites are  $|z\rangle$ , and  $|zzz\dots zzy\rangle$ , where the state at site  $N$  is  $|y\rangle$  and the rest of the sites are  $|z\rangle$ .

Other states with the same  $\{W_n\}$  can be constructed from these two states by the action of the Hamiltonian  $H_d$  as defined in Eq. (3.51). For convenience we redefine this in terms of the original spin variables below

$$H_d = \sum_{i=1}^N H_i \quad \text{where} \quad H_i = S_i^x S_{i+1}^y. \quad (3.68)$$

$H_i$  changes  $|z_i z_{i+1}\rangle \rightleftharpoons |y_i x_{i+1}\rangle$ . This process can be thought of as a hard-core particle deposition-evaporation process, as in the previous section. The state  $|zz\rangle$  represents no particles on either site and  $|yx\rangle$  represents a particle at  $y$  and none at  $x$ . For the  $|xzz\dots zzz\rangle$  state,  $H_i$  deposits or removes particles on sites from  $i = 2$  to  $N - 1$ .  $H_1$  annihilates the state. Similarly for the  $|zzz\dots zzy\rangle$  state, the particles can be added and removed on sites from  $i = 1$  to  $N - 2$ , with  $H_{N-1}$  annihilating the state.

Thus, the states in this sector fall into two categories,  $|xzz\dots zzz\rangle$  along with states built from placing particles on it, and  $|zzz\dots zzy\rangle$  along with the corresponding states formed by adding particles. We represent the first type of state  $|xS\rangle$  by  $|XC\rangle$  where  $S$  is a string of  $x, y, z$  and  $C$  is the corresponding configuration of particles,  $C \equiv 0n_2n_3\dots n_{N-1}$ , with  $n_i$  being the occupation number of the site  $i$  (0 or 1). The second category of states is represented by  $|Ty\rangle \equiv |DY\rangle$  where  $T$  is a string of  $x, y, z$  and  $D$  represents the configuration of particles in this state,  $D \equiv n_1n_2\dots n_{N-2}0$ .  $H_N$  converts the  $|zx\rangle$  on the  $N$ 'th plaquette to  $-|yz\rangle$  and vice versa only if the site  $N - 1$  (and 1) is unoccupied, thereby converting  $|XC\rangle$  to  $-|CY\rangle$ .

Now, from the action of the Hamiltonian on the basis states  $|XC\rangle$  and  $|DY\rangle$ , it is easy to see that the ground state wave function is of the form

$$|\psi_{\text{var}}\rangle = \frac{1}{\sqrt{2}} \left( \sum_C \sqrt{\text{Prob}(XC)} |XC\rangle - \sum_D \sqrt{\text{Prob}(DY)} |DY\rangle \right), \quad (3.69)$$

where  $\text{Prob}(XC)$  is computed as the probability of the configuration  $C$  occurring in the equilibrium ensemble of a hard core lattice gas on an open chain of length  $N - 2$  with a suitably chosen classical Hamiltonian, and similarly for  $\text{Prob}(DY)$ . The negative sign between the two terms ensures that the sign of the coefficients in the wave function are all

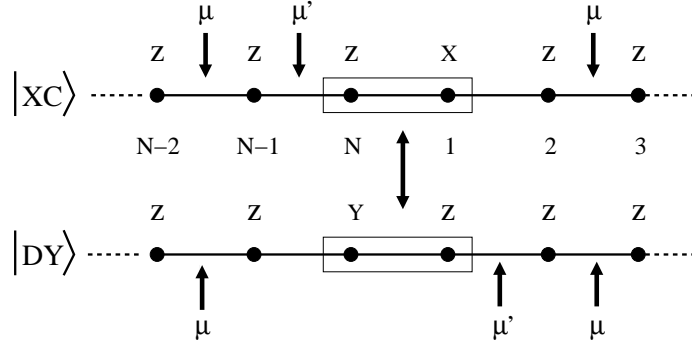


Figure 3.2: Figure depicting the two configurations  $|XC\rangle$  and  $|DY\rangle$ , in the  $W_N = -1$  sector. Dimers can be added at the sites 2 to  $N-1$  in the configuration  $|XC\rangle$  and correspondingly at  $N-2$  to 1 in the configuration  $|DY\rangle$ . Addition of particles at the end of the chain carries a different weight  $\mu'$  from the rest.

positive. It is easy to see that

$$\langle \psi_{\text{var}} | \psi_{\text{var}} \rangle = 1. \quad (3.70)$$

The Hamiltonian is invariant under the following transformation  $|XC\rangle \rightarrow |C^T Y\rangle$ , where  $C^T$  is the configuration  $C$  with the order of particles reversed ( $n_i \rightarrow n_{N-i}$ ). Hence the ground state wave function must also be invariant under this symmetry transformation. We incorporate this symmetry explicitly in the wave function  $|\psi_{\text{var}}\rangle$  by the condition

$$\text{Prob}(XC) = \text{Prob}(C^T Y). \quad (3.71)$$

We choose the classical lattice gas Hamiltonian to be that of a nearest neighbour exclusion gas with equal fugacities for deposition or evaporation of particles at all sites except at the end of the chain. As placing a particle on the site adjacent to the  $N$ 'th site is less favourable than the others, we set the activity of this site as different from the rest. We have

$$H_{cl}^C = +\infty \sum_{i=2}^{N-2} n_i n_{i+1} - \sum_{i=2}^{N-2} \mu n_i - \mu' n_{N-1}. \quad (3.72)$$

The probability of each configuration is then given by

$$\text{Prob}(C) = \exp[-\beta H_{cl}^C(C)] / \Omega_{N-2}(z, z'), \quad (3.73)$$

where  $z = \exp(\beta\mu)$  and  $z' = \exp(\beta\mu')$  and  $\Omega_{N-2}(z, z')$  is the grand partition function of an open chain with the above classical Hamiltonian. We now calculate the expectation value of the energy of the Hamiltonian for this wave function. In the calculation below we find the largest eigenvalue of the system, since the eigenvalues come in pairs. We have

$$\sum_{i=1}^{N-1} \langle \psi_{\text{var}} | H_i | \psi_{\text{var}} \rangle = \frac{2}{\sqrt{z'}} \text{Prob}(1_{N-1}^C) + \sum_{i=2}^{N-2} \frac{2}{\sqrt{z}} \text{Prob}(1_i^C), \quad (3.74)$$

where  $\text{Prob}(1_i^C)$  is the probability of the occurrence of a dimer at site  $i$  in the configuration  $|XC\rangle$  and similarly for D. We use the fact that  $\text{Prob}(1_i^D) = \text{Prob}(1_{N-i}^C)$  in the above calculation.

The term  $H_N$  connects the states  $|XC\rangle$  and  $|DY\rangle$ . Using (3.71) we get

$$\langle \psi_{\text{var}} | H_N | \psi_{\text{var}} \rangle = 1 - \text{Prob}(1_{N-1}^C). \quad (3.75)$$

These probabilities can be computed from the grand partition function as

$$\begin{aligned} \sum_{i=2}^{N-2} \text{Prob}(1_i^C) &= z \frac{d}{dz} \log(\Omega_{N-2}(z, z')), \\ \text{Prob}(1_{N-1}^C) &= z' \frac{d}{dz'} \log(\Omega_{N-2}(z, z')). \end{aligned} \quad (3.76)$$

Thus we have

$$\begin{aligned} \langle \psi_{\text{var}} | H_d | \psi_{\text{var}} \rangle &= 1 + (2\sqrt{z'} - z') \frac{d}{dz'} \log(\Omega_{N-2}(z, z')) \\ &\quad + 2\sqrt{z} \frac{d}{dz} \log[\Omega_{N-2}(z, z')]. \end{aligned} \quad (3.77)$$

We can calculate the partition function using a transfer matrix technique.  $\Omega_{N-2}(z, z')$ , the partition function of a chain of length  $N - 2$ , where the last site has a fugacity  $z'$ , is given by

$$\Omega_{N-2}(z, z') = \Omega_{N-3}(z) + z' \Omega_{N-4}(z), \quad (3.78)$$

where  $\Omega_{N-3}(z)$  and  $\Omega_{N-4}(z)$  are partition functions of an open chain (with all fugacities equal to  $z$ ) of length  $N - 3$  and  $N - 4$  respectively. In the limit of large  $N$  this reduces to

$$\Omega_{N-2}(z, z') = (\lambda_+ + z') \Omega_{N-4}(z) = \lambda_+^N \Omega', \quad (3.79)$$

where  $\Omega'$  is defined as

$$\Omega' = (z' + \lambda_+) \frac{(1 - \rho)}{\lambda_+^3}. \quad (3.80)$$

Now we have

$$\begin{aligned} \langle \psi_{\text{var}} | H_d | \psi_{\text{var}} \rangle &= 1 + (2\sqrt{z'} - z') \frac{d}{dz'} \log(\Omega') + 2\sqrt{z} \frac{d}{dz} \log(\Omega') \\ &\quad + 2\sqrt{z} \frac{d}{dz} \log(\lambda_+^N). \end{aligned} \quad (3.81)$$

The term  $2\sqrt{z} \frac{d}{dz} \log(\lambda_+^N)$  is exactly the value of  $\langle H_d \rangle$  in the sector with all  $W_n = +1$  which is the ground state sector (Eq. 3.61). This term is proportional to  $N$  and dominates over the other terms in the limit of large  $N$ . Hence the extremization of  $\langle H \rangle$  yields the value  $NE_0$  and  $z = z_g$  where  $E_0$  is the ground state energy per site of the Hamiltonian (in the sector with all  $W_n = +1$  sector,  $E_0 = -0.6005$ ) and  $z_g$  is the minimizing value of  $z$  in that sector ( $z_g = 0.4045$ ). Substituting this value of  $z$  back in (3.81) and extremizing over  $z'$  we obtain  $z' = 0.2537$  yielding

$$\langle \psi_{\text{var}} | H_d | \psi_{\text{var}} \rangle = -N(0.6005) + 0.1875. \quad (3.82)$$

This implies the following bound on the lowest eigenvalue in this sector

$$E'_0 \leq NE_0 + 0.1875. \quad (3.83)$$

Thus we arrive at an estimate of the energy gap  $\Delta = 0.1875$  for this system. This estimate can be improved by adding more parameters in the wave function, or equivalently in the classical lattice gas Hamiltonian. In an open chain, the occupation numbers at the ends of the chain are different from the ones in the bulk. We incorporate this fact by successively changing the fugacities at the ends of the chain. A two parameter wave function would have  $z'$  and  $z''$  at the two opposite ends. Extremizing with respect to these parameters we find the energy gap to be 0.1642 with  $z' = 0.2537$  and  $z'' = 0.6670$ . A four parameter wave function would have fugacities  $z'z'''$  at one end and  $z''z''''$  at the other, and similarly for higher parameter wave functions. Table 3.9 shows the improvement in the value of the energy gap with the number of parameters used.

We thus obtain a variational estimate of the gap of the first excited state from the ground state energy. This matches quite well with the numerical estimates of the energy gap [21].

### 3.10 Study of Ground States in Other Sectors

We now define a related, more general Hamiltonian for the system that explicitly contains a defect energy term

$$H(\lambda) = H_K + \lambda \sum_n W_n. \quad (3.84)$$

Since the  $W_n$ 's commute with  $H_K$ , all the eigenvectors of  $H_K$  can be chosen to be

No. of Parameters	$\Delta$
1	0.18751
2	0.16419
4	0.15845
6	0.15642
8	0.15578
10	0.15556

Table 3.1: Table showing the estimates of the energy gap with varying number of parameters in the trial wave function.

simultaneous eigenvectors of  $H(\lambda)$ , for all  $\lambda$ . However, if we vary  $\lambda$ , we can get different eigenvectors to have the lowest energy. Clearly, if  $\lambda$  is large and positive, the ground state will lie in the sector with all  $W_n = -1$ . Conversely, if  $\lambda$  is large and negative, the ground state is the lowest energy eigenvector in the sector with all  $W_n = +1$ . In both these regions, the gap in the excitation spectrum is of order  $|\lambda|$ . As we vary  $\lambda$  from  $-\infty$  to  $+\infty$ , initially the gap decreases and becomes zero at some value  $\lambda_1^c$ . We then expect a gap to open up again when  $\lambda$  is greater than a second critical point  $\lambda_2^c > \lambda_1^c$ .

We can extend the treatment of the previous section to sectors with two or more  $W_n$ 's negative. There is an energy  $\Delta$  required to create a single negative  $W_n$ . Thus  $\lambda_1^c = \Delta/2$ . If two defects are spaced far apart, the energy required to create two defects will be nearly  $2\Delta$ , with the correction term decreasing exponentially with the distance between the defects. For  $n$  defects, the energy would be minimized if the defects are equally spaced. Thus the distance between the defects is  $N/n$ , and the energy cost of creating  $n$  defects  $\Delta E(n)$  in  $H(\lambda)$ , for small  $n$ , is well approximated by

$$\Delta E(n) \approx -2n\lambda + n\Delta + nA \exp(-BN/n), \quad (3.85)$$

where  $A$  and  $B$  are some constants. This then implies that for  $\lambda = \lambda_1^c + \epsilon$ , the density of defects in the true ground state of  $H(\lambda)$  will vary as  $1/|\log \epsilon|$ .

We consider a sector with exactly two of the  $W_n$ 's equal to  $+1$ , and the rest negative. Let us start with the state  $|zxxx \cdots zxxx \cdots\rangle$ , where the spins at two sites  $i = 1$  and  $i = m + 1 \leq N$  are in the state  $z$  (these states will be referred to as  $z$ -spins in the following discussion). This corresponds to  $W_N = W_m = +1$ . Then, under the action of  $H(\lambda)$ , this state mixes with other states where the positions of the  $z$ -spins can change; the general state in this sector may be labelled by the positions of the  $z$ -spins,  $r_1$  and  $r_2$ . We denote the vector as  $|r_1, r_2\rangle$ , where  $1 \leq r_1 \leq m < r_2 \leq N$ . Then, for  $1 < r_1 < m$  and  $m + 1 < r_2 < N$ , we get

$$H_K |r_1, r_2\rangle = -|r_1, r_2 + 1\rangle - |r_1 + 1, r_2\rangle - |r_1, r_2 - 1\rangle - |r_1 - 1, r_2\rangle. \quad (3.86)$$

If the first  $z$ -spin is at  $m$  and the second is not at  $m + 1$ , the first spin cannot move to  $m + 1$ , as that site would be in spin state  $y$ , and the state  $zy$  cannot change [Eqs. (3.47)]. Similarly, if  $r_2 = N$ , and  $r_1 \neq 1$ , then the second spin cannot move to the right. However, if the two  $z$ -spins are adjacent, then they can change to a state  $zz \rightleftharpoons yx$  [Eqs. (3.47)]. But from the state  $yx$  the state can only return to  $zz$ .

If we disallow the transitions to state  $yx$ , the  $z$ -spins act as independent particles moving in two disjoint regions of space,  $1 \leq r_1 \leq m$  and  $m + 1 \leq r_2 \leq N$ . In this case, the minimum energy of this system is just the sum of the energies of two particles. This energy is an upper bound on the true ground state energy of this system. Thus, we find that the ground state energy in this sector,  $E_{2\text{-sector}}^g$ , has the upper bound

$$E_{2\text{-sector}}^g \leq -2J \cos\left(\frac{\pi}{m+1}\right) - 2J \cos\left(\frac{\pi}{N-m+1}\right) - \lambda(N-4). \quad (3.87)$$

Next, suppose that the state with the  $m$ -th site in the  $y$ -state and the  $(m+1)$ -th in the  $x$ -state is called the state  $r_1 = m + 1, r_2 = 1$ , and a similar definition for the other end. Then the range of  $r_1$  is at most  $m + 1$ , and the range of  $r_2$  is at most  $l - m + 1$ . By excluding some states (here  $r_1 = m + 1, r_2 \neq r_1$ ), the kinetic energy can only increase, and hence we have

$$E_{2\text{-sector}}^g \geq -2J \cos\left(\frac{\pi}{m+2}\right) - 2J \cos\left(\frac{\pi}{N-m+2}\right) - \lambda(N-4). \quad (3.88)$$

For  $N, m \gg 1$ , these bounds can be expanded in powers of  $1/m$ , and have the same leading order correction. Also, the minimum energy corresponds to equally spaced defects, with  $m = N/2$ .

We can easily extend the discussion to sectors with three, four or more  $W_n$ 's equal to  $+1$ . In case the lengths of the intervals between the positive  $W_n$ 's are  $m_1, m_2, m_3, \dots, m_r$ , the bounds on the lowest energy in this sector  $E_{r\text{-sector}}^g$  become

$$-2J \sum_{i=1}^r \cos\left(\frac{\pi}{m_i+2}\right) - \lambda(N-2r) \leq E_{r\text{-sector}}^g \leq -2J \sum_{i=1}^r \cos\left(\frac{\pi}{m_i+1}\right) - \lambda(N-2r). \quad (3.89)$$

Thus, we see that for  $\lambda > J$ , the ground state belongs to the sector with all  $W_n$ 's equal to  $-1$ . If  $\lambda = J(1 - \epsilon)$ , the ground state will be in the sector with  $n$  equispaced bonds with  $W_n = +1$ , where the spacing  $\ell$  between them  $\approx N/n$  is given by  $\epsilon^{-1/2}$ . The minimum energy per site of  $H(\lambda)$  for  $\lambda = J(1 - \epsilon)$  varies as  $\epsilon^{3/2}$  for small  $\epsilon$ . Equivalently, if we restrict ourselves to sectors with only a fraction  $\epsilon$  of  $W_n$ 's having the value  $+1$ , the minimum energy per site varies as  $-\epsilon^{3/2}$ . This is equivalent to the statement that for  $H_K$  corresponding to

$\lambda = 0$ , in the sector with the fractional number of positive  $W_n$ 's being equal to  $\Delta$ , the minimum energy per site varies as  $\Delta^{3/2}$ .

### 3.11 Summary

In this chapter, we first analysed the symmetries of a spin- $S$  Kitaev chain. We found a  $\mathbb{Z}_2$  invariant,  $W_n$ , associated with every link  $(n, n + 1)$ , namely,  $N$  invariants for the model defined on a ring with  $N$  sites. For integer  $S$ , these invariants commute with each other and the Hamiltonian. The Hilbert space can therefore be split into  $2^N$  sectors, where the Hamiltonian is block diagonal. For half-odd integer  $S$ ,  $W_n$  anti-commutes with  $W_{n\pm 1}$  and commutes with the rest. We showed that this implies that all the eigenstates of the half-odd-integer spin models are  $2^{N/2}$ -fold degenerate, thus showing a qualitative difference between the integer and half-odd-integer models. We outlined a procedure to compute the dimensions of the invariant sectors. We showed that the dimension of most of the sectors can be calculated in terms of products of  $2 \times 2$  matrices  $\mathbb{T}_+$  and  $\mathbb{T}_-$ . For  $S = 1$  the number of states in the sector with all  $W_n = 1$  grows as  $\gamma^N$ , where  $\gamma$  is the golden ratio,  $(1 + \sqrt{5})/2$ .

We then studied the spin-1 case in detail. We found that the ground state lies in a sector which can be mapped to a quantum lattice gas model with nearest-neighbour exclusion. We developed a variational wave function that relates the quantum mechanical averages to the correlation functions of a classical lattice gas with nearest-neighbour exclusion. We considered a more general Hamiltonian with a term proportional to the sum of the conserved quantities, and showed that as a function of the coupling constant  $\lambda$ , this would show gapless excitations in the range  $\lambda_1^c \leq \lambda \leq \lambda_2^c$ . We extended our variational calculation to study how the ground state energy and the defect density would vary near the two critical points  $\lambda_1^c$  and  $\lambda_2^c$ . At  $\lambda = \lambda_1^c$ , Eq. (3.85) implies that the energy of the lowest excited state in a system of length  $L$  goes as  $E \sim \exp(-BL)$ , corresponding to a state in which one  $W_n = -1$  while all the other  $W_n = 1$ . By the usual scaling arguments, the gap to the first excited state goes as  $1/L^z$ , where  $z$  is the dynamical critical exponent. We therefore conclude that  $z = \infty$ . At  $\lambda = \lambda_2^c$ , the low-energy excitations form a low-density gas of hard-core particles. In one dimension, this can be mapped to a system of non-interacting spinless fermions with a non-relativistic spectrum  $E \sim k^2$ . Hence in a system of size  $L$ , the gap to the lowest energy states goes as  $1/L^2$  corresponding to  $k \sim 1/L$ ; thus  $z = 2$ . The determination of the value of  $z$  in the critical region  $\lambda_1^c < \lambda < \lambda_2^c$  remains an open problem.

# References

- [1] X.-G. Wen, Phys. Rev. D **68**, 065003 (2003).
- [2] H. Yao and S. A. Kivelson, Phys. Rev. Lett. **99**, 247203 (2007).
- [3] S. Yang, D. L. Zhou, and C. P. Sun, Phys. Rev. B **76**, 180404(R) (2007).
- [4] S. Dusuel, K. P. Schmidt, J. Vidal, and R. L. Zaffino, Phys. Rev. B **78**, 125102 (2008).
- [5] G. Kells, N. Moran, and J. Vala, J. Stat. Mech. P03006 (2009).
- [6] H. Yao, S.-C. Zhang, and S. A. Kivelson, Phys. Rev. Lett. **102**, 217202 (2009).
- [7] C. Wu, D. Arovas, and H.-H. Hung, Phys. Rev. B **79**, 134427 (2009).
- [8] M. Kamfor, S. Dusuel, J. Vidal, and K. P. Schmidt, J. Stat. Mech. P08010 (2010).
- [9] X.-F. Shi, Y. Chen, and J. Q. You, Phys. Rev. B **82**, 174412 (2010)
- [10] T. Si and Y. Yu, Nucl. Phys. B **803**, 428 (2008).
- [11] S. Mandal and N. Surendran, Phys. Rev. B **79**, 024426 (2009).
- [12] V. Karimipour, Phys. Rev. B **79**, 214435 (2009).
- [13] D. Sen and S. Vishveshwara, EPL **91**, 66009 (2010).
- [14] A. Saket, S. R. Hassan, and R. Shankar, Phys. Rev. B **82**, 174409 (2010)
- [15] G. Baskaran, D. Sen, and R. Shankar, Phys. Rev. B **78**, 115116 (2008).
- [16] S. Chandra, K. Ramola, and D. Dhar, Phys. Rev. E **82**, 031113 (2010).
- [17] J. Villain, R. Bidaux, J. P. Carton, and R. J. Conte, J. Phys. (Paris) **41**, 1263 (1980).
- [18] R. Moessner and J. T. Chalker, Phys. Rev. B **58**, 12049 (1998).
- [19] C. L. Henley, Phys. Rev. B **71**, 014424 (2005).
- [20] M. V. Gvozdikova and M. E. Zhitomirsky, JETP Lett. **81**, 236240 (2005).

- 
- [21] Diptiman Sen, R. Shankar, Deepak Dhar, and K. Ramola, *Phys. Rev. B* **82**, 195435 (2010).
- [22] M. Barma, M. D. Grynberg, and R. B. Stinchcombe, *Phys. Rev. Lett.* **70**, 1033 (1993).



## Chapter 4

# The Hard Square Lattice Gas

### 4.1 Introduction

In this chapter we study the lattice gas model of particles on a square lattice with nearest and next-nearest-neighbour exclusion (hard squares). This model undergoes a transition from a fluid phase at low density to a columnar ordered phase at high density. In order to understand the nature of the columnar ordered phase, we develop a high activity perturbation expansion for the free energy per site about a state with perfect columnar order. This is a singular perturbation series in powers of  $1/\sqrt{z}$ , where  $z$  is the fugacity associated with each particle. We show that the different terms of the series can be regrouped to get a Mayer-like series for a polydisperse system of interacting vertical rods in which the  $n$ -th term is of order  $z^{-(n+1)/2}$ . We sum this series to get the exact expansion to order  $1/z^{3/2}$ . We then analyse the nature of the transition from the columnar ordered phase at high density to the fluid phase at low density. We note that the ordered states are related to each other by  $\mathbb{Z}_4$  symmetry transformation. Using a simple coarse grained picture, we argue that the critical properties of the model are that of a more general Ashkin-Teller model. We use symmetry arguments to map the local densities in the model to the Ising energy densities in the corresponding Ashkin-Teller model. We then use Monte Carlo simulations to test our predictions. We locate the critical point of the system as  $z_c = 97.5 \pm 0.5$ . We also study the correlations between various quantities in the system in order to get a fairly precise estimate of the position of the transition on the Ashkin-Teller critical line.

### 4.2 The Model

We consider a system of particles with nearest and next-nearest-neighbour exclusion on the square lattice (Fig. 4.1). The Hamiltonian is either 0 for an allowed configuration and  $\infty$  for a disallowed configuration (if particles are closer than or at the next-nearest-neighbour). Thus we see that the temperature of the system plays no role and the nature of the phases are governed purely by the entropy of the particles. Associated with every particle, we have a fugacity  $z = \exp(-\mu)$ , where  $\mu$  is the chemical potential of the system. The grand

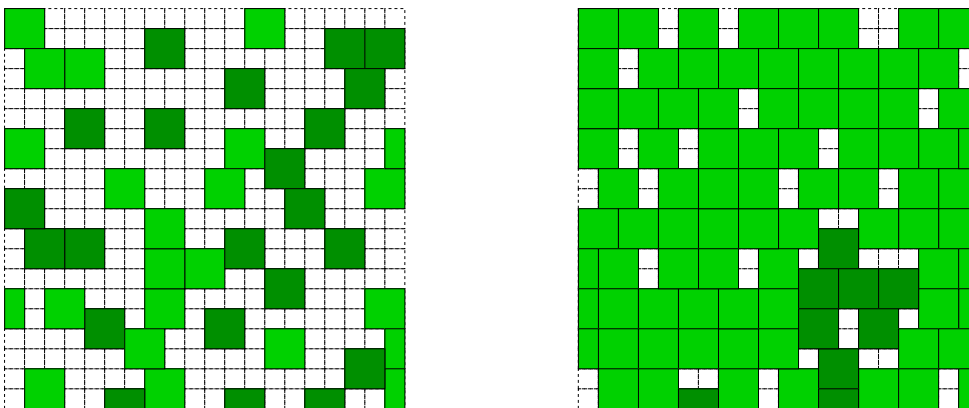


Figure 4.1: A typical configuration of hard squares on the lattice at (Left) low fugacity and (Right) high fugacity. The light green squares correspond to particles on row A, whereas the dark green squares correspond to particles on row B. At high densities, the system is in a columnar ordered phase. The figure depicts a section of a larger system.

canonical partition function of the hard square lattice gas model can be expressed as

$$\Omega(z) = \sum_C z^{n(C)}, \quad (4.1)$$

where  $z$  is the fugacity of the particles,  $n(C)$  is the number of particles in the configuration  $C$  and the sum is over all allowed configurations of hard squares on the lattice.

The Landau free energy per site is defined as

$$f(z) = \lim_{N \rightarrow \infty} -\frac{1}{N} \log \Omega(z), \quad (4.2)$$

where  $N$  is the total number of sites in the lattice. From this we can calculate other thermodynamic quantities. The density of particles at a particular fugacity is given by

$$\rho(z) = -z \frac{d}{dz} f(z). \quad (4.3)$$

The low density Virial series of this model can be computed using standard techniques [1]. We have [2]

$$-f(z) = z - \frac{9}{2!} z^2 + \frac{194}{3!} z^3 - \frac{6798}{4!} z^4 + \dots \quad (4.4)$$

This expansion has a finite radius of convergence determined by the singularity closest to the origin at  $z_0 \approx -0.1$ . The low-density fluid phase has short-ranged correlations between particles, but the high-density columnar-ordered phase has long-range order.

### 4.3 Expansion about the Crystalline Ordered State

We consider the square lattice to be made up of four sublattices labelled 1 to 4 (Fig. 4.2). Rows containing the sites of sublattice 1 and 2 are called A-rows, and those containing

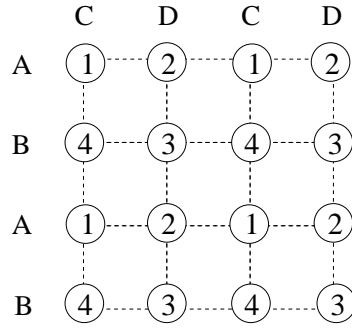


Figure 4.2: We define four sublattices 1 through 4 on the square lattice. Rows containing the sites of sublattice 1 and 2 (3 and 4) will be called A (B) rows. Similarly, columns with sublattice sites 1 and 4 (2 and 3) will be called C (D) columns.

sites of sublattice 3 and 4 are B-rows. Similarly, columns with sublattice sites 1 and 4 are called C-columns and those with sublattice sites 2 and 3 are D-columns. We will specify the position of the square by the position of the top left corner of the square.

At the point  $z = \infty$  the problem of computing the partition function reduces to one of calculating the number of perfect tilings of the lattice by hard squares. On a lattice of size  $L \times L$  (where  $L$  is assumed even), with open boundary conditions, clearly

$$\Omega_{\text{open}}(z \rightarrow \infty) = z^{L^2/4}. \quad (4.5)$$

For a lattice with periodic boundary conditions in both  $x$ - and  $y$ - directions, it is easy to see that we have  $\Omega_{\text{periodic}} = 4(2^{L/2} - 1)z^{L^2/4}$ .

As we decrease  $z$  from  $\infty$  there is a finite density of plaquettes not covered by squares in the system. Suppose we start with a fully packed configuration of squares, with all sites on sublattice 1 and introduce a single vacancy. By sliding squares in the corresponding row, we can break the vacancy into two half-vacancies with in-between squares on the 2-sublattice. These two vacancies can be moved arbitrarily far apart. Thus there are  $\mathcal{O}(L^2)$  configurations of half-vacancies on each row, and there are  $L/2$  possible rows. There is an equal number of configurations with half-vacancies along columns. This leads to

$$\Omega_{\text{open}}(z) = z^{L^2/4} \left( 1 + \frac{1}{z} \mathcal{O}(L^3) + \dots \right). \quad (4.6)$$

This phenomena, which may be called deconfinement of half-vacancies, is the reason behind the failure of the standard Mayer expansion technique, in which the order  $1/z$  term has a coefficient of the order of the volume of the system. Because the standard cumulant expansion fails, this series must be treated using different techniques.

We describe a simple qualitative picture of the system with a small density of defects introduced on the background with perfect crystalline order. The pairs of half-vacancies may be pictured as joined by straight rods, which may be horizontal or vertical. As the number of vacancies is increased, the system can be thought of as composed of horizontal

and vertical rods of arbitrary length which do not overlap, with half-vacancies at either end (Fig. 4.3). This gas of rods of width 2 has the same fugacity associated with rods of all lengths. Now, it is expected that the entropy of these rods is maximized when all of them are aligned, since the presence of a horizontal rod limits the number of allowed vertical rods more than it does a horizontal one. This leads to a nematic ordering of these objects in one particular direction. So as  $z \rightarrow \infty$  the system orders into a columnar ordered phase instead of a sublattice ordered one. This picture is valid only at low density of vacancies. We note that within this picture of defect rods on a starting state with all particles on sublattice-1, there are no occupied sites on sublattice-4. Clearly, this picture is not quantitatively accurate, however at high densities it is a good description of the system. The sublattice-4 particles represent a relevant perturbation at lower fugacities. We also note that not all allowed configurations of hard squares on the lattice are obtainable by such a sliding from the sublattice ordered state. There is a finite density of “fully jammed” states in the system, which are ignored in this simple rods picture.

The state with orientational (i.e. nematic) ordering of these rods corresponds to a state of the hard squares with columnar order. In fact, there is an exactly solved model of hard rods of variable length due to Ioffe *et al.* [3], in which the activity of a rod is independent of its length, which shows a phase transition at a finite value of the activity of the rods. This phase transition is in the Ising universality class. We note that in the above model, there is a weight for empty sites, which when translated to occupied sites gives a length dependent weight to the rods. The phase transition in Ioffe *et al.*'s model is therefore different from the hard squares case.

#### 4.4 Expansion about the Columnar Ordered State

In the columnar ordered state the system preferentially occupies one of the rows (A or B) or columns (C or D). In the A-ordered phase we have  $(\rho_1 = \rho_2) > (\rho_3 = \rho_4)$ , where  $\rho_i$  denotes the density of particles corresponding to the  $i$ th sublattice. The B, C, and D phases are defined similarly.

To quantify the nature of ordering in this system we define the following order parameters. The row order parameter of the system is defined to be

$$O_r = 4[(\rho_1 + \rho_2) - (\rho_3 + \rho_4)], \quad (4.7)$$

and the column order parameter is

$$O_c = 4[(\rho_1 + \rho_4) - (\rho_2 + \rho_3)]. \quad (4.8)$$

Equivalently, we can also define a single  $\mathbb{Z}_4$  complex order parameter

$$O_{\mathbb{Z}_4} = 4\sqrt{2}[(\rho_1 - \rho_3) + i(\rho_2 - \rho_4)]. \quad (4.9)$$

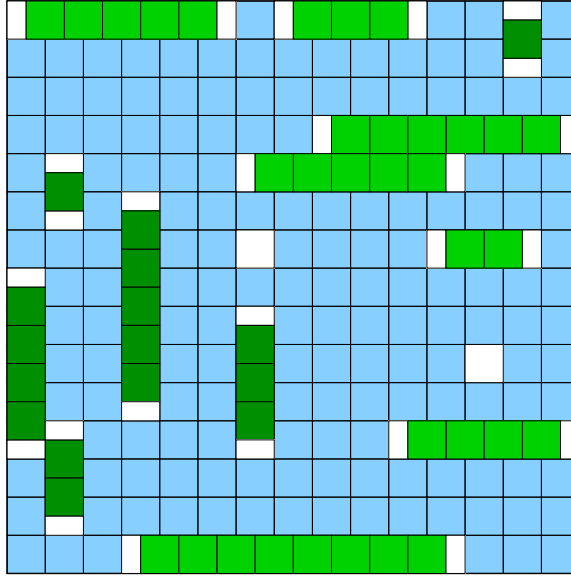


Figure 4.3: A configuration near full packing consisting only of horizontal and vertical rod defects. The single square vacancies can break up into half-vacancies and be moved arbitrarily far apart in the horizontal or vertical direction. The light blue squares represent particles on sublattice 1, the horizontal rods are made of squares on sublattice 2 and the vertical rods are composed of squares on sublattice 3.

The factor  $4\sqrt{2}$  has been introduced to make the maximum value of the order parameter  $|O_{z4}|$  equal to 1. The phase of the complex order parameter  $O_{z4}$  takes the values  $\pi/4, -3\pi/4, -\pi/4$  and  $3\pi/4$  in the A, B, C, and D phases respectively.

We now develop a high-activity perturbation series about the row-ordered state. As we will show, in this series, we effectively integrate out the horizontal rods, and this generates a longer-ranged effective interaction between the vertical rods, in addition to the excluded volume interactions.

We begin by associating different fugacities to the particles on the A and B rows. The fugacities of the particles on row A is  $z_A$  and on row B is  $z_B$ .  $\Omega(z_A, z_B)$  is the partition function of the system with this explicit symmetry breaking between the odd and even rows.  $\Omega(z_A, 0)$  corresponds to the fully columnar ordered state. We expand the partition function of the system about a state with perfect columnar order in the A phase. This approach is similar to methods developed in earlier studies [4].

We write the partition function of the system as a formal expansion in terms of the fugacities of the particles on the B rows (defects) and the corresponding partition functions of the A rows. The partition function expansion about the columnar ordered state is

$$\frac{\Omega(z_A, z_B)}{\Omega(z_A, 0)} = 1 + z_B W_1(z_A) + \frac{z_B^2}{2!} W_2(z_A) + \dots \quad (4.10)$$

The calculation of  $W_n(z_A)$  involves fixing a configuration  $\mathcal{B}_n$  of  $n$  particles on the B-sites. The weight of this configuration is defined to be  $z_B^n \text{Prob}(\mathcal{B}_n)$ , where  $\text{Prob}(\mathcal{B}_n)$  is the

probability that in the reference system with only  $A$ -particles, no site excluded by these  $B$ -particles will be occupied. We then sum these weights over all configurations  $\mathcal{B}_n$ . The negative of the logarithm of  $\text{Prob}(\mathcal{B}_n)$  is defined to be the effective interaction between the  $B$  particles when the  $A$  particles are integrated out.

Now, taking the logarithm of Eq. (4.10), we arrive at the cumulant expansion

$$\frac{1}{N} \log \Omega(z_A, z_B) = \kappa_0(z_A) + z_B \kappa_1(z_A) + \frac{z_B^2}{2!} \kappa_2(z_A) + \dots, \quad (4.11)$$

where  $N$  is the total number of sites in the system and  $\kappa_n$  denotes the connected part of the  $n$ 'th term in the expansion.  $\kappa_0$  denotes the contribution to the free energy expansion from the perfectly columnar ordered state. The terms in the series can be evaluated from the standard cumulant expansion as

$$\begin{aligned} \kappa_1(z_A) &= \frac{1}{N} W_1(z_A), \\ \kappa_2(z_A) &= \frac{1}{N} \left[ W_2(z_A) - W_1(z_A)^2 \right], \\ &\vdots \end{aligned} \quad (4.12)$$

It is straightforward to evaluate the first few terms in this expansion. When there are no  $B$ -particles in the lattice, the partition function of the system breaks up into a product of 1-d partition functions of particles on the  $A$ -rows (particles on different  $A$ -rows do not interact). These  $A$ -particles thus behave as a 1-d lattice gas with nearest neighbour exclusion. Thus we have

$$\Omega(z_A, 0) = [\Omega_{1d,L}(z_A)]^{L/2}, \quad (4.13)$$

where  $\Omega_{1d,L}(z_A)$  is the 1-d partition function of particles with nearest neighbour exclusion on a periodic ring of length  $L$ . This is easily seen to be

$$\Omega_{1d,L}(z_A) = \lambda_+^L + \lambda_-^L, \quad (4.14)$$

where  $\lambda_{\pm}$  are the eigenvalues of the 2 X 2 transfer matrix

$$\begin{aligned} \mathbf{T} &= \begin{bmatrix} 1 & 1 \\ z_A & 0 \end{bmatrix}, \\ &\text{with} \\ \lambda_{\pm} &= \frac{1 \pm \sqrt{1 + 4z_A}}{2}. \end{aligned} \quad (4.15)$$

Eq. (4.14) is valid for all  $L > 1$ . In the limit of large  $L$ , this gives us

$$\kappa_0(z_A) = \frac{1}{2} \log \lambda_+. \quad (4.16)$$

We now evaluate the first few terms in the cumulant expansion.

#### 4.4.1 Single Defect

We begin by deriving the expression for  $\kappa_1(z_A)$ , which involves a single B-defect on the lattice.  $W_1(z_A)$  involves fixing the position of a single particle on a B-site, say at  $(x, y)$ . Then the sum over A-particle configurations is restricted to those in which the sites  $(x \pm 1, y \pm 1)$  and  $(x, y \pm 1)$  are not occupied. The partition function of a single row with this constraint is the partition functions of a system of particles on an open chain of length  $L - 3$ , and is easily calculated. Let  $f_{000}$  be the probability that the sites in a randomly picked interval of length three on an A-row are all empty, in a 1-dimensional lattice gas with nearest neighbour exclusion at activity  $z_A$ . Then,

$$W_1(z_A) = \frac{N}{2} (f_{000})^2. \quad (4.17)$$

The expression for  $f_{000}$  is easy to derive using the properties of the 1-d nearest-neighbour exclusion lattice gas. We have  $f_{000} = \frac{1}{z_A} f_{010}$ , where  $f_{010}$  is the probability that a randomly picked site in the gas will have the occupation numbers 010 at the three consecutive sites. Clearly,  $f_{010} = \rho_{1d}(z_A)$ , the density of the gas. Using Eq. (4.15), we get

$$\rho_{1d}(z_A) = \frac{1}{2} - \frac{1}{2\sqrt{1+4z_A}}. \quad (4.18)$$

Therefore we obtain

$$\kappa_1(z_A) = \frac{1}{2} (f_{000})^2 = \frac{1}{2} \left( \frac{\rho_{1d}(z_A)}{z_A} \right)^2. \quad (4.19)$$

Thus  $\kappa_1(z_A)$  has the following expansion in inverse powers of  $z_A$

$$\kappa_1(z_A) = \frac{1}{8} \left( \frac{1}{z_A^2} \right) - \frac{1}{8} \left( \frac{1}{z_A^{5/2}} \right) + \mathcal{O} \left( \frac{1}{z_A^3} \right). \quad (4.20)$$

Therefore the leading contribution to the cumulant expansion from the single particle term is of order  $\mathcal{O} \left( \frac{z_B}{z_A^2} \right)$ .

In general, any term involving an arbitrary number of B-particles can be decomposed into a product over partition functions of open chains and hence can be evaluated using a product over two-particle correlators. The terms in the series can be easily expressed in terms of the correlation function of occupied sites in the reference system. Let the pair correlation function at a separation  $\Delta$  between the centres of two unoccupied 000 triplets in the 1-d nearest neighbour exclusion gas be  $G(\Delta)$ . This involves the computation of partition functions of particles on open chains. The partition function for an open chain of length  $r$  is given by

$$\Gamma_{1D,r}(z_A) = f_{000}\lambda_+^{r+3} \left[ 1 - \left( \frac{\lambda_-}{\lambda_+} \right)^{r+2} \right]. \quad (4.21)$$

Then it is easily seen that

$$\begin{aligned} G(\Delta) &= (f_{000}) \quad \text{for } \Delta = 0, \\ &= (f_{000}) \frac{1}{\lambda_+} \quad \text{for } |\Delta| = 1, \\ &= (f_{000})^2 \left( 1 - \alpha^{|\Delta|-1} \right) \quad \text{for } |\Delta| \geq 2, \end{aligned} \quad (4.22)$$

where

$$\alpha = \frac{\lambda_-}{\lambda_+} = -1 + \frac{1}{z_A^{1/2}} - \frac{1}{2} \left( \frac{1}{z_A} \right) + \mathcal{O} \left( \frac{1}{z_A^{3/2}} \right). \quad (4.23)$$

#### 4.4.2 Two Defects

Next, we consider the case where there are two  $B$ -particles on the lattice. The first particle can be placed on any of the  $N_B$   $B$ -sites. The second particle can then be placed in the following distinct ways, 1) on the same row, 2) on an adjacent row (above or below) and 3) on any of the other rows. The contribution from these terms are  $\kappa_{2,\text{same-row}}(z_A)$ ,  $\kappa_{2,\text{adjacent}}(z_A)$  and  $\kappa_{2,\text{rest}}(z_A)$  respectively. It is easy to see that the term  $\kappa_{2,\text{rest}}(z_A)$  contains terms that can be factored into a product of two independent  $B$ -defects and thus is exactly cancelled in the corresponding cumulant expansion. We thus have

$$\kappa_2(z_A) = \kappa_{2,\text{same-row}}(z_A) + \kappa_{2,\text{adjacent}}(z_A). \quad (4.24)$$

We calculate the contributions from these two terms below.

##### Same row

The second particle can be placed at a distance  $\Delta$  from the first on the same row. The weight  $w[\Delta]$  of each configuration in the partition function expansion (Eq. 4.22) is given by

$$\begin{aligned} w[\Delta] &= 0 \quad \text{for } |\Delta| \leq 1, \\ &= (f_{000})^4 \left( 1 - \alpha^{|\Delta|-1} \right)^2 \quad \text{for } |\Delta| \geq 2. \end{aligned} \quad (4.25)$$

Summing over all  $\Delta$ , and subtracting the disconnected term we arrive at

$$\kappa_{2,\text{same-row}}(z_A) = \frac{(f_{000})^4}{2} \left( -\frac{4\alpha + 2}{1 - \alpha^2} - 1 \right). \quad (4.26)$$

The contribution from the sum over all  $\Delta$  yields a factor of the type  $\frac{1}{1-\alpha^2}$ , which tends to  $\sqrt{z_A}$  at large  $z_A$ . Therefore the leading order contribution from the  $\kappa_{2,\text{same-row}}$  term is of order  $\frac{1}{z_A^{7/2}}$ .

### Adjacent Rows

In the calculation of the term  $\kappa_{2,\text{adjacent}}(z_A)$  we consider two defects on adjacent B-rows ( $\Delta Y = 1$ ), separated by a distance  $\Delta$  in the  $X$  direction. The weight of each configuration in the expansion is

$$\begin{aligned} w[\Delta] &= (f_{000})^3 \quad \text{for } \Delta = 0, \\ &= (f_{000})^3 \frac{1}{\lambda_+} \quad \text{for } |\Delta| = 1, \\ &= (f_{000})^4 \left( 1 - \alpha^{|\Delta|-1} \right) \quad \text{for } |\Delta| \geq 2. \end{aligned} \quad (4.27)$$

Summing over all  $\Delta$ , and subtracting the disconnected term we arrive at

$$\kappa_{2,\text{adjacent}}(z_A) = \frac{(f_{000})^3}{2} \left( 1 + \frac{2}{\lambda_+} \right) + (f_{000})^4 \left( -\frac{2\alpha}{1 - \alpha} - 1 \right). \quad (4.28)$$

The first term represents the contact term obtained from the region  $|\Delta| \leq 1$ . This has contributions from  $\Delta = 0$  and 1 which have leading contributions of order  $1/z_A^3$  and  $1/z_A^{7/2}$  respectively. The second term represents the contribution from the sum over all  $\Delta > 2$  which is of order  $1/z_A^4$ . Thus the leading contribution from  $\kappa_{2,\text{adjacent}}(z_A)$  is of order  $\frac{1}{z_A^3}$ .

Hence the two particle term in the cumulant expansion has the following expansion in inverse powers of  $z_A$

$$\frac{\kappa_2(z_A)}{2!} = \frac{1}{16} \left( \frac{1}{z_A^3} \right) + \frac{3}{64} \left( \frac{1}{z_A^{7/2}} \right) - \frac{21}{64} \left( \frac{1}{z_A^4} \right) + \mathcal{O} \left( \frac{1}{z_A^{9/2}} \right). \quad (4.29)$$

### 4.4.3 Higher Orders

The calculation of higher order terms  $W_n(z_A)$  for  $n > 2$  is similar. We can compute the terms in the cumulant expansion in defect fugacities to arbitrarily high orders. It is possible to write down closed-form expressions for each term in the cumulant expansion in defect fugacities, as the series arising from the sum over all configurations of  $n$  particles is

algebraically summable. As an illustrative example, we quote the result for the third term in the cumulant expansion,  $\kappa_3(z_A)$  in Appendix B.

However, working order by order in  $n$  is not very effective. In the series given in Eq. (4.11), the series in powers of  $z_B$ , with coefficients that are functions of  $z_A$ . Eventually, We would like to put  $z_A = z_B = z$ , and expand the series in inverse powers of  $1/z$ . Unfortunately, the leading behaviour of  $W_n(z_A)$  for large  $z_A$  is only  $z_A^{-n-1}$ . Then, arbitrarily large orders in  $n$  are required even to get the correct result to order  $1/z$ .

This may be seen as follows: Consider the configuration of  $n$   $B$ -particles vertically above each other. It is easy to see that the probability that such a configuration would be allowed in the unperturbed ensemble is  $[f_{000}]^{n+1}$ , and hence is  $\mathcal{O}(z_A^{-(n+1)})$ . Hence the contribution of this term to the perturbation expansion is of order  $z_B^n z_A^{-(n+1)}$ . For  $z_B = z_A = z$  this is  $\mathcal{O}(1/z)$  for all  $n$ .

It is easy to check that only these vertical rod-like configurations of  $B$ -particles contribute to order  $1/z$ . Hence, if we want to sum over all terms to order  $1/z$ , we group these configurations together, and identify them as a single vertical rod. A general configuration of  $B$ -particles would then be a group of non-overlapping vertical rods.

## 4.5 High-Activity Expansion in terms of Rods

We now develop an expansion in terms of the number of rod defects. In any configuration of  $B$ -particles, we define a rod containing a given occupied  $B$ -site  $\vec{r}$  to be the set of all the consecutively occupied  $B$ -sites in the same column reachable from  $\vec{r}$  using vertical steps of length 2. Clearly, any configuration of  $B$ -sites has a unique description as a set of non-overlapping vertical rods. To avoid over counting, two rods cannot sit directly on top of each other.

We attach an additional activity factor  $\epsilon$  to each rod, and now rewrite the summation in Eq.(4.10) as a sum over configurations involving different numbers of rods

$$\frac{\Omega(z_A, z_B)}{\Omega(z_A, 0)} = 1 + \epsilon R_1(z_A, z_B) + \epsilon^2 R_2(z_A, z_B) + \dots, \quad (4.30)$$

where  $R_n(z_A, z_B)$  denotes the contribution of the configurations with exactly  $n$  rods to the partition function expansion. Now taking the logarithm, we arrive at the free energy expansion

$$\begin{aligned} \mathcal{F}(z_A, z_B) &= -\frac{1}{N} \log(\Omega(z_A, z_B)) \\ &= F_0(z_A, 0) + \epsilon F_1(z_A, z_B) + \epsilon^2 F_2(z_A, z_B) + \dots, \end{aligned} \quad (4.31)$$

where  $\mathcal{F}(z_A, z_B)$  denotes the free energy per site of the hard square lattice gas and

$$\begin{aligned}
F_1(z_A, z_B) &= -\frac{1}{N}R_1(z_A, z_B), \\
F_2(z_A, z_B) &= -\frac{1}{N}\left(R_2(z_A, z_B) - \frac{R_1(z_A, z_B)^2}{2}\right), \\
&\vdots
\end{aligned} \tag{4.32}$$

We evaluate the free energy expansion formally in powers of  $\epsilon$ . At the end of the calculation, we set  $\epsilon = 1$ .  $F_0$  denotes the contribution from the term when there are no  $B$ -particles in the system. From Eq. 4.31 we have

$$F_0 = -\kappa_0(z_A). \tag{4.33}$$

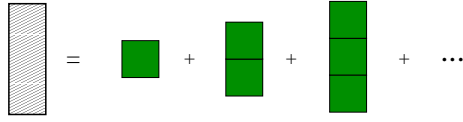


Figure 4.4: The configurations contributing to a single rod term

Now consider configurations with exactly one rod. The weight of a rod with exactly  $n$   $B$ -sites exactly above each other is easily seen to be  $f_{000}^{n+1}w_B^n$ . There are  $N_B = N/2$  possible positions for each size  $n$  of the rod. Summing over all possible values of  $n$ , we get

$$F_1 = -\frac{N_B}{N} \sum_{n=1}^{\infty} (f_{000})^{n+1} z_B^n. \tag{4.34}$$

Which yields

$$F_1 = -\frac{1}{2} \left( \frac{z_B f_{000}^2}{1 - z_B f_{000}} \right). \tag{4.35}$$

It is convenient to define a parameter  $\gamma = z_B f_{000}$ . Then we have

$$F_1 = -\frac{\gamma f_{000}}{2(1 - \gamma)}. \tag{4.36}$$

We next evaluate the two rod term

$$F_2 = - \sum_{\vec{r}_1, l_1} \sum_{\vec{r}_2, l_2} \left[ w(\vec{r}_1, l_1; \vec{r}_2, l_2) - \frac{w(\vec{r}_1, l_1)w(\vec{r}_2, l_2)}{2} \right]. \tag{4.37}$$

where  $w(\vec{r}_1, l_1; \vec{r}_2, l_2)$  denotes the weight of the two-rod configuration, with a rod at position  $r_1$  and length  $l_1$  and another at position  $r_2$  with length  $l_2$ , in the partition function expansion.  $w(\vec{r}_1, l_1)$  denotes the weight of a single rod configuration.

It is easy to see that rods that do not have a finite interaction are exactly cancelled

in the corresponding cumulant expansion. We thus deal with only the following two rod terms:

- 1) Adjacent rods (two rods whose ends lie on the same row) (Fig. 4.5)
- 2) Two rods with a finite Y-overlap (Fig. 4.6)
- 3) Intersecting rods (The weight of the configuration  $w(r_1, r_2)$  is zero, but  $w(r_1)w(r_2)$  is finite)(Fig. 4.7)

We deal with these three terms separately. We have

$$F_2 = t_1 + t_2 + t_3. \quad (4.38)$$

### Adjacent rods

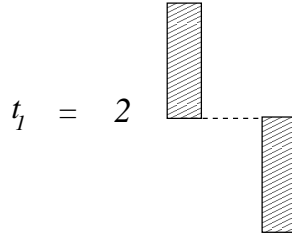


Figure 4.5: The configurations contributing to the adjacent rods term

In the calculation of the term  $t_1$ , we deal with all configurations in which two rods touch an A-row from different sides. Then for this row, we need to calculate the correlation function in the reference problem that two triplets of three consecutive sites at a given distance are both empty. One of the rods extends upwards with length  $n_a$  and the other rod extends downwards with a length  $n_b$  (Fig. 4.5), the factor of 2 accounts for the symmetry related diagrams. Summing over all configurations and subtracting the disconnected part, we have

$$t_1 = - \sum_{n_a=1}^{\infty} \sum_{n_b=1}^{\infty} \gamma^{n_a+n_b} \left( \left( \frac{f_{000}}{\lambda_+} - f_{000}^2 \right) + \sum_{\Delta \geq 2} f_{000}^2 \left[ (1 - \alpha^{|\Delta|-1}) - 1 \right] \right).$$

This series can be easily summed. We have

$$t_1 = - \frac{\gamma^2 f_{000}}{(1-\gamma)^2} \left( \frac{1}{\lambda_+} - \frac{f_{000}}{1-\alpha} \right). \quad (4.39)$$

### Rods with a finite Y-overlap

In the evaluation of the term  $t_2$ , we have two rods, with  $n_o$   $B$ -particles overlapping in the Y-direction. Now, one of the rods can have a part extending above these fully overlapping

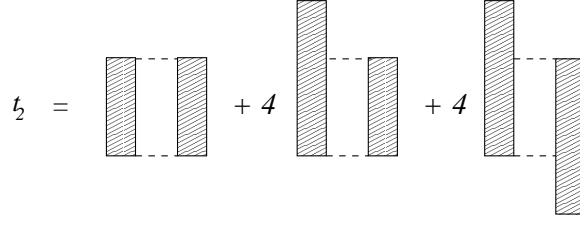


Figure 4.6: The configurations contributing to the rods with a finite Y-overlap term. The factors multiplying the diagrams account for the other symmetry related configurations of overlapping rods.

rods (Fig. 4.6), this can happen in 4 ways. The two rods can both have a finite extension above the overlapping section, this can occur in two distinct ways, one of the rods extends both above and below the other, or one rod extends above and the other below. Both these cases yield the same weights. The extending sections above and below the overlap are of lengths  $n_a$  and  $n_b$ . We have

$$t_2 = -\frac{1}{2} \left( 1 + 4 \sum_{n_a=1}^{\infty} \gamma^{n_a} + 4 \sum_{n_a=1}^{\infty} \sum_{n_b=1}^{\infty} \gamma^{n_a+n_b} \right) \left( \sum_{n_o=1}^{\infty} \sum_{\Delta \geq 2}^{\infty} \gamma^{2n_o} (f_{000})^2 \left[ (1 - \alpha^{|\Delta|-1})^{n_o+1} - 1 \right] \right). \quad (4.40)$$

The sum within the first brackets can be performed trivially. We have

$$t_2 = -\frac{1}{2} \left( \frac{1+\gamma}{1-\gamma} \right)^2 (f_{000})^2 \left( \sum_{n_o=1}^{\infty} \sum_{\Delta \geq 2}^{\infty} \gamma^{2n_o} \left[ (1 - \alpha^{|\Delta|-1})^{n_o+1} - 1 \right] \right). \quad (4.41)$$

The sum over  $n_o$  is straightforward, we have

$$t_2 = -\frac{1}{2} \left( \frac{1+\gamma}{1-\gamma} \right)^2 \gamma^2 (f_{000})^2 \left( \sum_{\Delta \geq 2}^{\infty} \frac{(1 - \alpha^{|\Delta|-1})^2}{1 - \gamma^2 (1 - \alpha^{|\Delta|-1})} - \frac{(f_{000})^2 \gamma^2}{1 - \gamma^2} \right).$$

We can rewrite this in a better form as

$$t_2 = -\frac{1}{2} \left( \frac{1+\gamma}{1-\gamma} \right)^2 (f_{000})^2 \left( \sum_{r=1}^{\infty} \frac{(1 - \alpha^r)^2}{\gamma^{-2} - (1 - \alpha^r)} - \frac{1}{\gamma^{-2} - 1} \right). \quad (4.42)$$

Now, since  $\alpha$  is negative, the terms in the summand series are oscillatory. We thus split the terms into even and odd powers of  $\alpha$ . We have

$$S = \left( \sum_{r=1}^{\infty} \frac{(1 - \alpha^r)^2}{\gamma^{-2} - (1 - \alpha^r)} - \frac{1}{\gamma^{-2} - 1} \right). \quad (4.43)$$

We write

$$S = S_{odd} + S_{even}, \quad (4.44)$$

with

$$S_{even} = \left( \sum_{n=1}^{\infty} \frac{(1 - \alpha^{2n})^2}{\gamma^{-2} - (1 - \alpha^{2n})} - \frac{1}{\gamma^{-2} - 1} \right), \quad (4.45)$$

and

$$S_{odd} = \left( \sum_{n=0}^{\infty} \frac{(1 + |\alpha|^{2n+1})^2}{\gamma^{-2} - (1 + |\alpha|^{2n+1})} - \frac{1}{\gamma^{-2} - 1} \right). \quad (4.46)$$

For large  $z$ ,  $\alpha \approx -1 + z^{-1/2}$ , and the summand in  $S_{odd}$  and  $S_{even}$  is a slowly varying function of  $n$ . To evaluate these expressions we can approximate the sum over the discrete values by an integral over the appropriate range of  $n$ . The error is only of order  $1/z$ . We get

$$\begin{aligned} S_{even} &= \int_{n=\frac{1}{2}}^{\infty} dn \left( \frac{(1 - \alpha^{2n})^2}{\gamma^{-2} - (1 - \alpha^{2n})} - \frac{1}{\gamma^{-2} - 1} \right), \\ &= \frac{1}{-2 \log(-\alpha)} \left( -\alpha - \frac{\gamma^{-4}}{\gamma^{-2} - 1} \log \left( \frac{\gamma^{-2} - 1 + \alpha}{\gamma^{-2} - 1} \right) \right), \end{aligned} \quad (4.47)$$

and

$$\begin{aligned} S_{odd} &= \int_{n=-\frac{1}{2}}^{\infty} dn \left( \frac{(1 + |\alpha|^{2n+1})^2}{\gamma^{-2} - (1 + |\alpha|^{2n+1})} - \frac{1}{\gamma^{-2} - 1} \right), \\ &= \frac{1}{2 \log(-\alpha)} \left( 1 + \frac{\gamma^{-4}}{\gamma^{-2} - 1} \log \left( \frac{\gamma^{-2} - 2}{\gamma^{-2} - 1} \right) \right). \end{aligned} \quad (4.48)$$

We thus have

$$t_2 = -\frac{1}{2} \left( \frac{1 + \gamma}{1 - \gamma} \right)^2 (f_{000})^2 (S_{odd} + S_{even}). \quad (4.49)$$

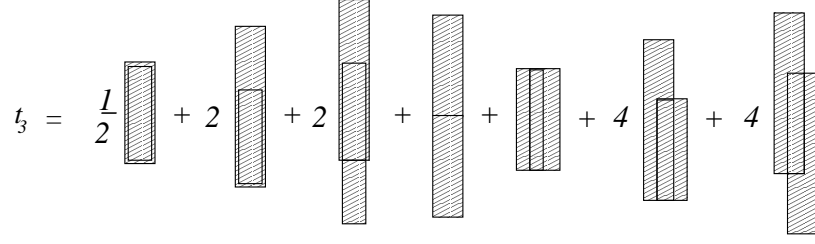


Figure 4.7: The configurations contributing to the overlapping rods term

### Overlapping Rods

In the calculation of the overlapping rods term, we deal with all possible configurations in which two rods which partially or fully overlap. In this case the two rods can be at a distance  $\Delta = 0$  or  $\Delta = \pm 1$  away from each other. The length of the overlap is  $n_o$  and the parts extending above and below are of lengths  $n_a$  and  $n_b$  respectively. There is also a contribution from the term in which two rods sit directly on top of each other, since this configuration is not counted as a two rod term, but has a weight in the disconnected part. We have

$$t_3 = \frac{3}{4} \left( 1 + 4 \sum_{n_a=1}^{\infty} \gamma^{n_a} + 4 \sum_{n_a=1}^{\infty} \sum_{n_b=1}^{\infty} \gamma^{n_a+n_b} \right) \left( \sum_{n_o=1}^{\infty} (f_{000})^2 \gamma^{2n_o} \right) + \frac{1}{2} \sum_{n_a=1}^{\infty} \sum_{n_b=1}^{\infty} (f_{000})^2 (\gamma)^{n_a+n_b}. \quad (4.50)$$

Hence

$$t_3 = \frac{3}{4} \left( \frac{1+\gamma}{1-\gamma} \right)^2 \left( \frac{f_{000}^2 \gamma^2}{1-\gamma^2} \right) + \frac{1}{2} \left( \frac{f_{000} \gamma}{1-\gamma} \right)^2. \quad (4.51)$$

#### 4.5.1 High-Activity Expansion for the Free Energy

Setting  $\epsilon = 1$  in Eq. (4.31) we obtain a high-activity expansion for the free energy of the system. The term  $F_1$ , corresponding to single rods, has a leading contribution of order  $1/z$ . The term  $F_2$ , corresponding to two-rod configurations has a leading contribution of order  $1/z^{3/2}$ . The order  $1/z^{3/2}$  contribution to the two-rod term comes from two sources, a) when two adjacent rods separated by a distance 1 touch the same row from opposite sides and b) a summation over the distance between two rods which share a finite interval in the Y-direction. The sum over the distance in this case yields a factor of order  $\sqrt{z}$  because the correlation length between the rods is  $\xi = \log \alpha \sim \sqrt{z}$ . The term of order  $1/z^2$  gets contributions from configurations involving three rods, in addition to the above single rod and two rod terms. For  $n$  rods, the summation over the distance between rods yields a

leading order contribution of at most  $z^{\frac{n-1}{2}}$ . Hence in the evaluation of the term of order  $z^{\frac{n+1}{2}}$ , only terms involving  $n$  rods need to be considered.

Using our expressions for  $F_0$ ,  $F_1$  and  $F_2$ , we can generate the exact series expansion for the free energy and the density of the hard square lattice gas up to order  $1/z^{3/2}$ . We have

$$-f(z) = \frac{1}{4} \log z + \frac{1}{4z^{1/2}} + \frac{1}{4z} + \frac{(3 \log(\frac{9}{8}) + \frac{11}{96})}{z^{3/2}} + \mathcal{O}\left(\frac{1}{z^2}\right), \quad (4.52)$$

and

$$\rho(z) = \frac{1}{4} - \frac{1}{8z^{1/2}} - \frac{1}{4z} - \frac{(\frac{9}{2} \log(\frac{9}{8}) + \frac{11}{64})}{z^{3/2}} + \mathcal{O}\left(\frac{1}{z^2}\right). \quad (4.53)$$

Higher order terms can in principle be evaluated in a similar manner. The term of order  $1/z^2$  gets contributions from terms involving three rods, in addition to the above single rod and two rod terms. This is much more involved, and will not be attempted here. In Appendix B we show how the above series can also be arrived at in an alternate way, by first summing over terms contributing at each order in  $z$ , and then over all sizes of the rods.

### 4.5.2 Order Parameter Expansion

In this section we compute the high-activity expansion for the row order parameter which is defined in Eq. (B.25). We have

$$O_r(z_A, z_B) = 4 \left[ z_A \frac{\partial}{\partial z_A} - z_B \frac{\partial}{\partial z_B} \right] (-\mathcal{F}(z_A, z_B)). \quad (4.54)$$

Using the terms in the free energy expansion above we can generate the exact order parameter expansion to order  $1/z^{3/2}$ . We have

$$O_r(z, z) = 1 - \frac{1}{2z^{1/2}} - \frac{5}{z} - \left( \frac{395}{16} + 50 \log\left(\frac{9}{8}\right) \right) \frac{1}{z^{3/2}} + \mathcal{O}\left(\frac{1}{z^2}\right). \quad (4.55)$$

Using the terms up to order  $1/z^{3/2}$  in the order parameter expansion, we estimate the critical point of the system by solving for the point  $O_r = 0$ . We obtain an estimate of the critical point  $z_c = 14.86$ , which is significantly better than the estimate  $z_c = 6.25$  obtained by using just the first three terms of the series.

## 4.6 Variational Study of the Free Energy

In this section we use the 1D nature of the perfectly ordered state to estimate the free energy (and rigorous upper bounds) of the system with periodic boundary conditions. We can generate each configuration of the hard square lattice gas by first filling up the A rows with particles (independently, as there is no interaction between particles on the different

A rows) and then placing B particles in the sites not disallowed by the occupied A-sites. The partition function of the system can therefore be expressed as

$$\Omega(z_A, z_B) = \sum_{\text{A-configurations}} z_A^{n_A} \Omega_{B/\{A\}}(z_B), \quad (4.56)$$

where  $\Omega_{B/\{A\}}(z_B)$  is the partition function of the B-sites given a configuration  $\{A\}$  of A-sites, and  $n_A$  denotes the number of A-particles in the configuration. The sum is over all possible allowed configurations of A-particles. Now, we can represent the partition function  $\Omega_{B/\{A\}}(z_B)$  as follows

$$\Omega_{B/\{A\}}(z_B) = \prod_{\text{all sites } x} \prod_l \Omega_{1D,l}(z_B)^{\eta(x,l)}, \quad (4.57)$$

where  $\Omega_{1D,l}(z_B)$  is the partition function of the system of particles on a 1D line of length  $l$  with nearest neighbour exclusion and fugacity  $z_B$ , this expression is provided in Eq. 4.21. The product is over the volume of the system and  $\eta(x,l)$  is an indicator function with value 1 if the site  $x$  is the leftmost site of  $l$  consecutively occupiable B-sites (i.e.- sites not forbidden for occupation by the configuration  $\{A\}$ ), and  $l$  ranges from 1 to  $L$ , the linear size of the system.

The total partition function thus becomes

$$\Omega(z_A, z_B) = \sum_{\text{A configs}} z_A^{n_A} \prod_{\text{all sites } x} \prod_l \Omega_{1D,l}(z_B)^{\eta(x,l)}. \quad (4.58)$$

We write the partition function as

$$\Omega(z_A, z_B) = \sum_{\text{A configs}} z_A^{n_A} \exp \left( \sum_{\text{all sites } x} \sum_l \eta(x,l) \log(\Omega_{1D,l}(z_B)) \right). \quad (4.59)$$

We define  $\theta(l, A)$  as the total number of sequences of length  $l$  of consecutively occupiable B-sites in a given configuration  $\{A\}$ . Thus  $\theta(l, A) = \sum_{\text{all sites } x} \eta(x,l)$ . We have

$$\frac{\Omega(z_A, z_B)}{\Omega(z_A, 0)} = \sum \frac{z_A^{n_A}}{\Omega(z_A, 0)} \exp \left( \sum_l \theta(l, \{A\}) \log(\Omega_{1D,l}(z_B)) \right). \quad (4.60)$$

We use the convexity inequality

$$\exp(\langle V \rangle) \leq \langle \exp(V) \rangle, \quad (4.61)$$

where the angular brackets denote the expectation value in a given ensemble. Using the above inequality and taking logarithms on both sides, we arrive at

$$\log \Omega(z_A, z_B) \geq \log \Omega(z_A, 0) + \sum_{\text{A configs}} \frac{z_A^{n_A}}{\Omega(z_A, 0)} \sum_l \theta(l, \{A\}) \log(\Omega_{1D,l}(z_B)). \quad (4.62)$$

We define

$$\text{Prob}(l, z_A) = \frac{1}{N_B} \sum_{\text{A configs}} \frac{z_A^{n_A}}{\Omega(z_A, 0)} \theta(l, \{A\}), \quad (4.63)$$

where  $\text{Prob}(l, z_A)$  is the expectation value of the number of sequences of length  $l$  in the A-ensemble. Therefore, we arrive at the following bound for the free energy of the system

$$\mathcal{F}(z_A, z_B) \leq F_0(z_A, 0) - \frac{1}{2} \sum_l \text{Prob}(l, z_A) \log(\Omega_{1D,l}(z_B)). \quad (4.64)$$

We can derive an expression for the probability  $\text{Prob}(l, z_A)$  as follows. We have

$$\text{Prob}(l, z_A) = \frac{1}{N_B} \sum_{\text{A configs}} \frac{z_A^{n_A}}{\Omega(z_A, 0)} \sum_x \eta(x, l). \quad (4.65)$$

We now interchange the summation over the configurations and the positions so that

$$\text{Prob}(l, z_A) = \frac{1}{N_B} \sum_x \left( \sum_{\text{A configs}} \frac{z_A^{n_A}}{\Omega(z_A, 0)} \eta(x, l) \right). \quad (4.66)$$

Due to the periodicity of the lattice, the quantity within the brackets is translationally invariant, therefore we have

$$\text{Prob}(l, z_A) = \sum_{\text{A configs}} \frac{z_A^{n_A}}{\Omega(z_A, 0)} \eta(0, l). \quad (4.67)$$

We can compute  $\text{Prob}(l, z_A)$  in the following manner. We need to sum over configurations which have a sequence of  $l$  non-forbidden sites with the leftmost being at 0. For the site  $-1$  to be forbidden, one or both of the A-sites (directly above or below the B-row) at the  $X$  position  $-2$  must be occupied. A similar condition holds for the A-sites at the  $X$  position  $l+2$ . This probability can be calculated to be

$$\text{Prob}(l, z_A) = (f_{000})^2 \frac{1}{\lambda_+^{2l}} \left( \frac{4z^2}{\lambda_+^2} + \frac{4z^3}{\lambda_+^4} + \frac{z^4}{\lambda_+^6} \right). \quad (4.68)$$

Using the above expression in Eq. 4.64 we obtain a rigorous upper bound on the free energy of the system and therefore bounds on the individual terms in the series expansions. We note that this free energy expression ignores the correlations along the axis perpendicular to the ordering direction.

We can use this estimate of the free energy to estimate the critical point of this system.

We start by estimating the density of particles on the B-rows  $\rho_B$ , given the density of particles on the A-rows  $\rho_A$  (calculated from  $z_A$ ). Using this value of  $\rho_B$ , we then calculate  $\rho_A$ .

We thus have the following set of coupled equations

$$\rho_B(z_B, \overline{z}_A(\rho_A)) = \sum_{l=1}^{\infty} \text{Prob}(l, \overline{z}_A(\rho_A)) \rho_{\text{open}}(z_B), \quad (4.69)$$

$$\rho_A(z_A, \overline{z}_B(\rho_B)) = \sum_{l=1}^{\infty} \text{Prob}(l, \overline{z}_B(\rho_B)) \rho_{\text{open}}(z_A). \quad (4.70)$$

Where  $\overline{z}_i(\rho_i)$  is determined by the equation

$$\rho_i = \rho_{1d}(z_i) \quad i \equiv A, B. \quad (4.71)$$

We solve these equations self consistently to establish the point where this system of equations becomes unstable. Using this technique, we estimate the critical point of this system to be  $z_c = 2.993$ . We note that even this somewhat elaborate variational technique fails to capture the correlations that lead to a high value of the critical point in this system.

## 4.7 Fluid to Columnar Order Transition

We have seen above that the high density state of the hard square lattice gas exhibits columnar order. Proving the finiteness of the radius of convergence of the expansions developed above would amount to a rigorous proof of the existence of this phase (we have not succeeded in doing this here). While at high densities the system is in a long range ordered state, the low density state is disordered with short ranged correlations between particles, as can be seen by the finite radius of convergence of the low activity series (Eq. (4.4)). Therefore there is a phase transition from fluid to columnar order behaviour as a function of density (or activity) in this system. This transition has been the subject of several studies in the past, but there is as yet no consensus on the exact nature of the transition.

We now focus our attention on this transition. As described in Section 4.4, the system can order into any of four columnar ordered states. The transition from disorder to columnar order thus represents a  $\mathbb{Z}_4$  symmetry breaking. There are several well studied models that exhibit a transition that break a  $\mathbb{Z}_4$  symmetry in two dimensions such as the Eight-Vertex model [5] and the Ashkin-Teller-Potts model [6]. As discussed in Chapter 1, a likely paradigm for the critical behaviour of the hard square lattice gas is Ashkin-Teller criticality. We describe a coarse grained mapping of the hard square lattice gas to the Ashkin-Teller model in the next section.

## 4.8 Mapping to the Ashkin-Teller Model

The boundaries between the different phases in the hard square lattice gas are hard to define in a microscopic sense. Although, at large length scales it is possible to describe the phase corresponding to the state of the system, at the lattice scale there is a degeneracy in the definition of the phases. For example, a cluster of particles on the 1-sublattice can be in either of the phases  $A$  or  $C$ . Thus, to find a good description of the system in terms of a local order parameter, we need to look at the system at a scale that allows an unambiguous definition of the phase. A coarse grained description is therefore a natural way to understand the nature of this system.

Near the critical point, the correlation length of the system diverges. The behaviour of the system at large length scales can be understood by dividing the system into patches of larger sizes as we approach the critical point. This is in essence a real space renormalization procedure. Each patch has a linear size  $l$  with  $1 \ll l \ll \xi$ , where  $\xi$  is the correlation length of the system. Then, every block has very good order within it. As we coarse grain the system, we expect the energy (in the case of the hard square lattice gas, the configurational entropy) between the different phases to be linearly proportional to the perimeter of the interface between two phases. This “surface tension” is expected to flow to a fixed point value under repeated actions of this renormalization group.

If we coarse grain the system using square blocks parallel to the lattice axes, we see that the surface tensions between phases are not symmetric. For example, the interface between the C-phase and the D-phase separated by a vertical boundary, favours a C-phase on the left more than on the right, as this impedes less particles on the other side of the boundary. It therefore becomes necessary to find a different blocking algorithm in order to coarse grain the system. A natural choice is a grid at an angle  $\frac{\pi}{4}$  with respect to the lattice axes. We assign a single phase label to each resulting diamond corresponding to the majority rule (Fig. 4.8). In this coarse grained model, the phases have a finite surface tension with respect to each other. From symmetry, it is easy to see that there are two types of surface tensions in this high density phase. These two surface tensions are

$$\begin{aligned} \sigma_{AB} &= \sigma_{CD}, \\ &\text{and} \\ \sigma_{AC} &= \sigma_{CB} = \sigma_{BD} = \sigma_{DA}. \end{aligned} \tag{4.72}$$

where  $\sigma_{AB}$  denotes the surface tension between the A-phase and the B-phase. We can relate this 4-state model to the well known Ashkin-Teller model with a Hamiltonian that possesses a  $\mathbb{Z}_4$  symmetry and has two values of surface tension energies.

As described in Chapter 1, the Ashkin-Teller model is best described as a model of two coupled Ising models with a four spin coupling that has a varying strength of interaction.

The Hamiltonian is given by

$$H = - \left[ \sum_{\langle i,j \rangle} J_2 \sigma_i \sigma_j + J_2 \tau_i \tau_j + J_4 \sigma_i \sigma_j \tau_i \tau_j \right]. \quad (4.73)$$

This model has a line of critical points with continuously variable critical exponents, depending on the strength of the interactions  $J/K$ , where  $J = \beta J_2$  and  $K = \beta J_4$ . The surface tensions between the phases in the hard square lattice gas correspond to the surface energies  $K$  and  $2J - K$  of the above Ashkin-Teller model. Thus it seems plausible that the critical behaviour of this model is in the Ashkin-Teller-Potts universality class.

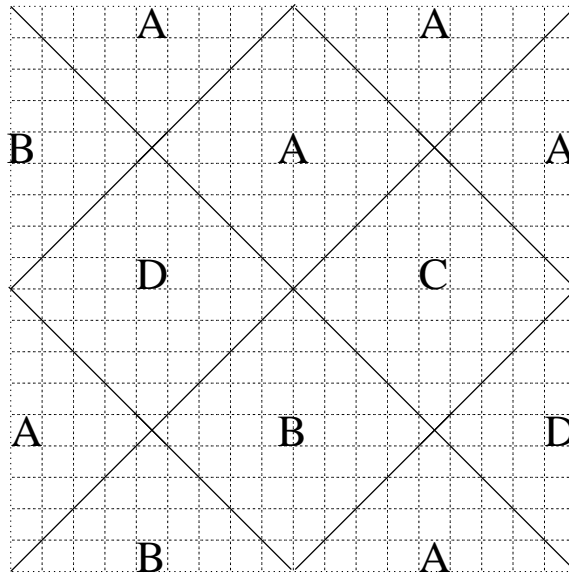


Figure 4.8: We coarse grain the system using a grid at an angle  $\frac{\pi}{4}$  with respect to the lattice. This ensures that the surface tensions between any two phases is symmetric. We assign a single phase label to each resulting diamond.

### 4.8.1 Ising Energy Densities

In this section we map the local degrees of freedom of the hard square lattice gas to the Ising degrees of freedom in the corresponding Ashkin-Teller model.

We begin by ascribing Ising labels to the phases in the hard square lattice gas. The four phases in the Ashkin-Teller model can be described by the values of the two Ising variables (which have different values  $\pm 1$ , in each of the phases). This can be described well in terms of a single complex valued “clock” variable  $\Theta$  with the following definition

$$\Theta_{AT} = \exp\left(\frac{i\pi}{4}\right) \frac{(\sigma + i\tau)}{\sqrt{2}}. \quad (4.74)$$

This variable takes values  $\exp(i\pi/2)$ ,  $1$ ,  $\exp(-i\pi/2)$  and  $-1$  in the phases corresponding to  $(\sigma, \tau) = (+, +), (+, -), (-, -)$  and  $(-, +)$  respectively.

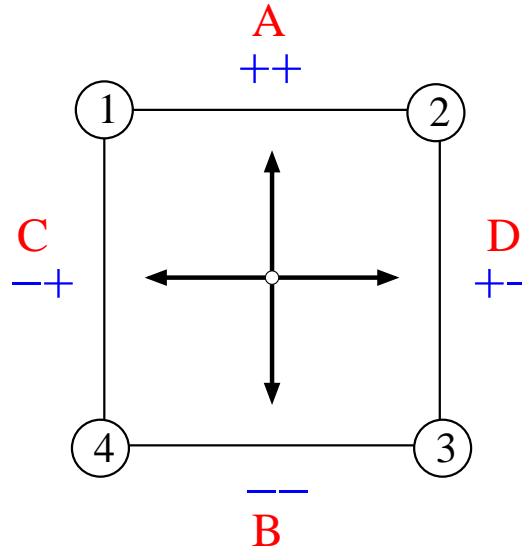


Figure 4.9: The four phases in the Ashkin-Teller model have a natural description in terms of a complex “clock” variable. The arrows represent the value of the clock variable in each phase. The identification to the four phases of the hard square lattice gas model is shown.

To mimic the action of this clock variable, we construct a similar variable for the hard square lattice gas which takes the same values in the four ordered states  $A$ ,  $D$ ,  $B$  and  $C$ . From Figure 4.9 we can see that

$$\Theta_{HS} = \exp\left(\frac{i\pi}{2}\right) 4(\rho_A + i\rho_C - \rho_B - i\rho_D), \quad (4.75)$$

is one such variable. This is related to the order parameter  $O_{Z_4}$  as

$$\Theta_{HS} = \exp\left(-\frac{i\pi}{4}\right) O_{Z_4}^*, \quad (4.76)$$

where  $*$  denotes complex conjugation.

Phase	$\sigma \tau$	$\rho_1$	$\rho_2$	$\rho_3$	$\rho_4$	$\Theta_{AT} \equiv \Theta_{HS}$
A	++	1	1	0	0	$i$
D	+-	0	1	1	0	1
B	--	0	0	1	1	$-i$
C	-+	1	0	0	1	$-1$

Table 4.1: The identification of the four phases in the Ashkin-Teller model and the hard square lattice gas

Now relating the two variables  $\Theta_{AT} \equiv \Theta_{HS}$ , we have the following natural mapping to the Ashkin-Teller Ising variables in terms of the local densities of the hard square lattice gas

$$\begin{aligned}\sigma(x) &\equiv (\rho_1(x) - \rho_3(x)), \\ \tau(x) &\equiv (\rho_4(x) - \rho_2(x)).\end{aligned}\tag{4.77}$$

We note that this identification is true only at the coarse grained level. We can now use these variables to determine the value and sign of the coupling between the two Ising models in the Ashkin-Teller description. We see that the energy densities for the two Ising degrees of freedom, at coarse grained level, are  $E_\sigma(x) \propto \sigma(x)^2$  and  $E_\tau(x) \propto \tau(x)^2$ . Therefore we can map the Ising energy densities to the hard square lattice gas densities as

$$\begin{aligned}E(\sigma) &\cong (\rho_1 + \rho_3), \\ E(\tau) &\cong (\rho_2 + \rho_4).\end{aligned}\tag{4.78}$$

Here  $E(\sigma)$  and  $E(\tau)$  represent the Ising energies in the entire system.

## 4.9 Monte Carlo Simulations

In this section we discuss Monte Carlo simulations we performed in order to test our predictions. In the simulations of high density states of exclusion gases, one often encounters the problem of “jamming”, where the number of available local moves for a system become very small. Since the transition to the columnar ordered phase in this system occurs at densities very close to full packing, it becomes necessary to use efficient non-jamming algorithms. We devised the following novel Monte-Carlo algorithm to simulate the hard square lattice gas.

### The Update Algorithm

1) We evaporate all particles that lie on an arbitrarily chosen 1D line (horizontal or vertical) of the system.

2) The resulting empty line of particles breaks up into regions that are occupiable by particles and regions forbidden for occupation, depending on the configuration of particles on the two adjacent lines of the lattice.

3) We then refill these smaller occupiable line segments using a configuration selected from the configuration space of a system of particles with nearest neighbour exclusion on a 1D chain of the corresponding length.

A lattice gas configuration for a chain of length  $r$  can be generated using the following simple algorithm. The probability of occupation of the edge of the chain is given by  $\text{Prob}(\dots 1) = z\Omega_{\text{open}}(r-2)/\Omega_{\text{open}}(r)$ . Starting with the edge of the chain, we successively occupy or leave empty each site at the edge with the above probability, until the entire

chain is filled. If a particle is deposited the length of the new chain decreases by 2, and if it is left empty, decreases by 1. If the configuration to be generated is that of a closed chain, the first site is occupied with the probability  $z\Omega_{\text{open}}(r-3)/\Omega_{\text{closed}}(r)$ . To speed up the simulations, the values of the various partition functions are stored in the program at the start.

Clearly, this update scheme obeys detailed balance. Since this algorithm updates an entire row or column at once, it is able to efficiently sample the phase space even at very high densities. Using this algorithm, we are able to obtain reliable estimates of thermodynamic quantities from lattices upto size  $1600 \times 1600$  (only for  $z$  close to  $z_c$ ).

## Results

Using finite size scaling we obtain an estimate of the critical point as  $z_c = 97.5 \pm 0.5$ . We find the corresponding critical density to be  $\rho_c = 0.23264(1)$ . The fluid to columnar order transition takes place very close to the full-packing point ( $\rho = 0.25$ ) In Fig. 4.11 we plot the second moment of the order parameter scaled by  $L^{-7/4}$ , showing a crossing at the value  $z_c = 97.5$  for different system sizes. The symmetry of the ordered states in this model suggests observables that are linear combinations of the sublattice densities  $\rho_i$  that have simple transformations under rotations by  $\frac{\pi}{2}$  as relevant quantities. These are

$$V_i = \rho_1 + \omega_i \rho_2 + \omega_i^2 \rho_3 + \omega_i^3 \rho_4, \quad (4.79)$$

where  $\omega_i$  with  $i = 1$  to  $4$  are the fourth roots of unity given by  $1, i, -1$  and  $-i$  respectively. We see that  $V_2 = V_4^*$  is equivalent to the complex order parameter  $O_{Z4} = 4\sqrt{2}V_2$ .

We define the variance of the observables in the system as

$$\text{Var}[V_i] = \frac{1}{L^2} \left( \langle V_i^2 \rangle - \langle V_i \rangle^2 \right), \quad (4.80)$$

where  $L$  is the linear size of the system. At the critical point the variance of  $V_i$  scales as  $L^{a_i}$  with  $a_1 \simeq 0.16$ ,  $a_2 = a_4 = \frac{7}{4}$  and  $a_3 = 0$ . We find that the variance of the observable  $V_1$  grows as a power law at large distances (Fig. 4.13). The variance of  $V_3$  saturates to a finite value (Fig. 4.16). We are able to verify that the scaling exponent  $\gamma/\nu$  is equal to  $7/4$  to very high accuracy, consistent with the critical behaviour of the Ashkin-Teller model (Fig. 4.14).

Due to the large correlation lengths in the columnar ordered phase, the determination of the exponent  $\nu$  is slightly harder. In Fig. 4.12 we present the finite size scaling collapse for the variance of the order parameter  $V_2$ . However, extracting a correlation length from these fits is a bit hard as a range of values for  $\nu$  yield a similar fit. At present our best estimates are  $\nu = 0.92 \pm 0.05$ .

We now use the mapping of particle densities in the hard square lattice gas to the coarse grained Ising energy densities illustrated in Section 4.8.1 to better understand the nature of the coupling between the Ising degrees of freedom in this system. From Eq. (4.78), we

have

$$\begin{aligned} E(\sigma) + E(\tau) &= V_1, \\ E(\sigma) - E(\tau) &= V_3. \end{aligned}$$

The variance of the quantities  $V_1$  and  $V_3$  are therefore a measure of the correlation between the two Ising degrees of freedom. Using the fact that the variance of  $V_1$  grows with a detectable power and that of  $V_3$  saturates, we see that the two Ising degrees of freedom in this model are ferromagnetically coupled (i.e.  $K > 0$ ). This is consistent with the fact that the floating exponent  $\nu$  falls between the value  $2/3$  and  $1$ , the Potts and Ising model values respectively. Therefore we are able to place the critical point of this model slightly to the ferromagnetic side of the Ising point on the critical line of the Ashkin-Teller model (Fig. 4.17).

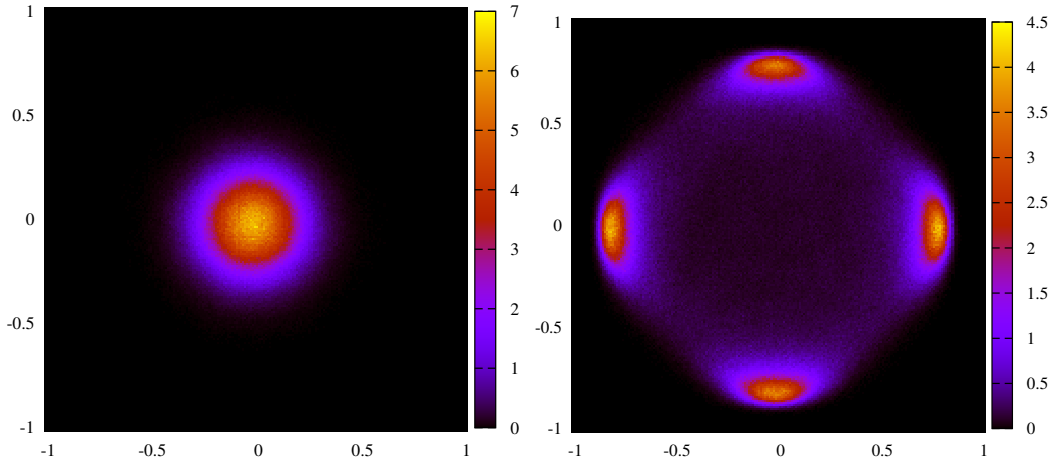


Figure 4.10: A histogram of the complex order parameter  $O_r + iO_c$  at  $z = 50$  (Left) and  $z = 100$  (Right). This illustrates the symmetry relation between the four columnar ordered states. The data above is for a lattice of size  $L = 120$ . Our algorithm samples over all possible ordered states, however, as the size of the system increases this symmetry is broken and the system remains in only one of the ordered states.

Finally it is worthwhile to compare our estimates of the critical exponents of this model with two recent studies [8] and [9]. To do this we use the hyperscaling law  $d\nu = 2 - \alpha = 2\beta + \gamma$ . Fernandes *et. al.* performed Monte Carlo studies on lattices of upto size  $L = 360$  and found  $\nu = 1.0 \pm 0.1$ , with  $\alpha/\nu = 0$ ,  $\beta/\nu = 0.125 \pm 0.05$  and  $\gamma/\nu = 1.75 \pm 0.05$ . This led them to conclude that the exponents are those of the Ising model, i.e.  $\nu = 1$ ,  $\alpha/\nu = 0$ ,  $\beta/\nu = 1/8$  and  $\gamma/\nu = 7/4$ . Feng *et. al.* performed Monte Carlo simulations on sizes upto  $L = 512$  and determined the scaling exponent  $y_t = 1.06(3)$ , which leads to  $\nu = 0.94 \pm 0.01$ ,  $\alpha/\nu = 0.12 \pm 0.01$ ,  $\beta/\nu = 0.125 \pm 0.01$  and  $\gamma/\nu = 1.75 \pm 0.002$ . Our present estimates using the exponent  $\alpha/\nu = 0.158(2)$  yield  $\nu = 0.92 \pm 0.01$ ,  $\beta/\nu = 0.125 \pm 0.01$  and  $\gamma/\nu = 1.75 \pm 0.002$ . We can compare these with the critical exponents of the four state Potts model which are

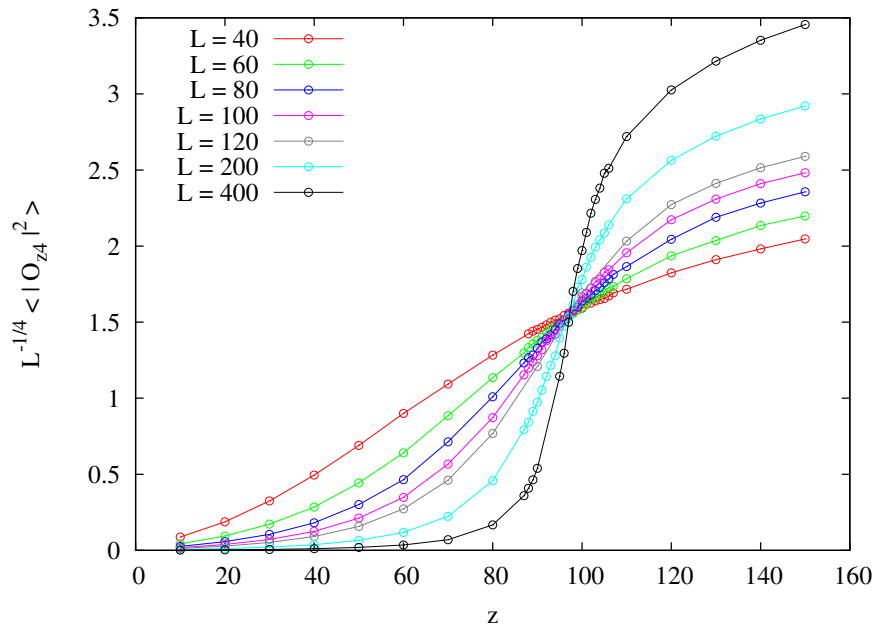


Figure 4.11: Plot of  $L^{-7/4} \langle |O_{Z4}|^2 \rangle$  with respect to  $z$ , showing a critical crossing at the value  $z_c = 97.5$ .

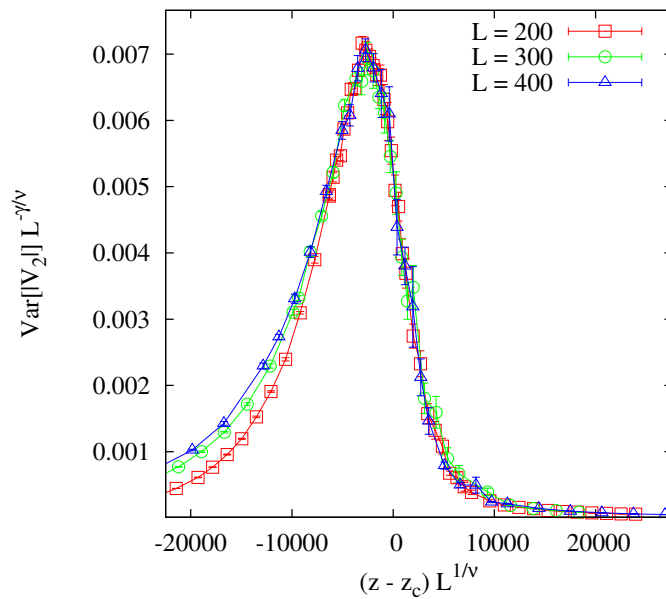


Figure 4.12: Finite size scaling collapse for the variance of  $|V_2|$ , with values  $z_c = 97.5$ ,  $\gamma/\nu = 7/4$  and  $\nu = 0.90$ .  $\text{Var}[|V_2|]$  is the susceptibility of the order parameter.

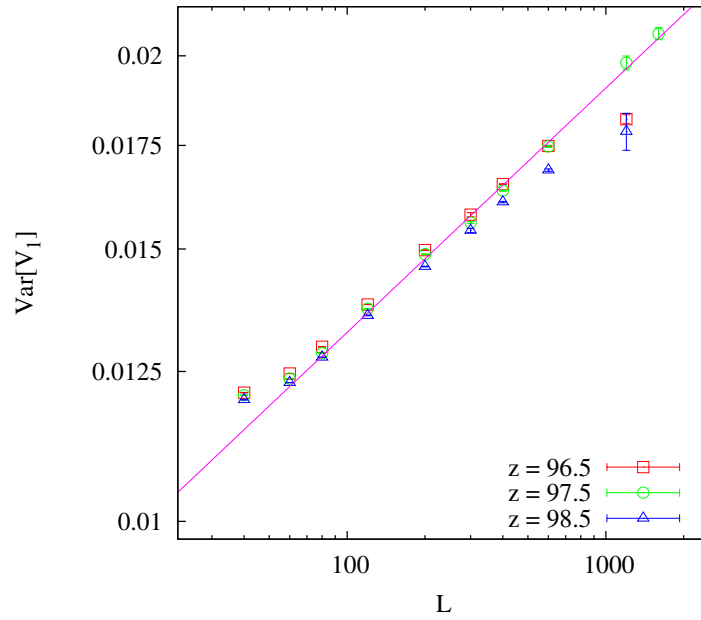


Figure 4.13: Plot of the variance of the vector  $V_1$  for various values of the system size at  $z = 96.5, 97.5$  and  $98.5$ . We find that the variance of  $V_1$  grows with a detectable power  $\approx 0.158 \pm 0.02$  with increasing system size at the critical point  $z_c = 97.5$ . The line has a slope of 0.158 (both axes are in log scale).

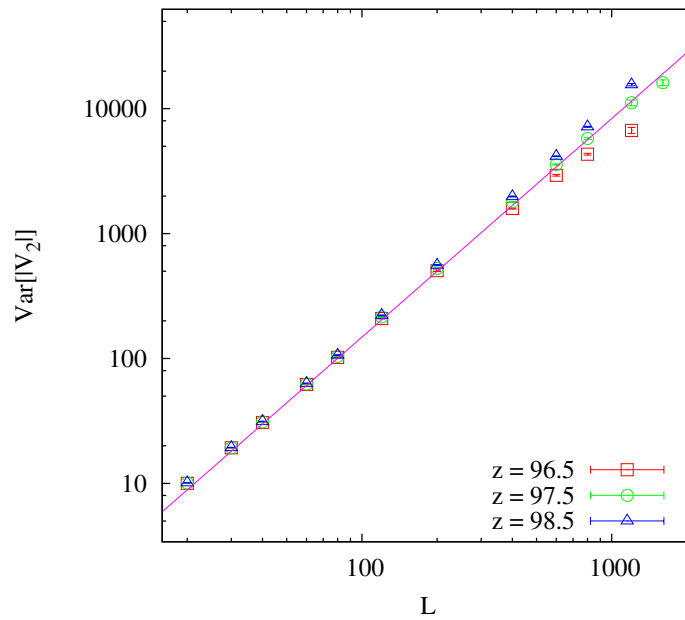


Figure 4.14: Plot of the variance of the vector  $|V_2|$  for various values of the system size at  $z = 96.5, 97.5$  and  $98.5$ . We find that this grows with a power  $1.75 \pm 0.002$  at the critical point  $z_c = 97.5$ . The line has a slope of 1.75.

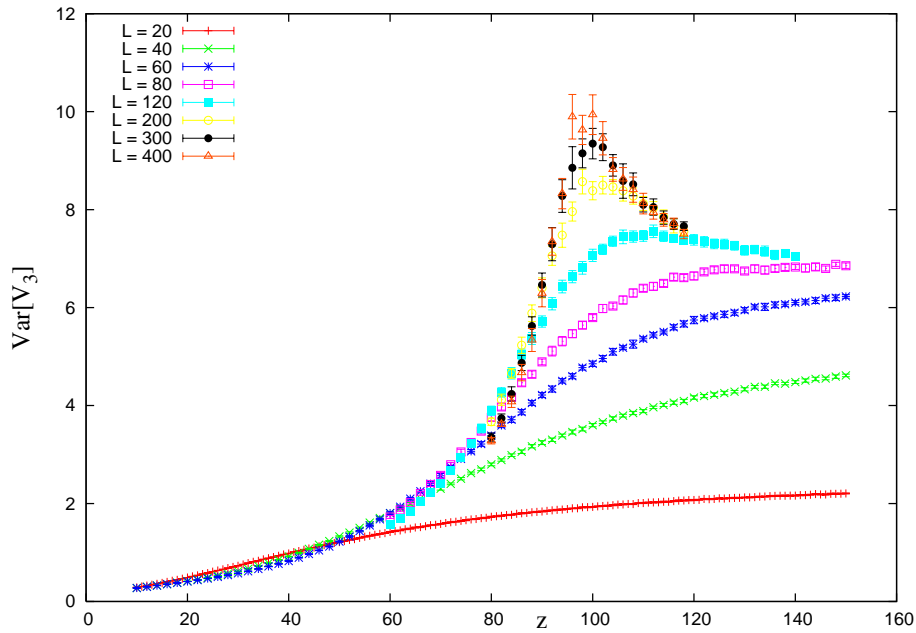


Figure 4.15: Plot of the variance of the vector  $V_3$  with respect to  $z$ , for various values of the system size.

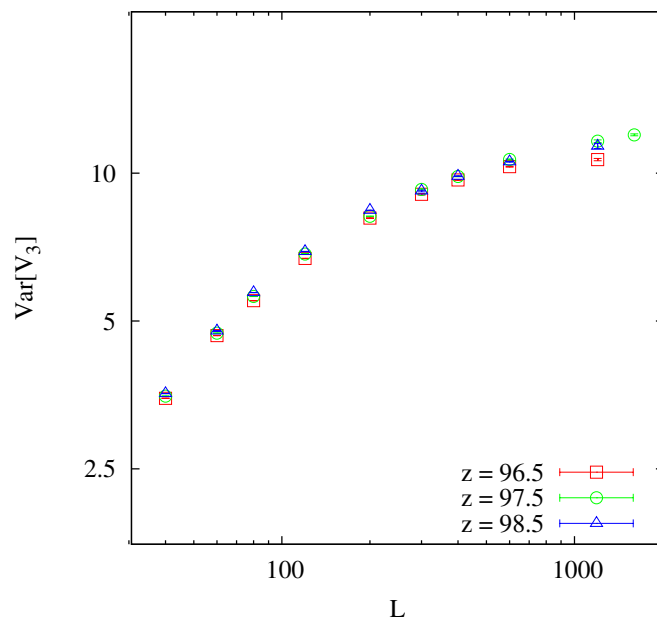


Figure 4.16: Plot of the variance of the vector  $V_3$  for various values of the system size at  $z = 96.5, 97.5$  and  $98.5$ . We find that this quantity saturates to a finite value at the critical point as the size of the system is increased.

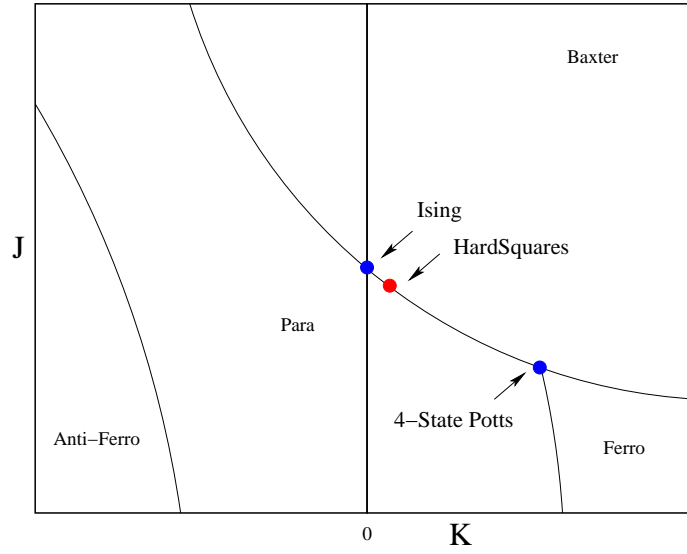


Figure 4.17: (Right) The phase diagram of the Ashkin-Teller model depicting the critical lines and the position of the phase transition of the hard square lattice gas.

$$\nu = 2/3, \alpha/\nu = 1, \beta/\nu = 1/8 \text{ and } \gamma/\nu = 7/4.$$

### Slidability

As we have seen in Section 4.3, the columnar ordered phases in the hard square lattice gas are characterised by the deconfinement of half vacancies along stacks of particles that can be slid to the left or right (and up or down) depending on the state of the system. In order to better understand the role of these long strings of defects, we define the following non-local variables, which we call the slidability variables.

We define a horizontal stack of particles as a (maximal) set of touching squares in the same row. A vertical stack is a set of touching squares in one column. A square can be a part of at most one horizontal and at most one vertical stack at the same time. A stack is slidable, if and only if it can be moved at least one space along the direction of the stack (i.e.- horizontally for a horizontal stack and vertically for a vertical stack). We assign a horizontal slidability index  $S_h(i) = +1$  at every lattice site  $i$  if it is occupied by a square that is part of a horizontally slidable stack, and 0 otherwise. A similar definition holds for the vertical slidability index  $S_v$ .

We then define the following variables that are a measure of the degree of sliding order in the system

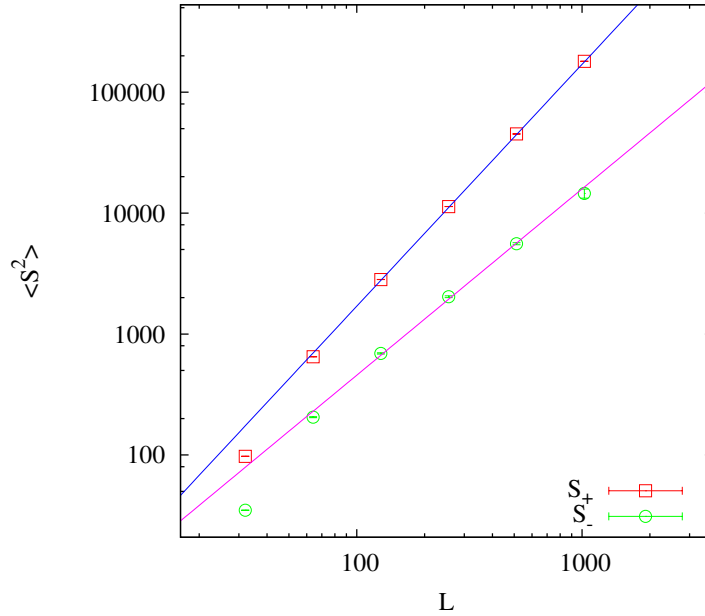


Figure 4.18: Plot of the second moment of the slidability variables  $\langle S_+^2 \rangle$  and  $\langle S_-^2 \rangle$  at  $z = z_c$  (normalized by  $\frac{1}{L^2}$ ).  $\langle S_+^2 \rangle$  grows with a power  $2 \pm 0.01$  with increasing system size, whereas  $\langle S_-^2 \rangle$  displays a non-trivial power law behaviour with exponent  $1.54 \pm 0.05$ . The lines have a slope of 2 and 1.54 respectively.

$$\begin{aligned}
 S_+ &= \sum_{i=1}^{L^2} [S_h(i) + S_v(i)], \\
 &\text{and} \\
 S_- &= \sum_{i=1}^{L^2} [S_h(i) - S_v(i)].
 \end{aligned} \tag{4.81}$$

The *A* and *B* phases have a large density of horizontally slidable rows of particles, and the *C* and *D* phases have a large density of vertically slidable columns. We measure the second moment of these slidability parameters  $S_+$  and  $S_-$ , for various system sizes at the critical point. This data is plotted in Fig. 4.18. These show a power law dependence on the size of the system, with the powers  $2 \pm 0.01$  and  $1.54 \pm 0.05$  respectively.

## 4.10 Hard-Cubes on the Cubic lattice

The series expansion developed in this chapter can be extended to three dimensional systems that exhibit columnar order. Consider a system of  $2 \times 2 \times 2$  hard cubes on the cubic lattice. In this case there are twelve distinct columnar ordered states available to the system. We label these states *A*, *B*, ... to *L* (Fig. 4.19 a). In any of the given ordered states, there can be three distinct types of defect particles depending on the which of the rows the particles

occupy in relation to the ordered row.

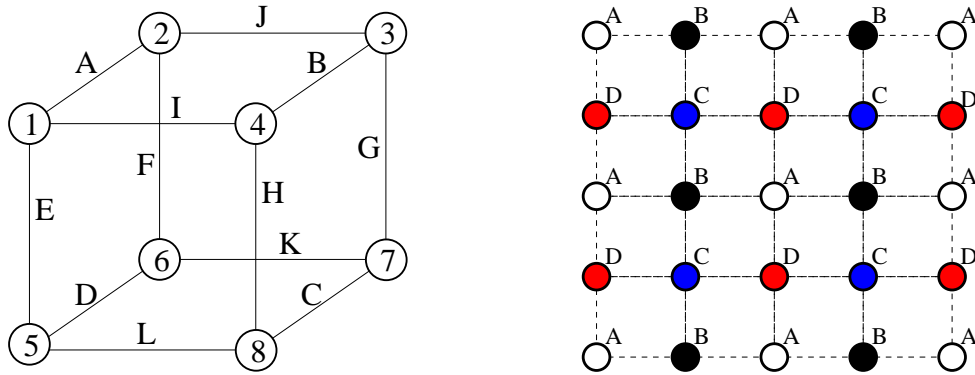


Figure 4.19: a) We define eight sublattices (1 to 8) on the cubic lattice. There are twelve columnar ordered states available to the system (labelled  $A, B, \dots$  to  $L$ ). b) A cross sectional segment of the cubic lattice depicting the positions of the defect rows ( $B, C$  and  $D$ ) with respect to the  $A$ -rows.

Consider a state with perfect columnar order, with columns along the  $z$ -direction. Now ascribing different fugacities to the rows  $A, B, C$  and  $D$ , we note that at the point where  $z_A = z_B \rightarrow \infty$  and  $z_C = z_D = 0$ , there is a large degeneracy of columnar ordered states available to the system, as particles on different planes can choose to align along independent columns ( $A$  or  $B$ ). The cross-section in the  $xy$ -plane would be a fully packed configuration of  $2 \times 2$  hard squares. Then, as discussed above, there are approximately  $2^{L/2}$  different fully-packed hard squares configurations.

The first correction term due to the  $C$  and  $D$  defects lying in between two planes is  $(f_{000})^4 + (f_{000})^2$ , when the two adjacent planes are both  $A$ -ordered or  $B$ -ordered, whereas the corresponding term when the two planes are in different ordered states is  $2(f_{000})^3$ . It is then easily seen that the contribution is largest when all the columns are arranged in a periodic superlattice with square symmetry (all  $A$ , or all  $B$ ). These states then outweigh all other states, for non-zero  $1/z$ , in the thermodynamic limit. This is an example of “order-by-disorder” [7] in this system. The extended objects that contribute to order  $1/z$  in the  $z_A = z_B = z$  series in this case turn out to be rigid rods along the  $x$ - or  $y$ - directions. The interactions between the rods are similar to the two dimensional case, but the summations are harder to do in closed form. This seems to be an interesting direction for future studies.

## 4.11 Summary and Discussion

In this chapter we have studied the high density columnar ordered phase and the transition from columnar order to a disordered phase in the hard square lattice gas. We developed a perturbation expansion about the columnar ordered state for the hard square lattice gas. We identified the basic objects of excitations about the ordered state, namely vertical rods. We showed that only configurations with at most  $n$  rods contribute up to  $\mathcal{O}(z^{-(n+1)/2})$

in the expansion in inverse powers of  $z^{-1/2}$ , and we explicitly summed the contribution from the terms containing two rods that provides exact results up to order  $1/z^{3/2}$ . We then analysed the nature of the transition from the columnar ordered phase at high density to the fluid phase at low density. We argued using a simple coarse grained picture, that the critical properties of the model can be mapped onto the critical line of a more general Ashkin-Teller model. We used symmetry arguments to map the local densities in the model to the Ising energy densities in the corresponding Ashkin-Teller model. We then studied the phase transition as a function of activity using Monte Carlo simulations to test our predictions. We located the critical point of the system and computed the correlations between various quantities in order to precisely locate the position of the transition on the Ashkin-Teller critical line. We established that the phase transition in the model corresponds to a ferromagnetically coupled point on the Ashkin-Teller phase diagram, between the 2D Ising model and the 4-state Potts model.

It is possible to extend the series expansion developed in this chapter to other systems that display columnar ordered behaviour at high densities. In particular for the  $k \times k$  hard square lattice gas a similar procedure can be used to generate the high-activity expansion with terms of powers of  $z^{-1/k}$  appearing. Other systems displaying columnar ordering at high densities such as hard rectangles on the square lattice are also amenable to treatments of this type. Another problem of interest is to establish lower bounds on the radius of convergence of these expansions. The columnar ordered phase studied in this chapter is characterised by very large correlation lengths as can be seen from the fact that the quantities of interest, for example the variance of the  $\mathbb{Z}_4$  eigenvectors reach their asymptotic values only at very large system sizes. It would be interesting to identify the reason for strong finite size corrections in such a columnar ordered phase.

# References

- [1] B. McCoy, *Advanced Statistical Mechanics* (International Series of Monographs on Physics) (Oxford University Press) (2010)
- [2] W. G. Hoover, B. J. Alder and F. H. Ree, *J. Chem. Phys.* **41**, 3528 (1964).
- [3] D. Ioffe, Y. Velenik and M. Zahradnik, *J. Stat. Phys.* **122**, 761 (2006).
- [4] A. Bellemans and R. Nigam, *J. Chem. Phys.* **46**, 2922 (1967).
- [5] R. J. Baxter, *Phys. Rev. Lett.* **26**, 832 (1971).
- [6] J. Ashkin and E. Teller, *Phys. Rev.* **64**, 178 (1943).
- [7] J. Villain, R. Bidaux, J. P. Carton, and R. J. Conte, *J. Phys. (Paris)* **41**, 1263 (1980).
- [8] H. C. M. Fernandes, J. J. Arenzon and Y. Levin, *J. Chem. Phys.* **126**, 114508 (2007).
- [9] X. Feng, H. W. J. Blote and B. Nienhuis, *Phys. Rev. E.* **83**, 061153 (2011).



# Chapter 5

## Conclusions

In this thesis, we have studied the spin- $S$  Kitaev model, and the hard square lattice gas model.

We analysed the spin- $S$  Kitaev model in the limit of large  $S$  where the spins are classical 3-vector (Heisenberg) spins. We derived the ground states of this model and were able to parametrise the full set of states using height variables living on the plaquettes of the lattice. We showed that for a system with  $2N$  sites, the ground states form an  $N + 1$  dimensional manifold. We then used an analogy to a two dimensional electrostatics problem. We parametrised the non-ground state configurations of this system using additional real valued charge variables at each site. Using this characterisation of the entire set of states, we were able to take the limit of temperature  $T \rightarrow 0$  without resorting to any approximation. We showed that in this limit, all the states in the ground state manifold have an equal weight and thus this model does not display thermal order-by-disorder. We then mapped the zero temperature system of Heisenberg spins interacting via Kitaev couplings onto that of a solid-on-solid model with nearest neighbour interaction. We found that at zero temperature, this model is still in its rough phase. This implies a power law decay of the spin-squared correlations. We also mapped the model of interacting spins at a finite temperature onto that of a solid-on-solid model, but with non-local coupling. We were able to show that for the entire range of temperatures  $[0, \infty]$  of the spin model, the corresponding solid-on-solid model remains in its rough phase. We then performed Monte-Carlo simulations on this model and verified our predictions.

We next investigated the quantum spin- $S$  Kitaev model. We derived an exact lower bound for the ground state energy of this model. We then analysed the case in which the coupling between the spins in one direction are set to zero, reducing the problem to a one dimensional spin chain. For this one dimensional case, we found constants of motion at each bond that commute with the Hamiltonian, and each other. We were able to classify the states of this model according to the eigenvalues of these invariants. We developed a way to count the number of states in each of these sectors using a simple transfer matrix technique. We then investigated the ground state energy of this spin chain for the case

$S = 1$ . We mapped the Hamiltonian of the  $S = 1$  model onto that of an  $S = 1/2$  model. We then used trial wave functions whose coefficients were chosen from a one dimensional lattice gas ensemble to find the ground state of this system. We also estimated the energy gap to the first excited state using this technique. We also investigated a related model with an extra parameter added, and found that this model exhibits a quantum phase transition from a phase that has a finite energy gap to a gapless phase.

In Chapter 4 we studied the lattice gas model of  $2 \times 2$  hard squares on the square lattice. This model does not order into a crystalline ordered state at high densities because there is a vacancy-induced sliding instability that makes this type of order unstable. However, a partial order survives in the form of columnar order, where only two of the four possible ordered states mix with each other. To better understand the nature of the columnar ordered phase, we developed exact series expansions in this phase. We found that this series is a singular series in the activity of particles,  $z$ , with half integer powers appearing. This is due to the deconfinement of half-vacancies in the high density phase. We showed that the series can be grouped in terms of arbitrarily long vertical columns of defects that are the natural excitations in the high density phase. We derived a series for the free energy and order parameter of this system in inverse powers of  $z$ , that is exact to order  $1/z^{3/2}$ . We then analysed the nature of the transition from fluid to columnar order as a function of density in this system. Using a simple symmetry argument we showed that this model can be mapped onto the more general Ashkin-Teller-Potts model at its critical point. We used this mapping to identify the individual Ising components of the Ashkin-Teller model in terms of the local densities of the hard square lattice gas model. We then used Monte Carlo simulations to test our predictions. In order to efficiently sample the configuration space, we used a non-local algorithm that updates an entire line of sites at once. Using this technique we were able to estimate thermodynamic quantities from lattices of sizes upto  $1600 \times 1600$ . From our simulations we find that the two Ising degrees of freedom in the corresponding Ashkin-Teller description are ferromagnetically coupled. Thus we were able to place the transition of the hard square lattice gas model in the Ashkin-Teller universality class with critical exponents between the values of the two dimensional Ising model and the four state Potts model.

## Appendix A

# Height Correlations at Infinite Temperature

In this Appendix we calculate the asymptotic behaviour of the height correlation functions at infinite temperature in the Kitaev model with classical Heisenberg spins.

At infinite temperature, the spins at different sites are completely uncorrelated. This simplifies the calculation of the  $\langle (f_R - f_0)^2 \rangle$  correlation function. There are two independent degrees of freedom at each A-site. We can choose these to be  $\epsilon(l, m; z)$  and  $\epsilon(l, m; y)$ .  $\epsilon(l, m; x)$  is trivially  $-\epsilon(l, m; z) - \epsilon(l, m; y)$ . At infinite temperature

$$\begin{aligned}\langle \epsilon(l, m; z) \epsilon(l', m'; z) \rangle &= \frac{4}{45} \delta_{l,l'} \delta_{m,m'}, \\ \langle \epsilon(l, m; y) \epsilon(l', m'; z) \rangle &= -\frac{2}{45} \delta_{l,l'} \delta_{m,m'}.\end{aligned}\tag{A.1}$$

For a field  $\phi(l, m)$  on the lattice, we define the Fourier and inverse Fourier transforms as follows

$$\begin{aligned}\phi(\vec{k}) &= \frac{1}{\sqrt{LM}} \sum_{\vec{r}} \exp[i\vec{k} \cdot \vec{r}] \phi(\vec{r}), \\ \phi(\vec{r}) &= \frac{1}{\sqrt{LM}} \sum_{\vec{k}} \exp[-i\vec{k} \cdot \vec{r}] \phi(\vec{k}).\end{aligned}\tag{A.2}$$

The vector  $\vec{r}$  denotes the point  $(l, m)$  in real space and  $\vec{k} \equiv (k_1, k_2)$  denotes the point  $(\frac{u}{2\pi L}, \frac{v}{2\pi M})$  in Fourier space, with  $\vec{k} \cdot \vec{r} = \frac{ul}{2\pi L} + \frac{vm}{2\pi M}$ . The charge  $Q_{b(l,m)}$  at each B-sublattice site is given by

$$\begin{aligned}Q_{b(l,m)} &= \epsilon(l, m; z) + \epsilon(l-1, m+1; y), \\ &\quad -\epsilon(l, m+1; z) - \epsilon(l, m+1; y).\end{aligned}\tag{A.3}$$

The discrete Poisson equation that determines the potential fields  $\phi$  is

$$\begin{aligned}\phi_a(l, m) + \phi_a(l-1, m+1) + \phi_a(l, m+1) - 3\phi_b(l, m) &= -Q_b(l, m), \\ \phi_b(l, m) + \phi_a(l+1, m-1) + \phi_a(l, m-1) - 3\phi_a(l, m) &= 0,\end{aligned}\tag{A.4}$$

where  $\phi_a(l, m) \equiv \phi(a(l, m))$  and  $\phi_b(l, m) \equiv \phi(a(l, m) + e_z)$ . Eq. (A.4) can be inverted in Fourier space as

$$\begin{bmatrix} \phi_a(\vec{k}) \\ \phi_b(\vec{k}) \end{bmatrix} = \frac{1}{g(\vec{k})g(\vec{k})^* - 9} \begin{bmatrix} 3 & g(\vec{k}) \\ g(\vec{k})^* & 3 \end{bmatrix} \begin{bmatrix} 0 \\ -Q_b(\vec{k}) \end{bmatrix},\tag{A.5}$$

where  $g(\vec{k}) = 1 + \exp[i(k_2 - k_1)] + \exp[ik_2]$ . Now, the difference in the  $f$  variables along the  $z$ -axis is given by

$$\begin{aligned}f(l+R, m+1) - f(l, m+1) &\equiv f_R - f_0 = \\ \sum_{r=1}^R \epsilon(l+r, m; z) + \sum_{r=1}^R [\phi_a(l+r, m) - \phi_b(l+r, m)].\end{aligned}\tag{A.6}$$

We can write this in terms of the Fourier components as follows (taking  $(l, m) = (0, 0)$ ):

$$\begin{aligned}[f_R - f_0] &= \sum_{r=1}^R \sum_{\vec{k}} [\alpha_{\vec{k}} \epsilon(\vec{k}; z) + \beta_{\vec{k}} \epsilon(\vec{k}; y)] \exp[-ik_1 r], \\ \text{where } \alpha_{\vec{k}} &= 1 + \frac{3 - g(\vec{k})}{g(\vec{k})g(\vec{k})^* - 9} (1 - \exp[-ik_2]), \\ \text{and } \beta_{\vec{k}} &= \frac{3 - g(\vec{k})}{g(\vec{k})g(\vec{k})^* - 9} (\exp[ik_1] - 1)(\exp[-ik_2]).\end{aligned}\tag{A.7}$$

The summation over the  $r$  variable is straightforward. The variance of the difference in the height variables at infinite temperature is thus given by

$$\langle (f_R - f_0)^2 \rangle_{\beta=0} = \sum_{\vec{k}} \left| \frac{1 - \exp[-ik_1(R+1)]}{1 - \exp[-ik_1]} \right|^2 \left[ \langle (\alpha_{\vec{k}} \epsilon(\vec{k}; z) + \beta_{\vec{k}} \epsilon(\vec{k}; y))^2 \rangle \right].$$

The term within the square brackets can be shown to be equal to

$$\frac{6}{45} \left( \frac{1 - \cos[k_1]}{3 - \cos[k_1] - \cos[k_2] - \cos[k_1 - k_2]} \right).$$

Thus the correlation function simplifies to

$$\langle (f_R - f_0)^2 \rangle_{\beta=0} = \frac{6}{45} \sum_{\vec{k}} \frac{1 - \cos[k_1(R+1)]}{3 - \cos[k_1] - \cos[k_2] - \cos[k_1 - k_2]}. \quad (\text{A.8})$$

For large lattice sizes, this summation can be approximated by an integral, using  $\sum_{\vec{k}} \rightarrow \int_{-\pi}^{\pi} \int_{-\pi}^{\pi} \left(\frac{dk_x}{2\pi}\right) \left(\frac{dk_y}{2\pi}\right)$ . After a change of basis  $\vec{k}_x = \frac{\vec{k}_1 + \vec{k}_2}{\sqrt{2}}$ ,  $\vec{k}_y = \frac{\vec{k}_1 - \vec{k}_2}{\sqrt{2}}$  the correlation function can be expressed as

$$\langle (f_R - f_0)^2 \rangle_{\beta=0} = \frac{12}{45} \int_{-\pi}^{\pi} \int_{-\pi}^{\pi} \left(\frac{dk_x}{2\pi}\right) \left(\frac{dk_y}{2\pi}\right) \frac{1 - \cos[\vec{k} \cdot \vec{R}]}{k_x^2 + 3k_y^2}, \quad (\text{A.9})$$

where  $\vec{k} \cdot \vec{R} = (k_x + k_y) \frac{R}{\sqrt{2}}$ . This is precisely the lattice Green's function on the triangular lattice. For large  $\vec{R}$ , only the  $\vec{k}$  near zero are important. This integral can be shown to behave as  $\frac{1}{2\pi\sqrt{3}} \log(R)$  at large  $R$  [1]. Thus we have

$$\langle (f_R - f_0)^2 \rangle_{\beta=0} = \frac{2\sqrt{3}}{45\pi} \log(R) + \text{const.} \quad \text{for large } R. \quad (\text{A.10})$$

The coefficient of  $\log(R)$  gives us the effective temperature of the SOS model, thus for  $T = \infty$  in the spin model we have  $\beta_{SOS} = \frac{2\sqrt{3}}{45\pi}$ .

# References

- [1] T. Horiguchi, J. Math. Phys 13, 1411 (1972)

## Appendix B

# Additional Details for the High-Activity Expansion

### B.1 Three B-defects on the lattice: Exact Expression

In this section we quote the exact expression for the three-defect term,  $\kappa_3(z_A)$  in the cumulant expansion.

Consider  $n$  B-defects on the lattice. If any of the defects are separated from the rest of the cluster by a distance  $\Delta Y > 1$  then the terms can be factored into a product of weights of lower order clusters and thus do not contribute in the cumulant expansion. We therefore consider diagrams with all the defects satisfying the criterion  $\Delta Y \leq 1$  with respect to their nearest neighbours.

It is possible to write closed form expressions for  $\kappa_n(z_A)$ . As an illustrative example we quote the result for the three-defect term  $\kappa_3(z_A)$ . We have

$$\kappa_3(z_A) = \kappa_{[3]}(z_A) + \kappa_{[21]}(z_A) + \kappa_{[111]}(z_A). \quad (\text{B.1})$$

The term within the square brackets in the subscript denotes the position of the particles in the  $Y$  direction.  $\kappa_{[3]}$  corresponds to the term with three particles placed on the same row,  $\kappa_{[21]}$  denotes the term corresponding to the first two particles on the same row and the third adjacent to them and  $\kappa_{[111]}$  denotes the term arising from all three particles on adjacent rows. We have

$$\kappa_{[3]}(z_A) = \frac{2(10 + \alpha(20 + (-7 + \alpha)\alpha))}{(-1 + \alpha)(-1 + \alpha^2)} f_{000}^6,$$

$$\begin{aligned} \frac{\kappa_{[12]}(z_A)}{3} &= \left( \frac{2-2\alpha}{\lambda_+^2} \right) f_{000}^4 + \left( -6 + \frac{\alpha \left( -8 - \frac{12}{\lambda_+} \right)}{1-\alpha^2} + \frac{\alpha^2 \left( -4 - \frac{12}{\lambda_+} \right)}{1-\alpha^2} - \frac{16}{\lambda_+} \right) f_{000}^5 \\ &\quad + \frac{2(10 + \alpha(10 + (-6 + \alpha)\alpha))}{(-1 + \alpha)(-1 + \alpha^2)} f_{000}^6, \end{aligned} \quad (\text{B.2})$$

$$\begin{aligned} \frac{\kappa_{[12]}(z_A)}{3} &= \left( 1 + \frac{4}{\lambda_+^2} + \frac{4}{\lambda_+} \right) f_{000}^4 + \left( -6 + \frac{\alpha \left( -4 - \frac{8}{\lambda_+} \right)}{1-\alpha} - \frac{12}{\lambda_+} \right) f_{000}^5 \\ &\quad + \frac{(-3 + \alpha)^2}{(-1 + \alpha)^2} f_{000}^6, \end{aligned} \quad (\text{B.3})$$

where  $f_{000} = \left( \frac{\rho_{1d}}{z_A} \right)$ . Expanding the above three-defect term in inverse powers of  $z_A$ , we have

$$\frac{\kappa_3(z_A)}{3!} = \frac{1}{32} \left( \frac{1}{z_A^4} \right) + \frac{3}{32} \left( \frac{1}{z_A^{9/2}} \right) - \frac{7}{32} \left( \frac{1}{z_A^5} \right) + \mathcal{O} \left( \frac{1}{z_A^{11/2}} \right). \quad (\text{B.4})$$

## B.2 Regrouping the Terms

In Chapter 4, we have developed a series expansion in terms of the number of rod defects. In this section we describe an alternate procedure to regroup the terms of the series at the point  $z_A = z_B = z$  in powers of  $z$ . Working order by order we identify the various diagrams that contribute to the expansion and evaluate the contribution from each term.

### B.2.1 Expansion for the Free Energy

The contribution from a single B defect in the expansion is given by the first term of the cumulant expansion  $\kappa_1(z_A)z_B$ . When we set  $z_A = z_B = z$ , we obtain an expansion in powers of  $z$  which contains fractional powers with the first term being of order  $1/z$  and the next being  $1/z^{3/2}$ . Similarly the two particle term also yields an expansion in terms of  $1/\sqrt{z}$  with the first correction of order  $1/z$  and so on. In general, terms at each order in inverse powers of  $z$  get contributions from an arbitrarily large number of defects. We regroup the  $n$ -particle terms in the cumulant expansion such that at the point  $z_A = z_B = z$  the terms are ordered in decreasing powers of  $1/z$ . We have the following expansion for the free energy of the system about the columnar ordered state

$$-\mathcal{F}(z_A, z_B) = -\mathcal{F}(z_A, 0) + f_1(z_A, z_B) + f_{\frac{3}{2}}(z_A, z_B) + \dots, \quad (\text{B.5})$$

where the term  $f_m(z_A, z_B)$  denotes the term obtained from the sum over all configurations that contribute to the free energy expansion at order  $m$  at the point  $z_A = z_B = z$ .

We have

$$f_m(z_A, z_B)|_{z_A=z_B=z} = \frac{g_m}{z^m}, \tag{B.6}$$

where  $g_m$  is the coefficient of the order  $1/z^m$  term in the free energy expansion.  $f(z_A, 0) = -\frac{1}{2} \log \lambda_+(z_A)$  is the contribution to the free energy from the perfectly columnar ordered state. At the point  $z_A = z_B = z$  we represent this term as  $f_{1D}(z)$ . We thus have the following expression for the free energy expansion about the columnar ordered state

$$-f(z) = -f_{1D}(z) + \frac{g_1}{z} + \frac{g_{\frac{3}{2}}}{z^{3/2}} + \mathcal{O}\left(\frac{1}{z^2}\right). \tag{B.7}$$

The order  $1/z$  term gets contributions only from defects aligned along the vertical direction (this excludes the least volume of A-particles). This is in effect the same object as a pair of half-vacancies separated by a vertical “rod” of B-sublattice particles. The free energy series at the point  $z_A = z_B = z$  can be written as a Mayer-like expansion of these rods. Each term in the expansion has a contribution from these columns of defects of arbitrary length. The term of order  $1/z^{\frac{n+1}{2}}$  involves at most  $n$  such rods, but one has to sum over all possible sizes of these objects.

**Order  $1/z$**

We now consider the terms that contribute to the cumulant expansion at order  $1/z$ . These are configurations where an arbitrary number of defects on adjacent rows are aligned so that  $\Delta = 0$  for each neighbour (single rods of arbitrary length. The weight of single rods in the partition function expansion is given by

$$w \left[ \begin{array}{|c|} \hline \square \\ \hline \end{array} \right] = \sum_{n=1}^{\infty} (f_{000})^{n+1} = \sum_{n=1}^{\infty} \left[ \frac{1}{2^{n+1}} \left( \frac{1}{z_A^{n+1}} \right) - \frac{n+1}{2^{n+2}} \left( \frac{1}{z_A^{n+3/2}} \right) + \mathcal{O}\left(\frac{1}{z_A^{n+2}}\right) \right], \tag{B.8}$$

where the diagram within the brackets denotes the class of rod configurations with an arbitrary number of aligned defects. The summation above is over all rods of length  $n = 1$  to  $\infty$ . Each weight is multiplied by the factor  $z_B^n$  due to the fugacity of the  $n$  B-defects (which yields the leading order contribution from each individual rod as order  $1/z$ ). Now for any other diagram, with  $\Delta > 0$ , the leading order term contributes to terms of order  $1/z^{3/2}$  or higher. Hence, to leading order in  $1/z$  we have

$$f_1(z_A, z_B) = \begin{array}{|c|} \hline \square \\ \hline \end{array}_1 = \frac{1}{2} \sum_{n=1}^{\infty} \frac{1}{2^{n+1}} \left( \frac{z_B^n}{z_A^{n+1}} \right), \tag{B.9}$$

where the subscript 1 on the diagram above represents the order  $1/z$  contribution to the free energy from the class of rods of arbitrary size. The disconnected terms arising from lower order cumulants are of order  $1/z^2$  or higher, and hence do not contribute in the above

expression. We thus have

$$g_1 = \frac{1}{4}. \quad (\text{B.10})$$

### Order $1/z^{3/2}$

At the next order in inverse powers of  $z$  we have contributions from terms involving two rods, in addition to the single rod terms. As illustrated in the cumulant expansion for two B-defects, the order  $1/z^{3/2}$  term gets a contribution from defects placed adjacent to each other separated by a single lattice spacing, and also from the sum over individual terms when the defects are placed on the same B-row. When we regroup the terms of the cumulant expansion, the terms arising from rods of all lengths behave in a similar manner. The configurations that contribute to the expansion at order  $1/z^{3/2}$  are as follows

- 1) The  $1/z^{3/2}$  contribution from individual rods,
- 2) Two adjacent rods separated by a single lattice spacing, and
- 3) Two rods that have a finite overlap along the  $Y$  direction with an  $X$  separation  $\Delta \geq 2$ . A sum over  $\Delta$  in this case yields a leading contribution of order  $\sqrt{z}$ , that gives such a term a leading contribution of order  $1/z^{3/2}$ . This can be understood as follows, the finite overlap term has a contribution  $[G(\Delta)]^n$ , where  $G(\Delta)$  is the correlation function for two particles separated by a distance  $\Delta$  for the 1D lattice gas.  $G(\Delta)$  decays exponentially with a correlation length  $\xi = \log \alpha \sim \sqrt{z}$  to leading order in  $z$ . Thus, a sum over  $\Delta$  yields a contribution of order  $\sqrt{z}$ .

We deal with each individual term separately. We have

$$f_{\frac{3}{2}}(z_A, z_B) = \begin{array}{|c|} \hline \square \\ \hline \end{array}_{\frac{3}{2}} + \begin{array}{|c|} \hline \square \\ \hline \square \\ \hline \end{array}_{\frac{3}{2}} + \begin{array}{|c|} \hline \square \\ \hline \square \\ \hline \end{array}_{\frac{3}{2}}. \quad (\text{B.11})$$

The subscript  $\frac{3}{2}$  on the diagrams above represents the order  $1/z^{3/2}$  contribution to the free energy from each class of diagrams. The corresponding coefficients for the diagrams above are  $T_1$ ,  $T_2$  and  $T_3$  respectively. We have

$$g_{\frac{3}{2}} = T_1 + T_2 + T_3. \quad (\text{B.12})$$

We compute the contribution from each of these terms to the free energy expansion below.

The order  $1/z^{3/2}$  contribution from single rods is given by Eq. B.8. We have

$$\begin{array}{|c|} \hline \square \\ \hline \end{array}_{\frac{3}{2}} = -\frac{1}{2} \sum_{n=1}^{\infty} \binom{n+1}{2n+2} \left( \frac{z_B^n}{z_A^{n+3/2}} \right), \quad (\text{B.13})$$

which leads to

$$T_1 = -\frac{3}{8}. \quad (\text{B.14})$$

The term  $T_2$  (the contribution from adjacent rods) involves configurations of two adjacent rods separated by an  $X$  distance  $\Delta = 1$ . The adjacency site is at a fixed position (on any of the  $N_B$  B-sites), and the two rods are composed of  $n_a$  and  $n_b$  (for the rod above and below) B-particles respectively. We also account for the fact that the second rod can be on either side of the first one. We have

$$\left[ \begin{array}{c} \text{rod} \\ \text{rod} \end{array} \right]_{\frac{3}{2}} = \sum_{n_a=1}^{\infty} \sum_{n_b=1}^{\infty} \frac{1}{2^{n_a+n_b+1}} \left( \frac{z_B^{n_a+n_b}}{z_A^{n_a+n_b+3/2}} \right), \quad (\text{B.15})$$

which leads to

$$T_2 = \frac{1}{2}. \quad (\text{B.16})$$

The computation of the term  $T_3$  involves two vertical rods with a finite  $Y$ -overlap. The size of the overlap is represented as  $n_o$ , the number of overlapping B-particles, where  $n_o$  varies from 1 to  $\infty$ . In addition, there can be sections of each rod that extend above and below the overlapping parts. The non-overlapping sections are parts of the rods extending above and below with  $n_a$  and  $n_b$  defects respectively, where  $n_a$  and  $n_b$  can vary from 0 to  $\infty$ . Once again the first rod can be on either side of the second one. The weight of this term in the partition function expansion is given by

$$w \left[ \begin{array}{c} \text{rod} \\ \text{rod} \end{array} \right] = \frac{1}{2} \left( 1 + 4 \sum_{n_a=1}^{\infty} (f_{000} z_B)^{n_a} + 4 \sum_{n_a=1}^{\infty} \sum_{n_b=1}^{\infty} \left( \frac{\rho_{\infty} z_B}{z_A} \right)^{n_a+n_b} \right) \\ \times \left( \sum_{n_o=1}^{\infty} \sum_{\Delta \geq 2} (f_{000})^{2n_o+2} z_B^{2n_o} (1 - \alpha^{|\Delta|-1})^{n_o+1} \right). \quad (\text{B.17})$$

The summation within the first bracket can be performed trivially and yields a factor  $\frac{9}{2}$ . To evaluate the term within the second bracket we use the binomial identity to expand the  $\alpha$ -term

$$(1 - \alpha^{|\Delta|-1})^{n_o+1} = \sum_{i=0}^{n_o+1} \binom{n_o+1}{i} (-\alpha^{|\Delta|-1})^i. \quad (\text{B.18})$$

The  $i = 0$  term corresponds to two disconnected rods on the lattice and hence is exactly cancelled in the corresponding cumulant expansion. Now, summing over  $\Delta$  yields



$z^{\frac{n+1}{2}}$ , only terms involving  $n$  rods need to be considered.

### B.2.2 Expansion for the Order Parameter

In this section we compute the high-activity expansion for the row order parameter which is defined in the text as

$$O_r = 4[(\rho_1 + \rho_2) - (\rho_3 + \rho_4)]. \quad (\text{B.25})$$

We thus have

$$O_r(z_A, z_B) = 4 \left[ z_A \frac{\partial}{\partial z_A} - z_B \frac{\partial}{\partial z_B} \right] (-f(z_A, z_B)). \quad (\text{B.26})$$

At the point  $z_A = z_B = z$  the expansion for the order parameter is

$$O_r = 4 \left( O_{1D}(z) + \frac{O_1}{z} + \frac{O_{\frac{3}{2}}}{z^{3/2}} + \dots \right), \quad (\text{B.27})$$

where  $O_{1D}(z)$  is the contribution to the order parameter expansion from the perfectly columnar ordered state. We have

$$O_{1D}(z) = z \frac{\partial}{\partial z} (-f_{1D}(z)) = \frac{1}{4} - \frac{1}{4\sqrt{1+4z}}. \quad (\text{B.28})$$

We now evaluate the order parameter expansion upto order  $1/z^{3/2}$ .

#### Order $1/z$

The contributions to the order  $1/z$  term come from single rod configurations of arbitrary length. We have

$$f_1(z_A, z_B) = \boxed{1} = \frac{1}{2} \sum_{n=1}^{\infty} \frac{1}{2^{n+1}} \left( \frac{z_B^n}{z_A^{n+1}} \right). \quad (\text{B.29})$$

Differentiating the expression with respect to  $z_A$  and  $z_B$  (Eq. B.26), we have the coefficient of the  $1/z$  term of the order parameter.

$$O_1 = -\frac{1}{2} \sum_{n=1}^{\infty} \frac{(2n+1)}{2^{n+1}} = -\frac{5}{4}. \quad (\text{B.30})$$

#### Order $1/z^{3/2}$

As discussed in Section B.2, at order  $1/z^{3/2}$  we have the following configurations contributing to the free energy and hence the order parameter expansion 1) single rods 2) two adjacent rods separated by a single lattice spacing and 3) two rods with a finite  $Y$ -overlap (summed over all  $X$ -separations  $\Delta$ ). We deal with each term separately. We have



$$\begin{aligned}
R_3 = & 4 \sum_{n_a=1}^{\infty} \sum_{n_b=1}^{\infty} \sum_{n_o=1}^{\infty} \left(\frac{1}{2}\right)^{2n_o+na+n_b+2} (4n_o + 2n_a + 2n_b + 3/2)\zeta \\
& + 4 \sum_{n_a=1}^{\infty} \sum_{n_o=1}^{\infty} \left(\frac{1}{2}\right)^{2n_o+na+2} (4n_o + 2n_a + 3/2)\zeta \\
& - \frac{1}{2} \sum_{n_o=1}^{\infty} \left(\frac{1}{2}\right)^{2n_o+2} (4n_o + 3/2)\zeta. \tag{B.37}
\end{aligned}$$

Now summing over  $n_a$  and  $n_b$  we have

$$\begin{aligned}
R_3 = & -\frac{51}{4} \sum_{n_o=1}^{\infty} \left(\frac{1}{2}\right)^{2n_o+2} \sum_{i=2,\text{even}}^{n_o+1} \frac{1}{i} \binom{n_o+1}{i} \\
& - 18 \sum_{n_o=1}^{\infty} (n_o + 1) \left(\frac{1}{2}\right)^{2n_o+2} \sum_{i=2,\text{even}}^{n_o+1} \frac{1}{i} \binom{n_o+1}{i}. \tag{B.38}
\end{aligned}$$

This series can be summed, as shown in Section B.2.3. We have

$$R_3 = \left(-4 - \frac{50}{4} \log\left(\frac{9}{8}\right)\right).$$

We therefore arrive at

$$O_{\frac{3}{2}} = -\left(\frac{99}{16} + \frac{25}{2} \log\left(\frac{9}{8}\right)\right). \tag{B.39}$$

We thus obtain the high-activity expansion for the order parameter upto order  $1/z^{3/2}$

$$O_r = 1 - \frac{1}{2z^{1/2}} - \frac{5}{z} - \left(\frac{395}{16} + 50 \log\left(\frac{9}{8}\right)\right) \frac{1}{z^{3/2}} + \mathcal{O}\left(\frac{1}{z^2}\right). \tag{B.40}$$

### B.2.3 Summing the Binomial Series

In this section we describe a procedure to sum the binomial series arising at order  $1/z^{3/2}$  in the expansions developed above. We define the generating function

$$\Sigma(Y, X) = \sum_{N=2}^{\infty} (Y)^N \sum_{i=2,\text{even}}^N \frac{1}{i} \binom{N}{i} X^i. \tag{B.41}$$

We evaluate  $\Sigma(Y, X)$  as follows. Let

$$S_{\pm} = \sum_{N=2}^{\infty} (Y)^N \sum_{i=1}^N \frac{(\pm 1)^i}{i} \binom{N}{i} X^i. \tag{B.42}$$

Therefore

$$\Sigma(Y, X) = \frac{S + S'}{2}. \quad (\text{B.43})$$

Differentiating with respect to  $X$ , we obtain

$$X \frac{\partial S_{\pm}}{\partial X} = \sum_{N=2}^{\infty} (Y)^N \sum_{i=1}^N \binom{N}{i} (\pm 1)^i X^i \quad (\text{B.44})$$

$$= \frac{1}{1 - (1 \pm X)Y} - \frac{1}{1 - Y} \mp XY. \quad (\text{B.45})$$

Therefore

$$\frac{\partial \Sigma}{\partial X} = \frac{1}{2X} \left( \frac{1}{1 - (1 + X)Y} + \frac{1}{1 - (1 - X)Y} - \frac{2}{1 - Y} \right). \quad (\text{B.46})$$

Integrating with respect to  $X$  and setting  $X = 1$ , we arrive at

$$\Sigma(Y, 1) = \frac{1}{2(1 - Y)} \log \left( \frac{(1 - Y)^2}{1 - 2Y} \right). \quad (\text{B.47})$$

Now, from Eq. B.21, the coefficient of the  $1/z^{3/2}$  contribution from the overlapping rods term in the free energy expansion can be expressed as

$$T_3 = 4 \Sigma \left( \frac{1}{4}, 1 \right). \quad (\text{B.48})$$

Using the expression in Eq. B.47 with  $Y = \frac{1}{4}$ , we arrive at

$$T_3 = \frac{9}{2} \Sigma \left( \frac{1}{4}, 1 \right) = 3 \log \left( \frac{9}{8} \right). \quad (\text{B.49})$$

In the calculation of the order parameter expansion we deal with the series

$$\chi(Y, X) = \sum_{N=2}^{\infty} N (Y)^N \sum_{i=2, \text{even}}^N \frac{1}{i} \binom{N}{i} X^i = Y \frac{\partial \Sigma(Y, X)}{\partial Y}.$$

We have

$$\chi \left( \frac{1}{4}, 1 \right) = \frac{2}{9} \left( 1 + \log \left( \frac{9}{8} \right) \right). \quad (\text{B.50})$$

From Eq. B.38, the coefficient of the  $1/z^{3/2}$  contribution from the overlapping rods term in the order parameter expansion can be expressed in terms of the functions  $\Sigma$  and  $\chi$  as follows

$$R_3 = -\frac{51}{4} \Sigma \left( \frac{1}{4}, 1 \right) - 18 \chi \left( \frac{1}{4}, 1 \right). \quad (\text{B.51})$$

Finally, using the expression in Eq. B.50, we arrive at

$$R_3 = \left( -4 + \frac{50}{4} \log \left( \frac{9}{8} \right) \right). \quad (\text{B.52})$$

